AN ABSTRACT OF THE THESIS OF

Jamie M. Kern for the degree of Master of Science in Geology presented on June 5, 2012

Title: Timescales of Large Silicic Magma Systems: Investigating the Magmatic History of Ignimbrite Eruptions in the Altiplano-Puna Volcanic Complex of the Central Andes through U-Pb Zircon Dating

Abstract approved:

_____

Shanaka L. de Silva

The Altiplano-Puna Volcanic Complex in the Central Andes is one of the youngest large silicic volcanic fields (LSVFs) in the world, erupting over 13,000 km^3 of material during multiple supereruptions from 11 to 1 Ma. Understanding the timescales over which magma is stored in the crust prior to eruption is crucial to understanding the development of LSVFs such as the APVC. The residence time of a magma is defined as the time between magma formation and its eruption. While the eruption age of a volcanic system is generally well constrained through $^{40}Ar/^{39}Ar$ dating of sanidine and biotite crystals, determining the time of magma formation offers a bigger challenge. U-Pb dating of zircon—an early crystallizing, ubiquitous

phase in silicic systems—is a commonly used method for determining the timing of magma formation.

U-Pb zircon ages were collected for 16 ignimbrites representing the temporal and spatial distribution of the APVC. Zircon crystallization histories show significant overlap between eruptive centers of similar age separated by as much as 200 km. Ignimbrites erupted from the same multicyclic caldera show little relationship. This suggests that ignimbrites may share a deeper, regional source. Timescales of zircon crystallization for individual ignimbrites range from ~400 ka to more than 1 Ma, with little correlation with age or erupted volume. Ignimbrites with longer crystallization timescales frequently exhibit a stepped age distribution and highly variable U contents, suggesting that these ignimbrites likely formed in a very crystalline, low melt fraction environment while ignimbrites with short crystallization times and constrained U concentrations crystallized in high melt fraction systems. Zircon crystallization histories record periods of continuous zircon crystallization in the APVC that extend over 1.5-2 Ma pulses and correlate well with eruptive pulses recognized by previous studies.

Overall, zircon crystallization histories of the magmas feeding ignimbrite eruptions in the APVC record long timescales of magmatic activity from a shared regional source, likely the Altiplano-Puna Magma Body currently detectable underlying the APVC.

Timescales of Large Silicic Magma Systems: Investigating the Magmatic History of Ignimbrite Eruptions In the Altiplano-Puna Volcanic Complex of the Central Andes through U-Pb Zircon Dating

by

Jamie M. Kern

A THESIS

submitted to

Oregon State University

in partial fulfillment of

the requirements for the

degree of

Master of Science

Presented June 5, 2012

Commencement June 2012

Master of Science thesis of Jamie M. Kern presented on June 5, 2012

APPROVED:

_____

Major Professor, representing Geology

_____

Dean of the College of Earth, Ocean and Atmospheric Sciences

_____

Dean of the Graduate School

I understand that my thesis will become part of the permanent collection of Oregon State University libraries. My signature below authorizes release of my thesis to any reader upon request.

_____

Jamie M. Kern, Author

ACKNOWLEDGEMENTS

The saying is that it takes a village to raise a child. The same can be said for raising a graduate student and seeing them through the long haul of achieving a M.S. degree. Because of this, there are quite a few people that I need to thank.

Most importantly, I need to thank my advisor Shan de Silva for welcoming me into his research group at OSU and providing guidance, opportunities, and support over the past two years.

Thanks to my committee members Adam Kent and Axel Schmitt for their feedback and support on completing this thesis.

I also thank the other members of the APVC group—Stephanie, Jason, Dale, Rodrigo, Trish, and Casey—for their help and friendship over the past two years. Thanks specifically to Steph for being an awesome role model and for giving excellent advice. Also thanks to my field buddies Jason and Rodrigo for helping me survive through a field season in Bolivia and research trips to other universities.

The VIPER research group is easily one of the best assets of OSU's geology department and I would like to thank all of the vipers for their amazing support.

Particular thanks to Christine Chan for listening to all of my complaints, grievances, and occasional euphoric ramblings and to Diana Di Leonardo and Kim Ogren for being awesome roommates, confidants, and bakers.

And finally, I wouldn't be where I am today without the incredible support of my family. Thanks Mom, Dad, Joey, and Jordan for letting me halfway across the country to pursue my dreams.

TABLE OF CONTENTS

Page

1.0 Introduction 1

1.1 Geologic Background 5

1.1.1 The Altiplano-Puna Volcanic Complex 5

1.1.2 Surface record of volcanism in the APVC 10

1.2 Magma Timescales 13

1.2.1 Zircon as a geochronometer 13

1.2.2 Magma timescales through zircon geochronology 14

1.2.3 APVC residence times 15

2.0 Goals and Objectives 17

3.0 Methods 20

3.1 Sample Collection 20

3.2 Mineral Separation 20

3.3 SIMS Analysis 21

4.0 Results 24

4.1 U-Pb Zircon Ages 24

4.2 Zircon Ages vs. $^{40}Ar/^{39}Ar$ Eruption Ages 25

4.3 Interior vs. Rim Ages 26

4.4 Cathodoluminescence Images 27

4.5 Zircon Age Spectra 28

4.5.1 Age spectra trends 28

TABLE OF CONTENTS (Continued)

Page

4.5.2 Overlapping zircon age spectra 29
5.0 Discussion 38
5.1 Zircon Populations and Trends 38
5.1.1 Xenocrysts 39
5.1.2 Antecrysts 40
5.1.3 Autocrysts 41
5.1.4 Population trends 41
5.2 Zircon Inheritance and Contemporaneous Crystallization 42
5.2.1 Evidence for true inheritance of zircon 43
5.2.2 Contemporaneous crystallization of magmas 45
5.3 Zircon Crystallization Times 51
5.4 Contrasting Styles of Magma Development 63
5.5 Integrating Crystallization Histories and Eruptive Histories 71
5.5 Integrated Model for APVC Magmatism 76
6.0 Conclusions 77
References Cited 80
Appendix 85

LIST OF FIGURES

Figure Page

Figure 1. Location map of APVC in the Central Andes. 4

Figure 2. Map of APVC calderas with geophysics. 7

Figure 3. Map of APVC ignimbrites and sources investigated in this study. 9

Figure 4. Overview of PDF plots of 16 ignimbrites over the temporal span of the APVC. 24

Figure 5. Zircon ages outside of APVC time span. 25

Figure 6. Rank order plots (ROP) of rim and interior ages with PDF curves for select ignimbrites. 27

Figure 7. CL images of representative zircon crystals. 28

Figure 8. ROP and PDF curves for ignimbrites erupted between 11 – 8.3 Ma. 30

Figure 9. ROP and PDF curves for ignimbrites erupted between 8 – 5.5 Ma. 32

Figure 10. ROP and PDF curves for ignimbrites erupted between 5.2 – 2.9 Ma 35

Figure 11. ROP and PDF curves for ignimbrites erupted between 2.7 – 1.0 Ma 37

Figure 12. Example PDF curve and histogram of the Toconao ignimbrite illustrating different zircon populations seen in APVC ignimbrites. 39

Figure 13. Spatiotemporal development of APVC magma systems. 50

Figure 14. Zircon crystallization times for 8 supereruptions in the APVC. 56

Figure 15. Zircon crystallization times compared to erupted volume and eruption age. 57

Figure 16. Probability plots for the Tara, Atana, and Guacha zircon age spectra 60

Figure 17. Normally distributed portions of zircon age spectra vs. zircon crystallization time.. 62

Figure 18. U abundances in zircon for 8 supereruptions in the APVC 65

LIST OF FIGURES (Continued)

Page

Figure 19. Variations in U abundance compared to the distribution of zircon ages for two ignimbrites. 66

Figure 20. Zircon saturation temperatures for ignimbrites examined in this study calculated based on whole rock pumice samples. 68

Figure 21. Cartoon representing two different end members of magma "chambers" feeding large ignimbrite eruptions 70

Figure 22. Zircon crystallization periods compared to eruptive pulses over the three stages of APVC development 72

Figure 23. Integrated model for the regional development of the APVC 76

LIST OF TABLES

Table Page

Table 1. Summary of ignimbrites used in this study.....19

Table 2. Summary of KS statistics for contemporaneous zircon age spectra.....46

Table 3. Summary of calculated zircon residence times 54

Table 4. Population statistics of normally distributed zircon ages for the Tara, Guacha, and Atana ignimbrites.....60

1.0 Introduction

A volcano-plutonic connection is founded on the geological, geophysical, geochemical kinship of spatiotemporally associated erupted and intruded rocks. Linking the surface record of volcanism to the associated plutonic record is one of the central challenges to understanding the volcano-plutonic connection. This challenge has been addressed particularly in large caldera-related systems where the surface eruptions are thought to be the "surface manifestations of batholiths" (Lipman 1984). Many of the largest calderas are parts of longer-lived volcanic fields or large silicic volcanic fields (LSVFs) that form during periods of intense caldera-forming volcanism known as ignimbrite flare-ups (de Silva 1989; Best & Christiansen 1991). Accounting for the volume of magma erupted during ignimbrite flare-ups and the associated plutonic roots invites a model where an extensive upper crustal batholith scale magma body was built during the lifetime of the LSVF (de Silva & Gosnold 2007; Lipman 2007). The link between LSVFs and batholiths has been best documented for the Southern Rocky Mountain Volcanic Field (SRMVF) of Colorado, and geophysical evidence suggests the presence of batholith-scale magma bodies beneath young LSVFs such as Yellowstone (Iyer et al. 1981), the Altiplano-Puna Volcanic Complex of the Central Andes (Zandt et al. 2003), and other locations compiled in Bachmann et al. (2007c).

Understanding the timescales over which magma is stored in the crust is crucial to understanding the development of LSVFs such as the APVC. The residence time of a

magma is defined as the time between magma formation and its eruption (Costa 2008). While the eruption age of a volcanic system is generally well constrained through $^{40}Ar/^{39}Ar$ dating of sanidine and, to a lesser extent biotite phenocrysts, determining the time of magma formation offers a bigger challenge. For one, sampling the underlying plutonic source in a young LSVF with little dissection can be problematic, and even if erosion exposes the underlying plutonic root, the timing of intrusion may not be concordant with eruption (Tappa et al. 2011). The most promising approach has focused on accessory minerals such as zircon found in erupted material. Zircon provides an invaluable window into the underlying magma system, allowing for linkages between the volcanic and plutonic realms and magma evolution and duration in the crust to be explored (Reid et al. 1997; Brown & Fletcher 1999; Vazquez & Reid 2002; Schmitt et al. 2003; Schmitt 2003; Bacon & Lowenstern 2005; Bachmann et al. 2007b; Miller et al. 2007; Simon et al. 2008; Walker et al. 2010; Folkes et al. 2011).

Advancements in high-precision U-Pb and U-Th zircon dating in the past 15 years allow for identification of zircon crystal populations that predate eruption ages. Many studies have successfully used pre-eruption zircon crystallization histories to infer residence times and the behavior of magmas prior to eruption (Reid et al. 1997; Brown & Fletcher 1999; Vazquez & Reid 2002; Schmitt 2003; Charlier 2005). In a silicic magma, zircon begins to crystallize once a magma of cools below the zircon saturation temperature determined by the melt composition (Watson &

Harrison 1983). Because the zircon saturation temperature is reached prior to eruption, zircons record an extended magma history between crystallization and eruption. U-Pb and U-Th zircon dating of young (<10 Ma) silicic systems compared to $^{40}Ar/^{39}Ar$ eruption ages shows that zircon can crystallize up to 100s of ka prior to eruption (Simon et al. 2008). This difference between zircon crystallization ages and eruption ages represents the crystal residence time for zircon and a minimum estimate for magma residence times (Reid et al. 1997).

This study explores the zircon crystallization histories of ignimbrites from the Altiplano-Puna Volcanic Complex (APVC) of the Central Andes (de Silva 1989; de Silva et al. 2006). The APVC is one of the youngest large silicic volcanic fields (LSVFs) in the world, erupting over 13,000 km^3 of magma during multiple supereruptions from 11 to 1 Ma that define an episodic volcanic history. The specific objectives of this research are to:

1. Use zircon crystallization histories to determine minimum residence times for the major APVC ignimbrites
2. Investigate relationships between zircon crystallization histories over the spatial and temporal span of the APVC
3. Relate the development of the plutonic system underlying the APVC eruptive centers to the erupted record

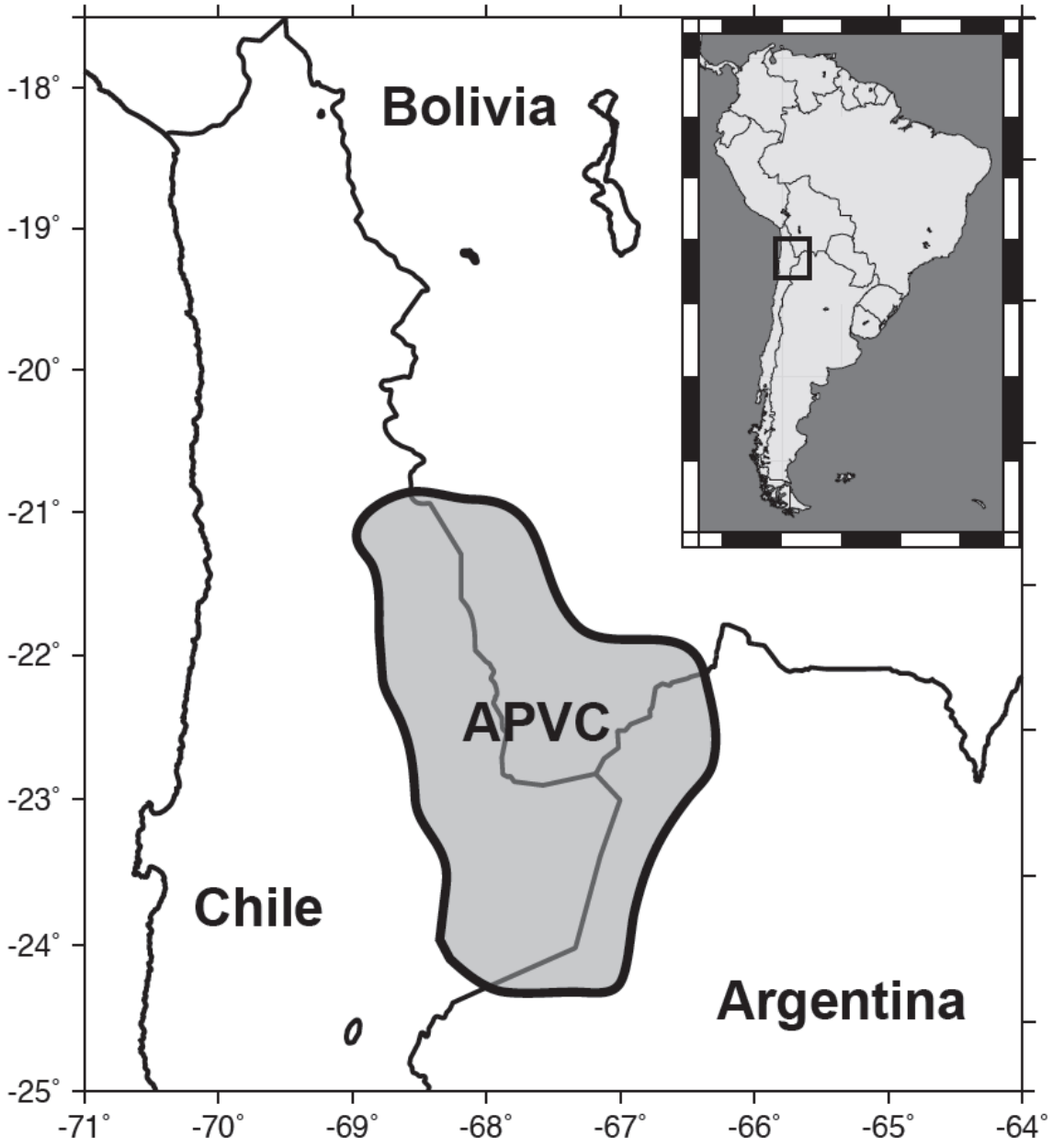

Figure 1. Location map of APVC in the Central Andes. Approximate extent of APVC is shaded in gray. Inset shows location on the western edge of South America.

1.1 Geologic Background

1.1.1 The Altiplano-Puna Volcanic Complex

The Altiplano-Puna Volcanic Complex in the Central Andes occupies an arid, high-elevation plateau at the political triple junction between Argentina, Chile, and Bolivia (Fig.1). The dry climate preserves multiple large caldera centers and their accompanying ignimbrites, providing an unparalleled view of some of the largest explosive silicic eruptions in the world. The APVC developed over the course of a catastrophic ignimbrite flare-up over a 10 Ma period which produced multiple large ignimbrite sheets from several large caldera sources (de Silva 1989). Today, the APVC is broadly studied from physical volcanological, geochemical, and geophysical viewpoints to better understand the development of large silicic volcanic fields and the potential for future APVC eruptions.

The APVC is situated on the Altiplano-Puna Plateau, which is rivaled only by the Tibetan Plateau in height and extent. The Altiplano-Puna Plateau is a major element of the Central Andes resulting from convergence of the Nazca and South American plates. Significant crustal shortening and magmatic addition over the Cenozoic produced a 70 km thick crust and an average elevation of 4000 m, with some stratovolcanoes on the plateau reaching 6000 m (Allmendinger et al. 1997).

Onset of volcanism in the APVC is correlated in time with a large degree of steepening of the subducting Nazca plate from nearly flat-slab subduction prior to

16 Ma to a ~30° dip today. The onset of steepening is thought to have induced decompression melting in the mantle, which produced voluminous mafic melt. The production of mafic magma triggered crustal melting and ignited the ignimbrite flare-up in the APVC from 11 to 1 Ma (Allmendinger et al. 1997; Kay & Coira 2009).

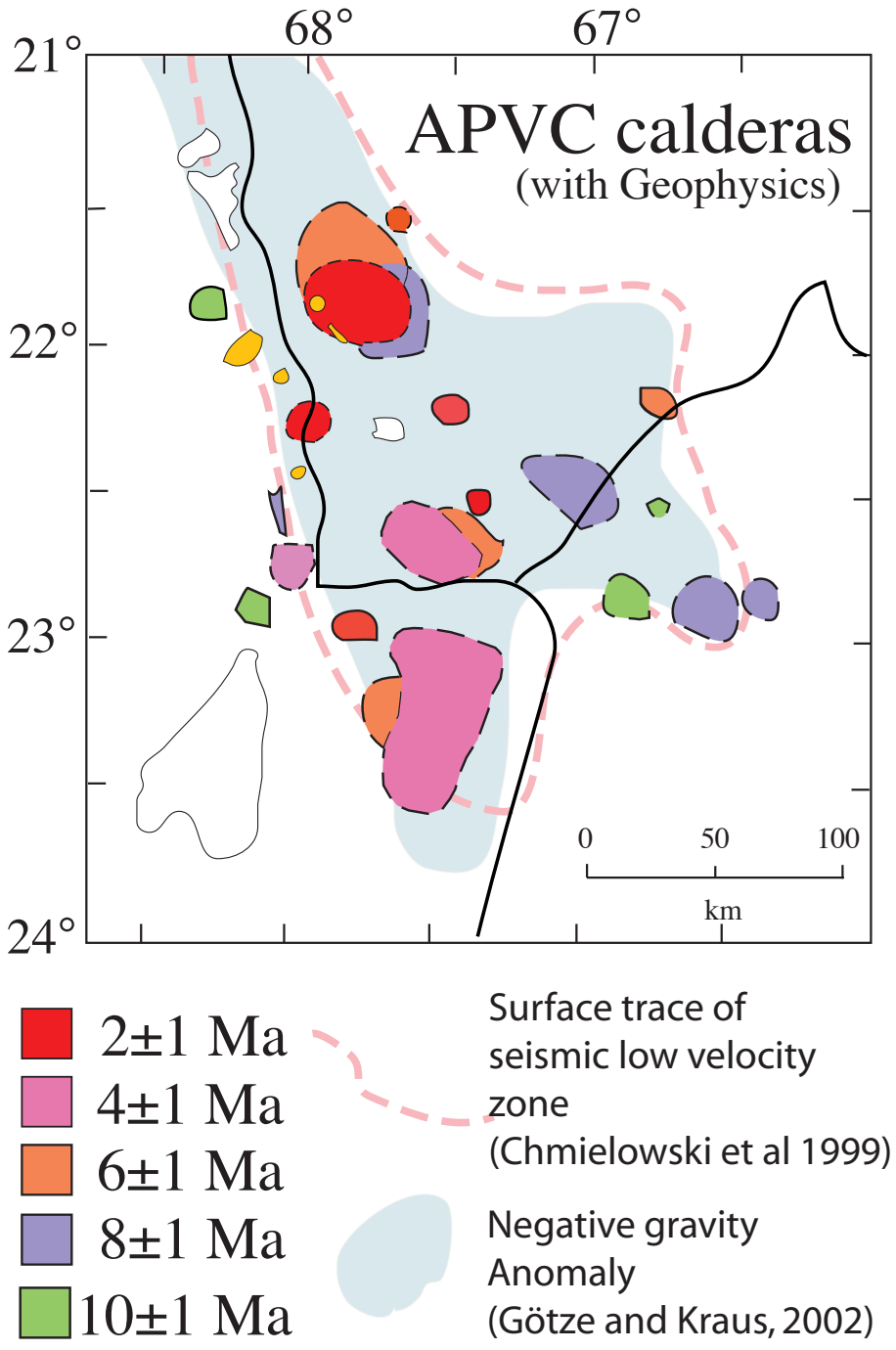

Figure 2. Map of APVC calderas with geophysics. Geophysics includes seismic and gravity surveys of the area. Extent of seismic low velocity zone and negative gravity anomaly approximates present extent of APMB (Chmielowski et al 1999; Gotze & Kraus 2002).

Today, multiple lines of geophysical evidence suggest that a large, partially molten magma storage zone—the Altiplano-Puna Magma Body (APMB)—sits ~17 km beneath much of the plateau (Fig. 2; Chmielowski & Zandt 1999; Zandt et al. 2003). The APMB is thought to be a large "mush" zone where mantle-derived melts stall and accumulate in the crust due to neutral buoyancy. The present extent of the APMB likely reflects at least 10 Ma of magma accumulation over the duration of the ignimbrite flare-up. Petrological evidence argues against the APMB as the direct source of the magmas supplying APVC eruptions. Instead, the APMB supplied more evolved silicic magmas to shallow-crustal staging areas at 4-8 km depth that fed surface volcanism. Over time, the development of the APMB and the upper crustal staging areas evolved the crustal geotherm, softening the crust to a point where it could store voluminous magma systems feeding ignimbrite eruptions on VEI 7-8 scales. Surface volcanism likely reflects the development of this vast plutonic system underlying the APVC (de Silva & Zandt 2006; de Silva et al. 2006).

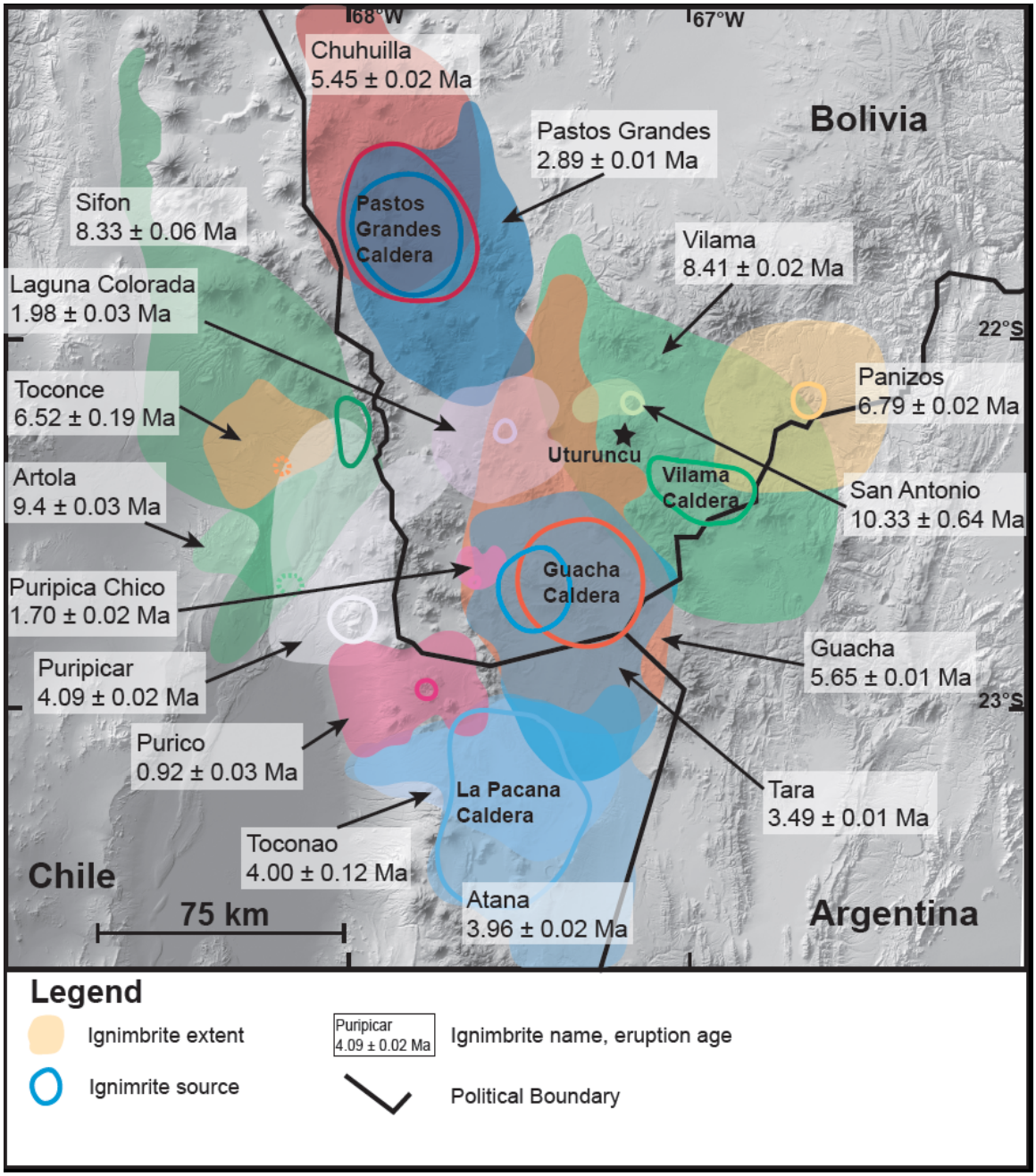

Figure 3. Map of APVC ignimbrites and sources investigated in this study. Sources and extent of ignimbrites are based on previously published research on individual APVC centers (Ort 1993; de Silva 1989; de Silva & Gosnold 2007; Lindsay, de Silva & Trumbull 2001a; Soler et al. 2007; Salisbury et al. 2011). Ages reported are compiled in Salisbury et al. (2011)

1.1.2 Surface record of volcanism in the APVC

The surface volcanic record of the APVC is dominated by large volume ignimbrite eruptions comprised primarily of high-K dacites and rhyodacites with minor rhyolites. Ignimbrite eruptions are sourced at large, multi-cyclic, nested calderas and smaller ignimbrite shields (Fig. 3; Table 1; de Silva et al. 2006). Seven eruptions from the La Pacana, Guacha, Pastos Grandes, and Vilama calderas exceed 1000 km^3. The space-time-volume record of APVC ignimbrites suggests three pulses of intense activity at ~8.4, ~5.5, and ~4.0 Ma and a centralization of volcanic activity over the course of the ignimbrite flare-up (de Silva & Gosnold 2007; Salisbury et al. 2011).

Initial activity from ~11 to 9 Ma represents a waxing stage of the flare-up. Eruptions occurred at separate, distant centers along the periphery of the APVC and produced small volume ignimbrites. These include the small Artola (<100 km^3) ignimbrite erupted from a buried source in the western edge of the APVC and the San Antonio ignimbrite that outcrops sparsely near Volcan Uturuncu (Fig. 3). These early eruptions suggest that an extensive plutonic system was already developing beneath the APVC at this time (de Silva & Gosnold 2007; Salisbury et al. 2011).

The first pulse of the ignimbrite flare-up at ~8.4 Ma includes the large-volume Sifon (1000 km^3) and Vilama (1400 km^3) ignimbrites (Salisbury et al. 2011). The Sifon ignimbrite erupted from an as yet unknown source, although the Piedras Grandes center in the western edge of the APVC near the Chilean border is the most probable

(Fig. 3). The crystal-rich, pumice-poor Vilama ignimbrite erupted from the Vilama caldera on the Bolivia-Argentina border (Soler et al. 2007).

The period between the first and second pulses of the ignimbrite flare-up is marked by several smaller-volume eruptions, including the Panizos and Toconce ignimbrites. Toconce erupted from an unknown source region in Chile (de Silva 1989), while Panizos ignimbrite constituting the Panizos ignimbrite shield erupted on the eastern edge of the APVC (Fig. 3; Ort 1993; de Silva & Gosnold 2007).

The eruptions of the Guacha (1300 km^3) and Chuhuilla (1200 km^3) ignimbrites mark the peak of the 5.5 Ma pulse. The Guacha ignimbrite, which covers over 5800 km^2, is sourced from the Guacha caldera in southern Bolivia near the Argentinian border. The Chuhuilla ignimbrite is the first eruption from the Pastos Grandes caldera in the northern part of the APVC (Fig. 3; Salisbury et al. 2011).

Flare-up intensity spiked at 4.0 Ma with the Atana (1600 km^3) and Puripicar (1500 km^3) eruptions, followed later by the eruptions of the Tara (800 km^3) and Pastos Grandes ignimbrite (1500 km^3). The source region for Puripicar, which outcrops extensively in Chile, was once considered to be the Guacha caldera (de Silva 1989; de Silva & Gosnold 2007); however, recent studies attribute the Tara ignimbrite to the Guacha caldera instead (Fig. 3; Salisbury et al. 2011). Puripicar likely has a Chilean source. The Atana ignimbrite is consanguineous with the smaller, crystal-poor Toconao ignimbrite and erupted from the La Pacana caldera. Together, these

eruptions comprise nearly 2700 km^3, making La Pacana one of the largest known calderas in the world (Lindsay, de Silva & Trumbull 2001a). The Tara ignimbrite marks the second eruption from the Guacha caldera while the Pastos Grandes ignimbrite is the second eruption from the Pastos Grandes caldera (Salisbury et al. 2011).

The waning stages of the ignimbrite flare-up include several small-volume ignimbrite eruptions from sources in the center of the APVC, including the Laguna Colorada (60 km^3), Puripica Chico (10 km^3), and Purico (100 km^3) ignimbrites (Salisbury et al. 2011). The Laguna Colorada ignimbrite forms the blanket of the Laguna Colorada ignimbrite shield erupted between the Pastos Grandes and Guacha calderas. Puripica Chico is generally associated with the Guacha caldera, although its source is a small lava dome on the western edge of Guacha (Salisbury et al. 2011). The Purico ignimbrite erupted from the Cerro Purico ignimbrite shield complex near the Chile-Bolivia border (Fig. 3; Schmitt et al. 2001).

Overall, the nearly 13,000 km^3 of material erupted over 11 million years likely reflects only a small portion of the entire volume of magma that makes the APVC. At plutonic to volcanic ratios estimated by previous studies of 3:1 to 5:1 (White et al. 2006), the APVC may contain anywhere from ~40,000 to ~65,000 km^3 of unerupted material left in the crust forming a gigantic upper crustal batholith (de Silva & Gosnold 2007).

1.2 Magma Timescales

1.2.1 Zircon as a geochronometer

Zircon has long been recognized as an excellent geochronometer because of its high partition coefficients for uranium and thorium radionuclides used in radiometric dating and its low affinity for ^{206}Pb (Mahood and Hildreth, 1983; Blundy and Wood, 2003). Extremely slow diffusion rates of tetravalent cations enable zircon to retain geochemical and isotopic information through multiple melting events (Cherniak et al. 1997). Additionally, zircon is a common accessory phase in silicic magmas, making it an abundant and readily obtained phase for U-Pb geochronology in crustal rocks (Harrison & Watson 1983).

Zircon crystallizes rapidly once saturation conditions are met and diffuses slowly in a Zr undersaturated melt, with larger zircon phenocrysts surviving preferentially over smaller zircon phenocrysts. When zircon crystallization conditions are reached in a new magma, surviving zircon crystal provide nucleation sites for additional zircon growth. In this way, zircon can record multiple magmatic events (de Silva et al. 2006). Zircon crystallization begins when a silicic melt cools below its zirconium saturation temperature, which has been constrained experimentally for a wide range of melt compositions and zirconium concentrations (Watson & Harrison 1983).

1.2.2 Magma timescales through zircon geochronology

Reid et al. (1997) pioneered the use of high-precision zircon age dating to understand the timescales of magma storage based on the principles that 1) zircons are frequently found as inclusions within major phenocryst phases suggesting that they formed early during the crystallization process and 2) zircon crystallizes once a magma cools below its zircon saturation temperature, which is higher than eruption temperatures. Based on these observations—which are backed by a plethora of recent high-precision U-series and U-Pb zircon crystallization ages with accompanying high-precision $^{40}Ar/^{39}Ar$ eruption ages (see examples below)—zircon dating proves to be an effective way to constrain the pre-eruption history of a magma in the shallow crust.

Defining residence times using zircon crystallization histories is complicated by the ability of zircon to survive multiple thermal events (Watson 1996). Zircon age populations can be divided into three categories: autocrysts, antecrysts, and xenocrysts. Zircon autocrysts crystallize in the magma that accumulates prior to an eruption and are used to constrain the residence time of a magma. The presence of an autocryst population suggests that magma is present and zircon saturation conditions are met, enabling new zircon growth. Zircon antecrysts are incorporated from material left from older episodes of magmatic activity at the same center. The presence of antecrysts can indicate that magma has been recycled from non-erupted, partially solidified material from the underlying plutonic system.

Xenocrysts are incorporated from surrounding country rock and bear no relationship to any magma pulses associated with autocryst or antecryst production (Miller et al. 2007).

Previous studies using U-Pb and U-Th zircon dating to determine residence times in large silicic systems show large variability in zircon crystallization histories (Costa 2008). Estimates for the Bishop Tuff at Long Valley Caldera are about 100 ka (Reid 2000; Reid et al. 1997; Simon & Reid 2005). Autocrystic zircon crystallization in ignimbrites erupted from the Cerro Galán volcanic system in the Central Andes exceeds 100 ka, with evidence for inheritance of zircon autocrysts from previous eruptions (Folkes et al. 2011). The voluminous Fish Canyon Tuff in the San Juan Volcanic Field yielded a range of zircon ages spanning 600 ka (Bachmann et al. 2007a). Zircons from ignimbrites erupted from the Taupo Volcanic Zone show a complicated distribution of ages with abundant evidence for inheritance from previous eruptions. The Oruanui eruption is interpreted to have a residence time range from 2.5 ka to 40 ka. The presence of an older zircon population peak ~50kyr before the eruption suggests that some of the zircons are inherited from an older magma system feeding a separate eruption (Charlier 2005).

1.2.3 APVC residence times

The APVC is considered to be analogous to other large silicic systems like the Great Basin (Best & Christiansen 1991) and the Southern Rocky Mountain Volcanic Field

(Lipman 2007). While calculated residence times for silicic, caldera-forming eruptions do vary significantly (10^1 to 10^5 years), most appear to be on the order of a few hundred thousand years (Costa 2008). APVC ignimbrites are expected to yield similar residence times to other LSVFs. Schmitt et al. (2003) reported U-Pb zircon ages for APVC ignimbrites yield residence times on the order of several 100 ka. The twelve zircon ages previously reported for the 3.96 ± 0.02 Ma Atana ignimbrite are indistinguishable from eruption ages, while six zircon ages from the consanguineous 4.0 ± 0.12 Ma Toconao ignimbrite predate the eruption by ~500 –750 ka (Schmitt et al. 2003). These preliminary data provide first order estimates for residence times based on zircon crystallization histories of APVC ignimbrites but the small sample size limits the interpretation of these data.

A recent study of Pleistocene lava domes erupted as part of the waning stages of magmatic activity in the APVC yielded residence times of ~200 ka based on a statistically robust data set of ~50 zircon ages per dome (Tierney 2011). However, it is difficult to know how these lava domes relate to the large-volume ignimbrites in terms of magma development, therefore they may not offer the best comparison.

Studies of volcanic centers near the APVC may offer additional insight into APVC magmatic residence times. The Aucanquilcha Volcanic Cluster (AVC) at the northern edge of the APVC yields continuous zircon age spectra of anywhere between ~0.5 to 2 m.y. for 13 different eruptions since 11 Ma, which coincides with the eruptive history of the APVC. In the AVC, the oldest and youngest eruptions

yield the longest age spectra (~ 2 m.y.) while the eruptions during the height of volcanic output yield the shortest age spectra (~0.5 Ma) (Walker et al. 2010).

2.0 Goals and Objectives

The primary goal of this study was to examine the pre-eruptive histories and timescales of APVC ignimbrite magmas using U-Pb zircon dating to investigate the volcano-plutonic connection linking voluminous ignimbrite volcanism to the plutonic source. To accomplish this, I examined the zircon age spectra from 16 different ignimbrites that represent a relevant portion of the spatial and temporal record of the APVC. The primary objectives of this study are as follows:

Objective 1 – Use zircon crystallization histories to determine the timescales of magma development and storage in the APVC

While the eruptive record has been well constrained over 20+ years of fieldwork in the Central Andes, little is known about the timescales of magmatic processes feeding each eruption. Preliminary studies suggest that APVC residence times are protracted and extend well over 500 ka, but this is based on very little data collected from only two ignimbrites and warrants further investigation (Schmitt et al. 2003). A better understanding of the timescales of magma development in the APVC will provide insight into the processes behind the development of LSVFs. How long are

magmas stored prior to a large ignimbrite eruption? Is there any relationship between erupted volume and storage time? Are there variations in storage time with age?

Objective 2 – Investigate relationships between zircon crystallization histories over the spatial and temporal span of the APVC

The APVC contains three multicyclic calderas, numerous monocyclic calderas and smaller ignimbrite centers. The largest eruptions usually occur within a fairly limited timespan of a few hundred thousand years and comprise the eruptive pulses of the APVC ignimbrite flare-up. However, these paired eruptions usually occur at caldera centers separated by over 100 km. While eruption ages only give single, constrained ages, zircon crystallization histories have the advantage of recording longer time frames of magmatic activity. This can be used to investigate the temporal relationships between a) contemporaneous ignimbrite eruptions separated by large distances and b) ignimbrites erupted from the same caldera but separated by significant time. Do ignimbrites erupted from a single, multicyclic caldera contain shared zircon histories despite the long repose interval between eruptions? How similar are zircon histories from contemporaneously erupted ignimbrites and if they are similar, at how are they physically related?

Objective 3 – Understand the relationship between the plutonic record and the eruptive history of the APVC

If the APVC is indeed the surface manifestation of a large upper-crustal batholith as hypothesized, then the zircon crystallization histories of individual ignimbrites provide the only means currently possible to investigate batholith development in the region. Zircon studies provide a window into the plutonic realm of surface volcanism. How does the zircon record relate to the surface record? Are the eruptive pulses reflected in the plutonic record as well?

Ignimbrite	Caldera/shield source	Eruption Age (Ma)	Erupted Volume (km^3)*	Total n Zircons
Purico	Purico	0.98 ± .03	100	34
Puripica Chico	Guacha	1.70 ± .02	10	46
Laguna Colorada	Laguna Colorada	1.98 ± .03	60	19
Pastos Grandes	Pastos Grandes	2.89 ± .01	1500	58
Tara	Guacha	3.49 ± .01	800	46
Atana	La Pacana	3.96 ± .02	1600	62
Toconao	La Pacana	4.00 ± .12	100	27
Puripicar	N.D.	4.09 ± .02	1500	62
Chuhuilla	Pastos Grandes	5.45 ± .02	1200	41
Guacha	Guacha	5.65 ± .01	1300	52
Toconce	N.D.	6.52 ± .19	N.D.	19
Panizos	Panizos	6.79 ± .02	650	31
Sifon	Piedras Grandes	8.33 ± .06	1000	53
Vilama	Vilama	8.41 ± .02	1400	31
Artola	N.D.	9.40 ± .03	>100	21
San Antonio	Cerro San Antonio	10.33 ± .64	<10	34

Table 1. Summary of ignimbrites used in this study. Eruption ages and volumes are previously reported in Salisbury et al. (2011). Volumes are reported as dense rock equivalent (DRE).

3.0 Methods

3.1 Sample Collection

Pumice samples from 16 ignimbrites representative of the temporal and spatial span of the APVC were chosen for this study (Table 1). The focus of this study is the nine large ignimbrite eruptions that comprise the ignimbrite flare-up. Of these nine, only one—the Pujsa ignimbrite erupted from La Pacana—was not sampled. Four ignimbrites preceding the flare-up were analyzed, as well as three that post-date the flare-up.

Pumice was selected as opposed to bulk ignimbrite as representative of the juvenile magma. Sampling juvenile material ensures that zircons analyzed are from the magma in question and not picked up from older ignimbrites during emplacement. Samples were collected by many workers over 20+ years of fieldwork in the APVC, most recently in the fall of 2010 when new samples were taken from the Guacha, Puripica Chico, Pastos Grandes, Chuhuilla, and Laguna Colorada ignimbrites. Selected samples were fist-sized or larger and had minimum alteration.

3.2 Mineral Separation

Samples were crushed and sieved to a <250 μm fraction that was washed and decanted to reduce the amount of fines present. The samples were separated magnetically using a Frantz magnetic separator in incremental steps up to 1.25

amps. The non-magnetic separate was mixed with methylene iodide (density of 3.325) and allowed to settle. The dense fraction containing the zircon crystals was separated out and rinsed in acetone. At minimum 20 representative zircon crystals with a target goal of 50-60 were hand picked for each ignimbrite using a fine acupuncture needle for dating. Zircon in all samples were easily identified based on their rose-colored hue.

3.3 SIMS Analysis

High-precision Secondary Ionization Mass Spectrometry (SIMS) has proven to be a highly effective tool for U-Pb zircon dating. Samples for SIMS analysis were mounted on 1 in aluminum disks using double-sided tape and mounted in epoxy resin. Each sample was polished first with 1200 grit paper until interiors were well exposed and then with 1 μm diamond paste for a final polish. Catholodoluminescence (CL) images were taken of each zircon mount using a secondary electron microscope at UCLA, after which the mounts received a 10 nm gold cold before SIMS analysis. $^{206}Pb/^{238}U$ zircon ages were obtained using the UCLA CAMECA ims 1270 ion probe based on Schmitt et al. 2003 procedures. A 10-20 nA $^{16}O^-$ beam was focused on a 30-35 μm spot. Secondary ions were extracted at 10kV using an energy-band pass of 35 eV. The mass spectrometer was tuned to a mass resolution of ~5000 to resolve molecular interference in the mass range analyzed. Relative sensitivities of U and Pb were determined based on reference zircon AS-3 (Paces and Miller, 1993).

Both interior and rim ages were analyzed for a minimum of 20 total analyses per sample, with an ideal goal of 50 analyses per sample. Rims were preferentially measured in order to examine more closely the last stages of zircon crystallization. Interior measurements comprised ~15-20% of analyses per sample. Ages with errors exceeding 2σ from the mean error were excluded. Additionally, rare zircon ages significantly younger than eruption ages were interpreted as experiencing Pb loss and excluded from final plots.

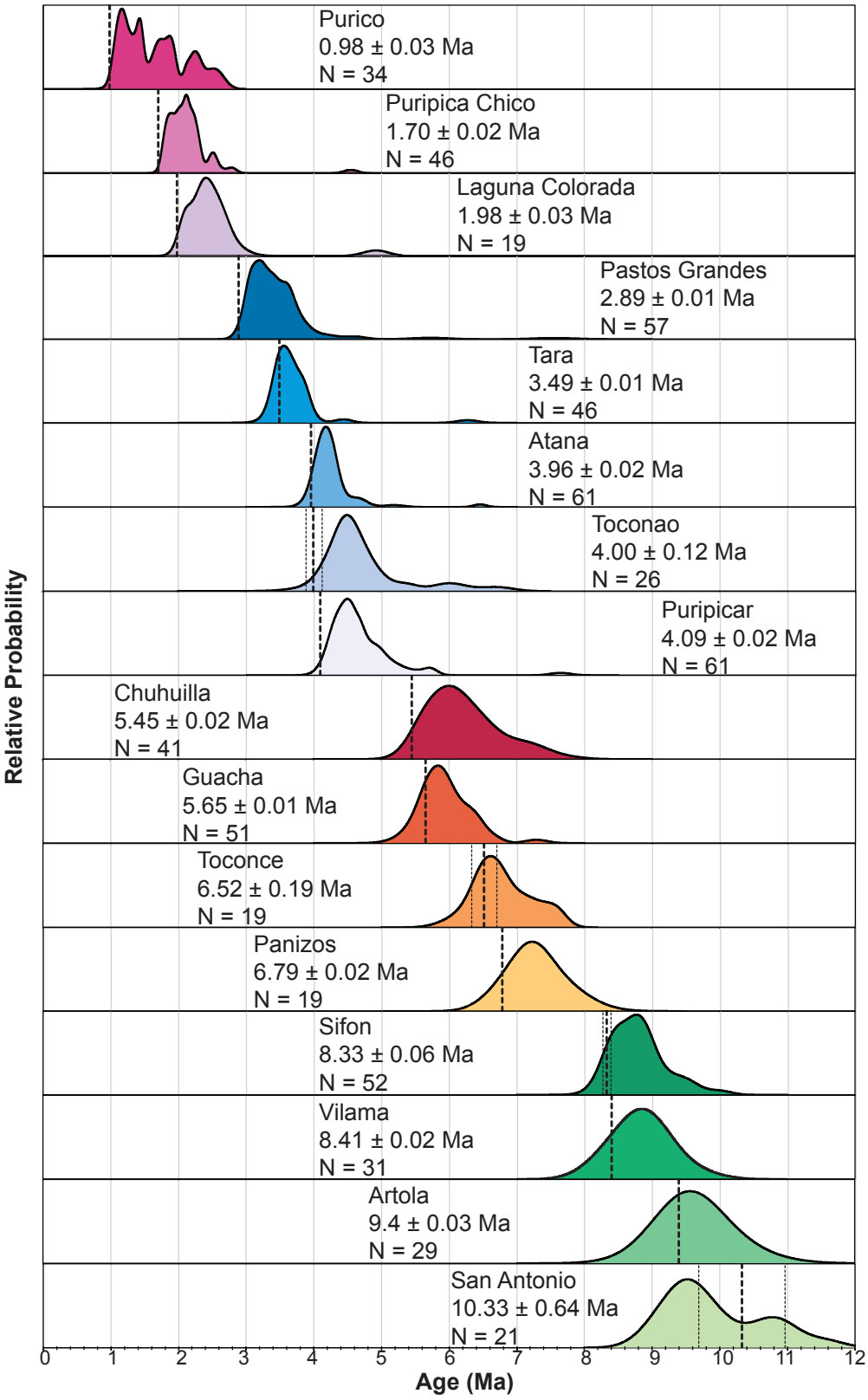
Purico
0.98 ± 0.03 Ma
N = 34
Puripica Chico
1.70 ± 0.02 Ma
N = 46
Laguna Colorada
1.98 ± 0.03 Ma
N = 19
Pastos Grandes
2.89 ± 0.01 Ma
N = 57
Tara
3.49 ± 0.01 Ma
N = 46
Atana
3.96 ± 0.02 Ma
N = 61
Toconao
4.00 ± 0.12 Ma
N = 26
Puripicar
4.09 ± 0.02 Ma
N = 61
Chuhuilla
5.45 ± 0.02 Ma
N = 41
Guacha
5.65 ± 0.01 Ma
N = 51
Toconce
6.52 ± 0.19 Ma
N = 19
Panizos
6.79 ± 0.02 Ma
N = 19
Sifon
8.33 ± 0.06 Ma
N = 52
Vilama
8.41 ± 0.02 Ma
N = 31
Artola
9.4 ± 0.03 Ma
N = 29
San Antonio
10.33 ± 0.64 Ma
N = 21
Relative Probability
0
1
2
3
4
5
6
7
8
9
10
11
12
Age (Ma)

Figure 4. Overview of PDF plots of 16 ignimbrites over the temporal span of the APVC. Varying colors represent groups of age spectra with overlapping distributions. Ignimbrites are ranked based on eruption ages represented by dashed lines with 1σ errors when discernible.

4.0 Results

4.1 U-Pb Zircon Ages

Over 600 U-Pb zircon ages from 16 ignimbrites representing the spatial and temporal span of the APVC were obtained for this study. Zircon ages for each ignimbrite form a continuous age spectrum with overlapping 1σ error bars. Few zircon ages fall greater than 1σ from the next youngest age. The difference between the oldest and the youngest zircon ages in the continuous distribution ranges from 500 ka to nearly 2 Ma. Within this continuous age spectrum, several different populations separated by small age gaps can be discerned. Probability density function (PDF) curves from all of the APVC ignimbrites show dominant peaks in zircon age density immediately prior to the eruption age (Fig. 4). These peaks approximate a range of strongly overlapping zircon ages with no significant age gaps and indicate the highest density of zircon ages. Most ignimbrites also show small inflections off the dominant peak or smaller peaks slightly older than but overlapping with ages comprising the dominant peak. These represent subpopulations within the overlapping zircon age spectrum. Only 24 zircon ages fall outside the age span of the APVC.

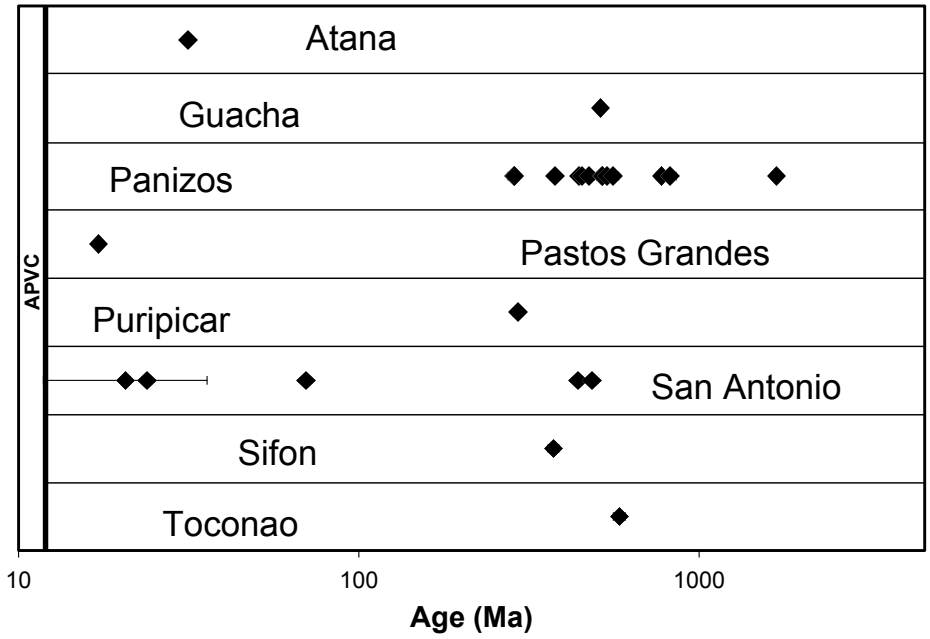

Figure 5. Zircon ages outside of APVC time span. Each row represents zircon crystals from a different ignimbrite. The furthest extent of APVC magmatism is shown in field to the left.

4.2 Zircon Ages vs. $^{40}Ar/^{39}Ar$ Eruption Ages

The youngest zircon ages in each age spectrum overlap within 1σ of the $^{40}Ar/^{39}Ar$ eruption age for each ignimbrite (Fig. 4). Amount of overlap varies between ignimbrites; in some cases, the youngest zircon ages overlay the eruption age (i.e. Guacha, Tara) while in other ignimbrites overlap is within error of only the youngest zircon ages (i.e. Pastos Grandes). In the APVC, eruption ages based on sanidine are thought to yield more accurate eruption ages than biotite crystals (Hora et al. 2010; Salisbury et al. 2011). The youngest zircon ages overlap within error of eruption ages in all ignimbrites with sanidine ages.

In rare cases, the eruption age may be significantly older than the youngest zircon ages. This is particularly evident in the San Antonio and Artola ignimbrites (Fig. 4). San Antonio yields $^{40}Ar/^{39}Ar$ single crystal fusion biotite age of 10.33 ± 0.64 Ma (Salisbury et al. 2011). The youngest zircon ages separated from the same sample from San Antonio are ~9.1 Ma. Artola $^{40}Ar/^{39}Ar$ biotite ages from multiple crystal fusion analysis of two samples produced a weighted mean age of 9.40 ± 0.03 Ma (Salisbury et al. 2011). The youngest Artola zircons yield ages of ~9.2 Ma. The strong correlation between eruption age and youngest zircon ages in other ignimbrites with sanidine eruption ages suggests that the youngest zircon ages provide better estimates of eruption age than the biotite ages for Artola and San Antonio.

4.3 Interior vs. Rim Ages

While both interior and rim ages were analyzed in each ignimbrite, the focus was to collect rim ages in order to better understand the last stages of crystallization of the magma. Interior and rim analyses on the same crystal show age differences ranging from analytically indistinguishable to several hundred thousand years (Fig. 6). In some cases, interiors yield ages outside of the APVC age span. Interior and rim ages fall on all portions of the continuous age spectra, with many rims yielding older ages

than interiors.

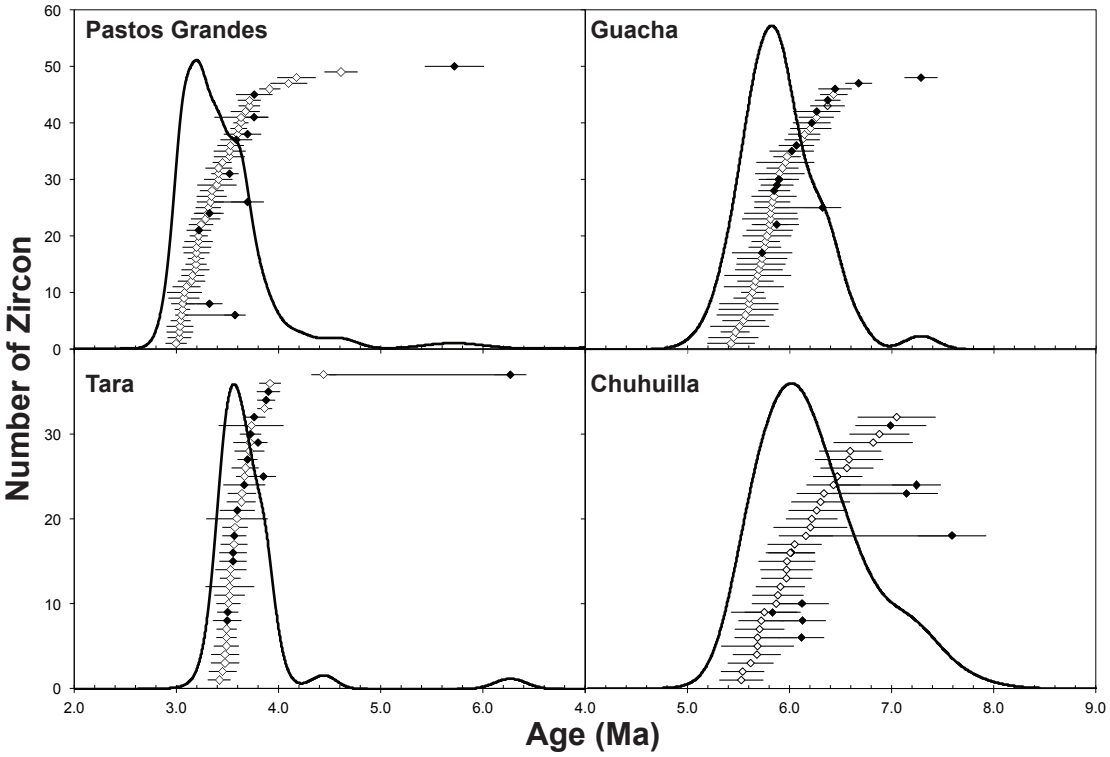

Figure 6. Rank order plots (ROP) of rim and interior ages with PDF curves for select ignimbrites. Diamonds represent individual zircon ages; open symbols are rim analyses, closed symbols are interiors. Lines connect single crystal interior-rim analyses.

4.4 Cathodoluminescence Images

Cathodoluminescence images reveal zoned zircon crystals in all ignimbrites. Crystal size varies greatly between ~50 to ~300 μm. Two separate populations of zircon crystals are present in each ignimbrite: equant, subhedral crystals and elongated, prismatic crystals (Fig. 7). There is no significant difference in the rim ages between zircon populations. Distinct interiors are often present in zircon crystals; however,

these usually have very regular boundaries with the apparent rim overgrowths and little evidence for resorption.

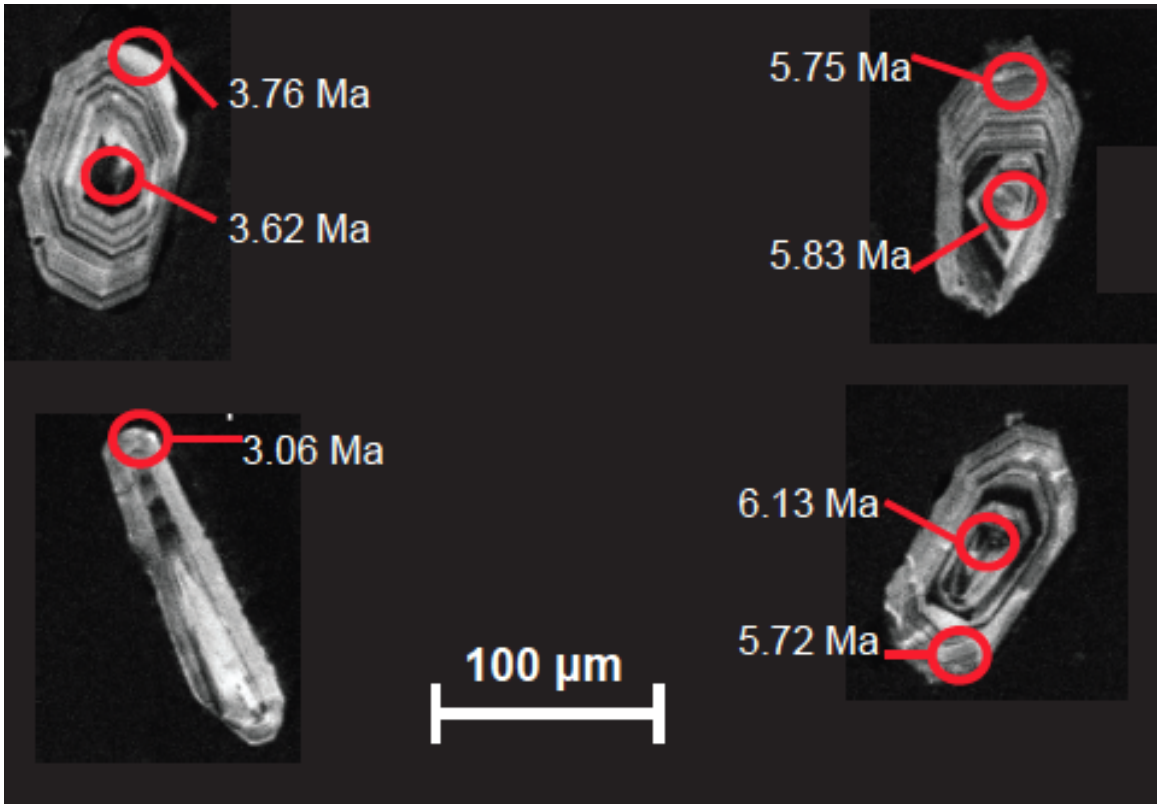

Figure 7. CL images of representative zircon crystals. Circles represent single spots analyses with corresponding ages. Zircons are from the Pastos Grandes (left) and Chuhuilla (right) ignimbrites.

4.5 Zircon Age Spectra

4.5.1 Age spectra trends

Patterns in PDF curves and population distributions appear over the temporal span of the APVC (Fig. 4). The oldest ignimbrites show largely unimodal zircon peaks

with few inflections or smaller peaks (i.e. Artola, Vilama). Progressively younger ignimbrites show more complex zircon crystallization histories with frequent satellite peaks off the prominent peak (i.e. Guacha, Toconao). Younger ignimbrites show isolated older peaks consisting of single zircon ages as well as satellite peaks. The youngest ignimbrites yield the most complex and variable PDF curves (i.e. Pastos Grandes, Puripica Chico).

4.5.2 Overlapping zircon age spectra

Each successive eruption in the APVC contains a zircon age spectra that often overlaps with previous eruptions. Ignimbrites with overlapping age spectra can be grouped into four periods (Fig. 4 color groups) with little significant overlap in age spectra between the groups. These periods cover ages between ~11 – 8.3 Ma, ~8 – 5.5 Ma, ~5.2 – 2.9 Ma, and ~2.7 to 1.0 Ma.

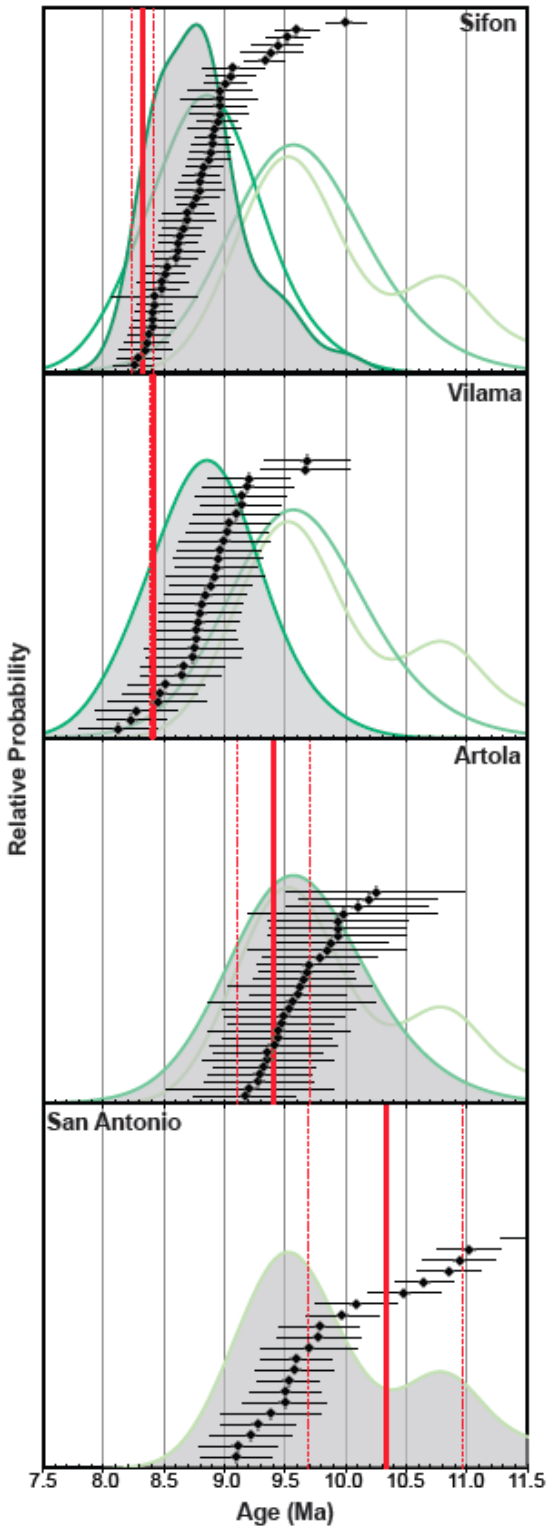

Figure 8. ROP and PDF curves for ignimbrites erupted between 11 – 8.3 Ma. Ignimbrites are arranged oldest to youngest from bottom to top, with PDF curves from previous eruptions for reference. Shaded PDF curve represents the distribution for the ROP displayed. Red lines represent eruption ages with errors for each ignimbrite.

11 – 8.3 Ma

The first period of overlapping ages includes the San Antonio, Artola, Vilama, and Sifon ignimbrites and lasts from ~11 to ~8.3 Ma (Figs. 4, 8). The earliest record of continuous zircon crystallization in the APVC begins at ~11 Ma with the oldest zircons in the San Antonio ignimbrite—one of the oldest ignimbrite eruptions in the APVC—and continues until the eruption of the Sifon ignimbrite at ~8.3 Ma.

The San Antonio age spectrum consists of a dominant peak centered at 9.5 Ma and a smaller peak at 10.8 Ma. Artola yields a single, dominant peak. Large errors in older ignimbrites may obscure some population trends. Overall, the San Antonio and Artola ignimbrites show nearly simultaneous zircon crystallization records (Fig. 8). The dominant peaks of these eruptions both span a period of about 1.5 Ma.

The first major pulse of ignimbrite activity (as defined by Salisbury et al., 2010) includes the Vilama ignimbrite erupted from the Vilama caldera on the eastern edge of the APVC and the Sifon ignimbrite likely erupted from a western caldera source. The Vilama contains a single peak while Sifon shows some small inflections and irregularities. Both ignimbrites contain antecrysts that correlate with the Artola and San Antonio peaks (Fig. 8). The PDF peaks of both age spectra overlap almost entirely and span ~1.3 Ma. Eruption ages overlap within error.

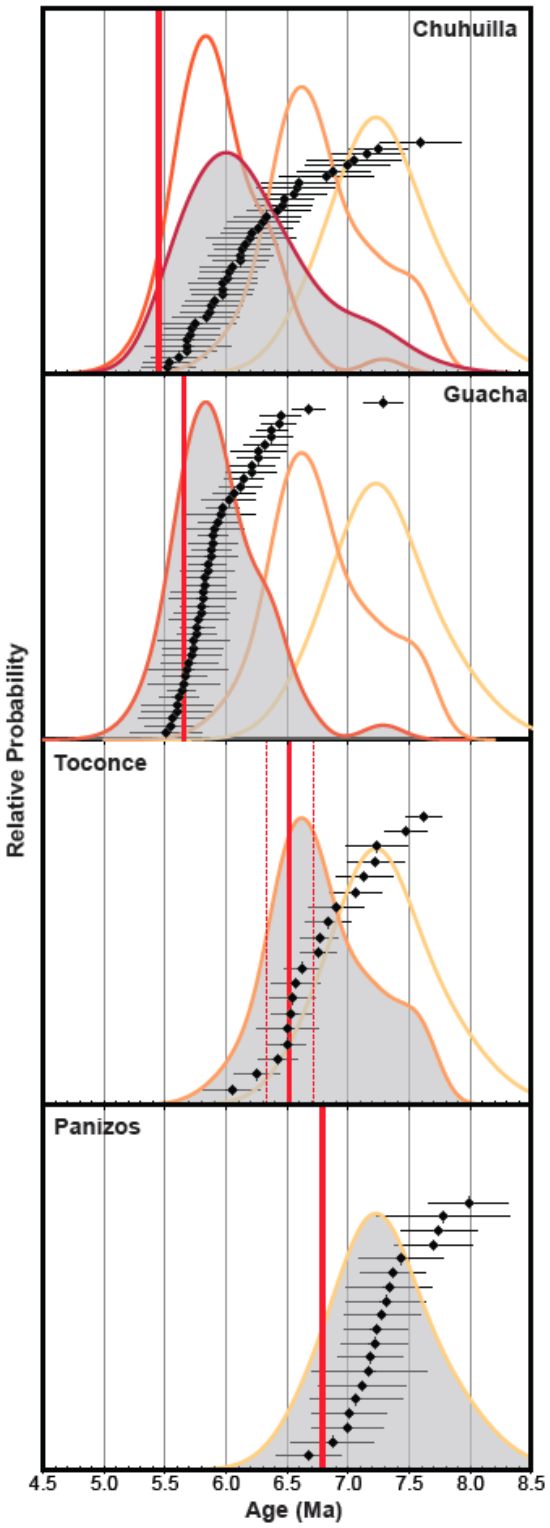

Figure 9. ROP and PDF curves for ignimbrites erupted between 8 – 5.5 Ma. Ignimbrites are arranged oldest to youngest from bottom to top, with PDF curves from previous eruptions for reference. Shaded PDF curve represents the distribution for the ROP displayed. Red lines represent eruption ages with errors for each ignimbrite.

8 – 5.5 Ma

The second period of overlapping age spectra from ~8 to 5.5 Ma includes zircon ages from the Panizos, Toconce, Guacha, and Chuhuilla ignimbrites (Figs. 4, 9). There is no significant overlap in zircon ages between the youngest zircon crystals from Sifon and Vilama ignimbrites of the preceding period and the oldest antecrysts from the next youngest ignimbrite, the Panizos ignimbrite. The second period of continuous zircon crystallization lasts from the onset of Panizos crystallization at ~8 Ma until the eruption of the Chuhuilla ignimbrite at ~5.45 Ma.

The Panizos age spectrum defines a single peak spanning ~1.5 Ma. Several younger ignimbrites have zircon ages that correlate with Panizos. This can be seen in Figure 9: an antecrystic peak from Guacha lies within the spread of the Panizos PDF and inflections off the prominent peaks in both Chuhuilla and Toconce correlate well with the Panizos peak. Isolated zircon ages from Pastos Grandes and Puripicar overlap with Panizos zircon ages.

The Guacha PDF curve consists of a dominant peak with a slight inflection at ~6.3 Ma represented by a kink in the slope of the rank order plot of zircon ages (Fig. 9). This correlates best with Chuhuilla zircon ages. The Guacha peak spans ~1 Ma.

The spread of the Chuhuilla PDF is noticeably wider than the other ignimbrites in this period, spanning almost 2 Ma (Fig. 9). Rank order plots show a slight stepped pattern compared to the continuous slopes seen in Guacha and Panizos. The oldest

Chuhuilla zircons sit well within the range of Panizos ages while the youngest overlap with the youngest Guacha zircons, suggesting that Chuhuilla zircons record crystallization over nearly the entire span of the second period.

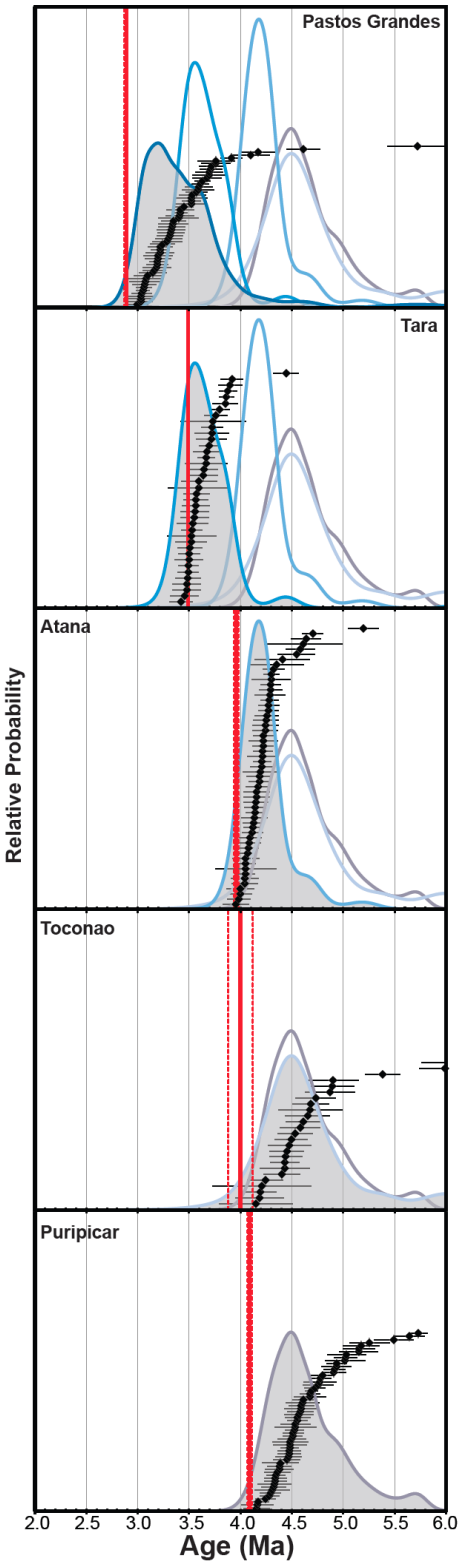

Figure 10. ROP and PDF curves for ignimbrites erupted between 5.2 – 2.9 Ma. Ignimbrites are arranged oldest to youngest from bottom to top, with PDF curves from previous eruptions for reference. Shaded PDF curve represents the distribution for the ROP displayed. Red lines represent eruption ages with errors for each ignimbrite.

5.2 – 2.9 Ma

The third period of overlapping age spectra includes the Puripicar, Toconao, Atana, Tara, and Pastos Grandes ignimbrites (Figs. 4, 10). A few isolated zircon ages from Puripicar and Toconao overlap in age with the zircon histories from Chuhuilla and Guacha in the preceding period, but the bulk of the age spectra that comprise the PDF peaks do not overlap. Zircon crystallization over this period begins at ~5.2 Ma and continues until the Pastos Grandes eruption at 2.89 Ma.

The Puripicar and Toconao zircon spectra overlap considerably and have eruption ages that overlap within error (Fig. 10). Both span ~1 Ma histories. While Toconao has a uniform peak, the Puripicar PDF shows some irregularities in the peak that do not correlate with any other zircon populations.

The Atana ignimbrite zircon age spectrum is the narrowest in the APVC, spanning only ~500 ka (Fig. 10). The small peak consisting of 5 zircon ages older than the dominant peak in the Atana ignimbrite overlaps well with the Toconao and Puripicar ages.

There is very little overlap between the age spectra from the Pastos Grandes and Tara ignimbrites and the Atana age spectrum (Fig. 10). The Pastos Grandes PDF defines a very irregular peak. Zircon ages comprising the inflection at approximately 3.6 Ma in the Pastos Grandes peak overlap with the dominant peak of

the Tara eruption. The Tara peak is largely uniform and covers a ~600 ka zircon history while the Pastos Grandes peak spans close to 1 Ma.

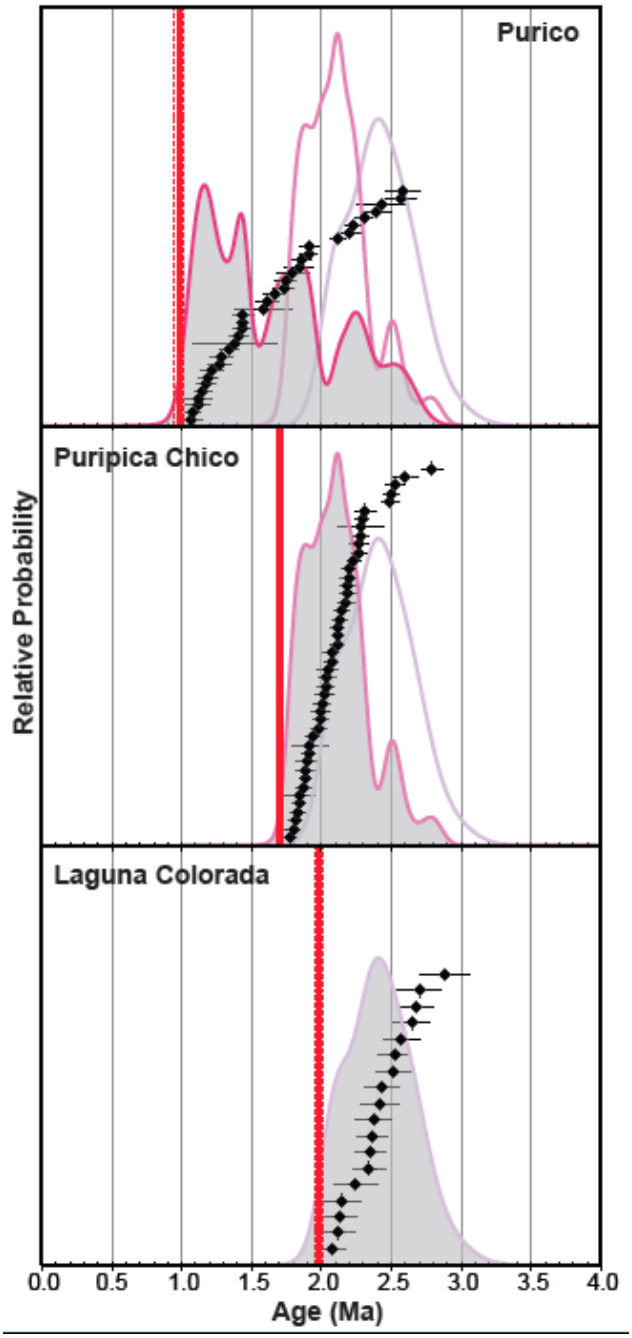

Figure 11. ROP and PDF curves for ignimbrites erupted between 2.7 – 1.0 Ma. Ignimbrites are arranged oldest to youngest from bottom to top, with PDF curves from previous eruptions for reference. Shaded PDF curve represents the distribution for the ROP displayed. Red lines represent eruption ages with errors for each ignimbrite.

2.7 – 1.0 Ma

The final period of overlapping age spectra consists of the Laguna Colorada, Puripica Chico, and Purico ignimbrites (Figs. 4, 11). Zircon ages are continuous between ~2.7 Ma until the eruption of the Purico ignimbrite at 0.98 Ma. The oldest zircon age from the Laguna Colorada ignimbrite overlaps within error of the Pastos Grandes eruption age. Laguna Colorada consists of a slightly irregular peak spanning ~ 1 Ma with no minor peaks. Purico and Puripica Chico both contain minor peaks consisting of multiple zircon ages that overlap the Laguna Colorada age spectrum. Puripica Chico peak ages span approximately 500 ka. The Purico ignimbrite is the only APVC ignimbrite that does not have a single dominant pre-eruption peak. Instead, Purico contains three distinct zircon age populations, the oldest of which overlaps significantly with the Laguna Colorada age distribution. Overall, Purico contains a nearly continuous zircon record extending over 1.5 Ma.

5.0 Discussion

5.1 Zircon Populations and Trends

Previous studies investigating zircon age distributions commonly identify three distinct population types: 1) zircon autocrysts that crystallize in the eruptible magma, 2) zircon antecrysts older episodes of magma formation, and 3) zircon

xenocrysts yielding significantly older ages thought to be incorporated from the country rock surrounding a magma chamber (Fig. 12). All three populations are identifiable in the zircon age distributions from APVC ignimbrites.

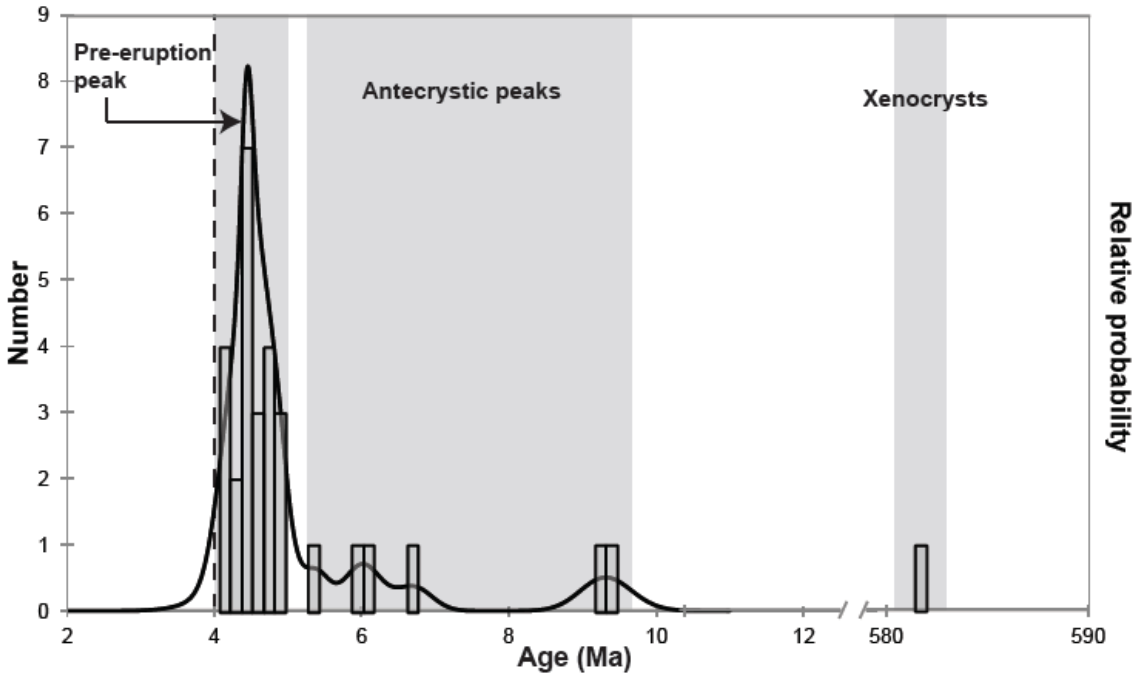

Figure 12. Example PDF curve and histogram of the Toconao ignimbrite illustrating different zircon populations seen in APVC ignimbrites. Dashed line is $^{40}Ar/^{39}Ar$ eruption age.

5.1.1 Xenocrysts

Zircon xenocrysts are represented by ages that fall outside of the 1-12 Ma APVC age range (Fig. 5). Most ignimbrites yielded a single xenocryst age; however, this may be due to biases in spot selection where we avoided analyzing highly irregular cores. Only the Panizos and San Antonio ignimbrites from the eastern edge of the APVC

yielded multiple zircon xenocrysts, with the Panizos xenocryst population comprising almost half of the analyses from that sample. The ages of zircon xenocrysts include a small early-Miocene population, a range of xenocrysts spanning the Phanerozoic, and a single Precambrian xenocryst (Fig. 5.).

5.1.2 Antecrysts

The term antecryst lacks a clear temporal definition in zircon age spectra (Schmitt 2011), but antecrystic zircons are usually interpreted as older populations that frequently define smaller peaks relative to the dominant pre-eruption peak in zircon ages (Charlier 2005; Walker et al. 2010). Older populations of zircons defined by smaller peaks are distinguishable in APVC ignimbrites (Fig. 12), and these can be considered antecrystic in origin based on their distinction from the bulk of zircon crystallization ages.

Resolving antecryst and autocryst populations within the dominant peaks in zircon age density preceding eruption is more difficult. Many of the zircon peaks contain inflections that can be associated with zircon histories from previous eruptions (Fig. 8-11). One excellent example of this is the inflection in the peak off the Pastos Grandes ignimbrite PDF at ~3.6 Ma that correlates with the peak in zircon crystallization within the older Tara ignimbrite (Fig. 10). Pastos Grandes and Tara erupt from two distinct caldera centers separated by ~115 km, therefore it is highly unlikely that the Tara-aged Pastos Grandes zircons are inherited from the Tara

magma system after eruption. However, because these zircon crystals overlap within age from another major eruption in the APVC, they can be considered antecrystic on a regional scale to the rest of the Pastos Grandes zircon population.

5.1.3 Autocrysts

Once zircon antecrysts have been teased out of the zircon population by either considerable offset from the primary peak in zircon ages or by association with other pulses of magmatic activity feeding ignimbrite eruptions in the APVC, the remaining zircons define the autocryst population. The autocryst populations define the peaks in zircon age density and consist of zircon ages that overlap at <1σ. In most cases, zircon ages define a continuous sequence and are normally distributed (i.e. Tara, Atana); however, in some ignimbrites the autocryst population exhibits a stepped behavior (i.e. Pastos Grandes, Sifon). Distinguishing between these distinct types of autocryst peaks will be discussed in section 5.4.

5.1.4 Population trends

Zircon age spectra become more complex with time in the APVC (Fig. 4). Younger ignimbrites (i.e. Pastos Grandes, Puripica Chico) contain more evidence for antecrystic zircons associated with zircon age spectra from preceding eruptions than older ignimbrites (i.e. Vilama, Panizos). Older zircon populations have larger errors averaging ~0.2 - 0.3 Ma, which can hide subtleties in zircon age differences while small errors (~0.05 - 0.15 Ma) in young zircon populations allow for PDF

curves to exhibit multiple peaks. It is notable, however, that older age spectra lack the isolated zircon ages found in younger age spectra.

The change in zircon populations over the history of the APVC likely reflects the development of a vast plutonic system in the shallow crust (~4 - 8 km; de Silva & Gosnold 2007). Each eruption is associated with an increment of intrusion into the shallow crust from the APMB. While much of the pluton is likely erupted, the presence of zircon antecrysts suggests that some fraction of the erupted magma remains behind. Younger ignimbrites contain more antecrysts because the upper crustal magmas feeding these eruptions are emplaced in a mature plutonic system.

5.2 Zircon Inheritance and Contemporaneous Crystallization

Inheritance of antecrystic zircons from the remnant magma left behind by previous eruptions is frequently observed in studies assessing the magmatic development of a volcanic system (Charlier 2005; Bacon & Lowenstern 2005; Walker et al. 2010; Folkes et al. 2011). In these examples, younger eruptions incorporate zircon crystals left over from a previous eruptive cycle from the same system. Inheritance is identified by correlating portions of age spectra of an eruption to age spectra of older eruptions.

While the presence of "inherited" zircon suggest that APVC magmas collect zircon left behind from previous eruptions, it is important to note the scale over which these centers are distributed. Contemporaneous ignimbrites erupted from calderas

separated by >100 km show more overlap in zircon age spectra than ignimbrites erupted several million years apart from the same caldera. The overlap of age spectra and contemporaneous zircon crystallization in magmas separated by > 100 km must be attributed to processes other than true "inheritance" of leftover zircon crystals.

5.2.1 Evidence for true inheritance of zircon

Three multicyclic caldera systems in the APVC—the Guacha, Pastos Grandes, and La Pacana calderas—provide the best insight into similarities in zircon age spectra between geographically related eruptions. Ignimbrites erupted from multicyclic caldera centers like these are most likely to show evidence for inheritance of zircon antecrysts leftover from previous eruptions.

The Guacha system produced the 5.65 ± 0.01 Ma Guacha ignimbrite and the 3.49 ± 0.01 Ma Tara ignimbrite. The Tara ignimbrite yielded a single zircon interior age of 6.27 ± 0.16 Ma that overlaps with the Guacha zircon age spectrum (Fig. 4). Pastos Grandes >100km to the northwest of Guacha erupted the 5.45 ± 0.02 Ma Chuhuilla ignimbrite and the 2.89 ± 0.01 Ma Pastos Grandes ignimbrite. Similar to the Guacha eruptions, the Pastos Grandes age spectrum contains a single interior age of 5.72 ± 0.29 Ma that overlaps with the Chuhuilla age spectrum. To the south of Guacha, the La Pacana center produced the 5.6 ± 0.2 Ma Pujsa ignimbrite, which was not analyzed in this study, and two younger eruptions—the 4.0 ± 0.12 Ma Toconao and the 3.96 ± 0.02 Ma Atana ignimbrite. Atana and Toconao yield 4 older zircon ages

between 5.2 ± 0.15 and 6.02 ± 0.25 Ma that could correlate with Pujsa; however, analysis of Pujsa zircons is needed to confirm this.

The lack of strong relationship in the crystallization histories between eruptions separated by several million years has multiple possible interpretations. It is possible that the older eruptions left behind very little in the plutonic system that could be incorporated into later eruptions. Later intrusions of zircon undersaturated magmas may also have dissolved the majority of zircons from older eruptions. Finally, because of sampling biases in which rims were preferentially measured over interiors, it may be that older interiors that reflect earlier periods of zircon crystallization in these systems were simply not analyzed.

The Toconao and Atana ignimbrites erupted within <100 ka of each other contain evidence for true inheritance and connectivity within a single center. Toconao is interpreted to be the silicic cap of the Atana magma (Lindsay, Schmitt & Trumbull 2001b). The Toconao zircon age spectrum shows a peak in zircon age density at ~4.5 Ma (Fig. 10, Toconao). This is defined by a strongly overlapping group of 13 zircon ages ranging from ~4.4 to 4.7 Ma. A small, subpopulation of 5 zircon ages is offset and slightly younger than the main group, ranging from ~4.15 to 4.25 Ma. The peak of the Atana age spectrum is defined by a series of strongly overlapping ages from eruption at 3.96 Ma to ~4.4 Ma (Figure 10, Atana). This overlaps well with the younger population of Toconao zircons. A smaller, slightly older Atana antecryst peak lies between 4.5 and 4.7 Ma, which overlaps significantly with the

older group of Toconao peak ages. The relationship between Atana and Toconao zircon crystallization histories suggests some level of shared zircon crystallization between Atana and Toconao, which likely approximates true inheritance given previous evidence for genetic relationship based on the work of Lindsay (2001a). This relationship is likely stronger than eruptions from other multicyclic calderas due to the temporal proximity between the Atana and Toconao eruptions.

5.2.2 Contemporaneous crystallization of magmas

Evidence for inheritance at multicyclic calderas is sparse in eruptions separated by long time spans (>1 Ma); however, there is evidence for contemporaneous zircon crystallization at centers separated by large distances (50 to 200 km). PDF curves from the Pastos Grandes and Tara eruptions—two successive large eruptions that occurred within 600 ka of each other but from calderas separated by over 100 km—overlap significantly, as do the PDF curves from the successive Guacha and Chuhuilla ignimbrites that erupted within about 200 ka of each other. This suggests that the magma systems of temporally related eruptions evolve contemporaneously to a point, at which one erupts while the other continues to develop.

In some cases, zircon age spectra overlap entirely, suggesting contemporaneous crystallization throughout the entire history of these magma systems. A statistical comparison known as a Kolomogorov-Smirnov (KS) test can be applied to quantitatively determine whether zircon populations comprising the overlapping age spectra come from the same distribution (Press et al. 1988). The KS test

measures the maximum distance between the cumulative probability function of two populations to determine the probability (P) that the populations come from the same distribution, with the null hypothesis being that they do come from the same distribution. The null hypothesis is confirmed if P>0.05.

Ignimbrites	Probability (P)
Artola – San Antonio	0.715
Vilama – Sifon	0.213
Chuhuilla – Panizos, Toconce, Guacha	0.242
Puripicar – Toconao	0.779

Table 2. Summary of KS statistics for contemporaneous zircon age spectra.

Comparing the distributions of the zircon ages comprising the prominent peaks using a KS test yields a high probability of relationship (P = 0.715) between Artola and San Antonio (Table 2, Fig. 8), two of the oldest ignimbrite eruptions in the APVC, suggesting that the magmatic development of these systems is contemporaneous, despite the fact that their sources are > 100 km apart (Fig. 3).

The first major pulse of ignimbrite activity (de Silva & Gosnold, 2007; Salisbury et al., 2010) includes the Vilama ignimbrite erupted from the Vilama caldera on the eastern edge of the APVC and the Sifon ignimbrite likely erupted from a western caldera source (Fig. 3). Both ignimbrites contain antecrysts that correlate with the

Artola and San Antonio peaks (Fig. 8). Autocryst populations comprising the prominent peaks from Sifon and Vilama are statistically indistinguishable (P = 0.213), again suggesting connectivity despite the distance between the two sources separated by >100 km.

The Chuhuilla ignimbrite contains a very broad zircon age spectrum that appears to correlate with three other ignimbrites from ~8 to 5.5 Ma (Fig. 9). A KS test comparing the Chuhuilla zircon distribution to the combined zircon distributions from Guacha, Toconce, and Panizos yields a high probability of relationship at P = 0.242. This suggests the plutonic development of Chuhuilla coincides with the magmatic development of at minimum three different ignimbrites erupted from separate centers over 2 Ma. The distance between each of these centers spans nearly the entire spatial distribution of the APVC (Fig.3). Panizos is the eastern-most eruption in the APVC. Toconce erupted from a buried source on the western edge. The Guacha caldera is located to the south, while Chuhuilla erupted from the northernmost caldera.

A KS test also shows a very high probability of fit (P = 0.779) between the Puripicar and Toconao zircon crystallization histories, suggesting that they developed contemporaneously (Fig. 10). Toconao erupted from the La Pacana caldera to the south while Puripicar erupted from a center ~50 km away (Fig. 3).

Qualitative peak matching also suggests contemporaneous zircon crystallization for portions of age spectra for temporally related eruptions. The onset of continuous zircon crystallization in both the Pastos Grandes and Tara ignimbrites overlaps within error at ~3.8 Ma (Fig. 10). Both ignimbrites have shared zircon crystallization histories until the Tara eruption at 3.49 Ma. Zircon crystallization continued at Pastos Grandes until eruption at 2.89 Ma.

The earliest crystallization in both the Puripica Chico and Purico magma systems overlaps with the peak of Laguna Colorada zircon crystallization (Fig. 11). About 70% of the Puripica Chico peak zircon ages overlap with the Laguna Colorada peak. Purico contains a population of 8 zircon ages that overlap entirely with the Laguna Colorada peak. It also contains ~7 zircon ages that overlap with the youngest Puripica Chico zircon ages. These youngest ignimbrite eruptions occur within ~75 km of each other (Fig. 4).

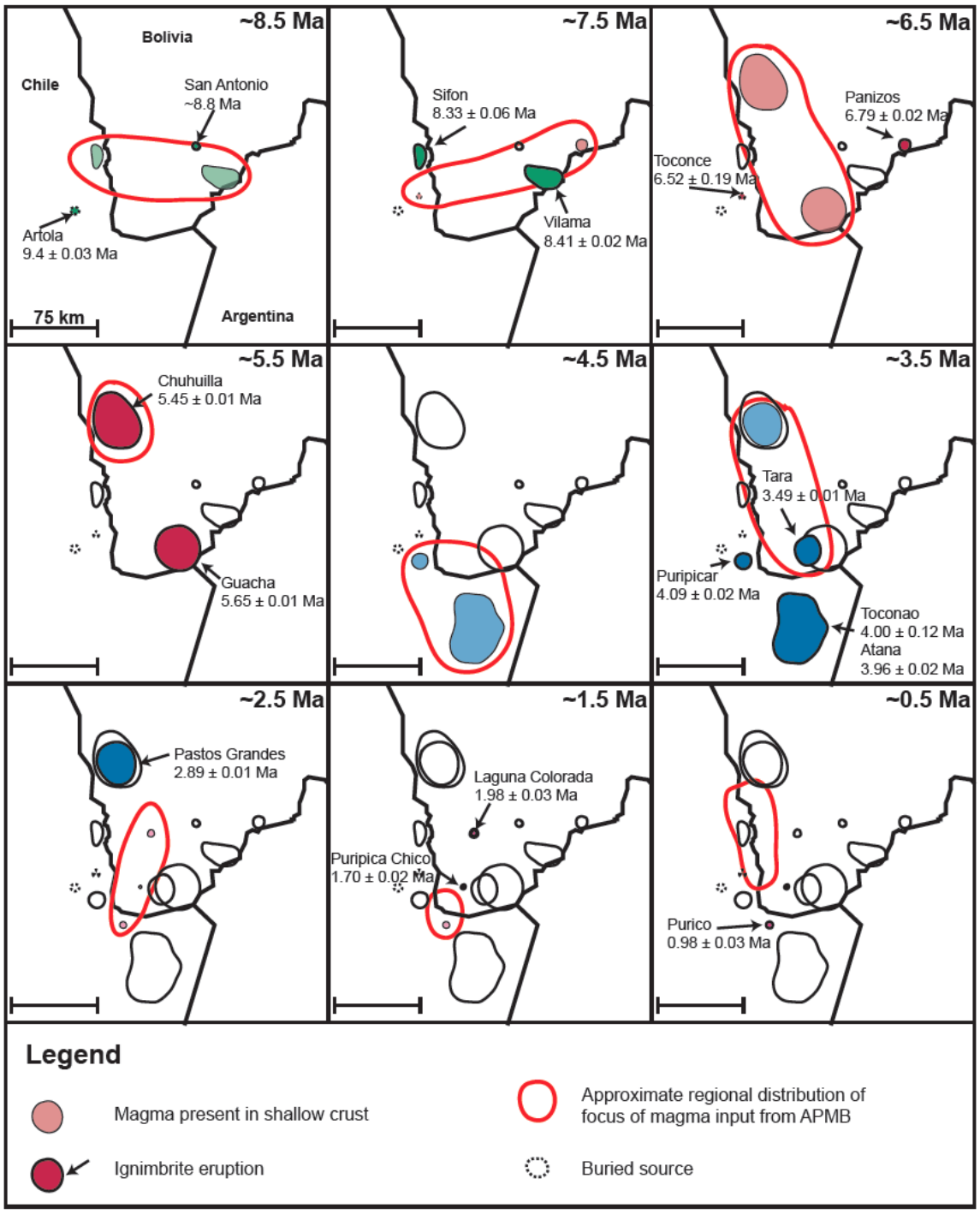
~8.5 Ma
Bolivia
Chile
San Antonio
~8.8 Ma
Artola
9.4 ± 0.03 Ma
75 km
Argentina
~7.5 Ma
Sifon
8.33 ± 0.06 Ma
Vilama
8.41 ± 0.02 Ma
~6.5 Ma
Panizos
6.79 ± 0.02 Ma
Toconce
6.52 ± 0.19 Ma
~5.5 Ma
Chuhuilla
5.45 ± 0.01 Ma
Guacha
5.65 ± 0.01 Ma
~4.5 Ma
~3.5 Ma
Tara
3.49 ± 0.01 Ma
Puripicar
4.09 ± 0.02 Ma
Toconao
4.00 ± 0.12 Ma
Atana
3.96 ± 0.02 Ma
~2.5 Ma
Pastos Grandes
2.89 ± 0.01 Ma
~1.5 Ma
Laguna Colorada
1.98 ± 0.03 Ma
Puripica Chico
1.70 ± 0.02 Ma
~0.5 Ma
Purico
0.98 ± 0.03 Ma
Legend
Magma present in shallow crust
Ignimbrite eruption
Approximate regional distribution of focus of magma input from APMB
Buried source

Figure 13. Spatiotemporal development of APVC magma systems. Each frame represents a single time slice separated by 1 Ma. Colored circles represent the approximate distribution of the sub-volcanic batholith as estimated by the location and approximate size of the collapse structure (de Silva & Gosnold 2007). Magma presence in the sub-volcanic system is indicated by the presence of zircon crystals at each time slice. Eruptions occurring between successive time slices are indicated by bold colors and arrows, with the eruption age given. The red line approximates the distribution of the focus of magma input from the APMB at each time slice.

Figure 13 explores the spatiotemporal development of APVC magmatic systems at increments of 1 Ma on both the surface and at the subsurface scale. Up until ~4.5 Ma, ignimbrites developed and erupted in pairs, usually on opposite sides of the APVC. After ~4.5, ignimbrite development and activity was more localized to the south around the La Pacana and Guacha calderas. The youngest eruptions show a centralization of magmatic activity.

The contemporaneous crystallization histories of APVC eruptive centers separated by > 100km suggest a significant level of temporal as opposed to geographic connectivity. While it is highly unlikely that magmas are connected at shallow levels (between 4-8 km) due to the immense scale of the APVC, it is very probably that separate systems are connected at a deeper level, likely at the partially molten Altiplano-Puna Magma Body sitting at ~20 km depth. The APMB presently underlying much of the APVC is considered to be the source of the magmas in the shallow crustal chambers that the feed APVC eruptions (de Silva & Gosnold 2007). The extent of overlap of zircon age spectra suggests that shallow crustal magma reservoirs separated by 10s to 100s of km are experiencing simultaneous thermal or material input from deeper levels. In this model, the addition of mafic material

into the APMB triggers output into the shallow crust, where the magma stalls in a staging area. With each successive input of material into the APMB, magma continues to accumulate in the shallow crust and each coexisting magma chamber records the same zircon history. Magmas either erupt nearly synchronously, as in the case of the Vilama and Sifon ignimbrites, or share a common history up until one erupts while the other continues to crystallize as observed in the Tara and Pastos Grandes zircon crystallization histories.

The red line in Figure 13 traces the potential evolution of the APMB over the history of the APVC. Early on in the APVC, including during the first pulse of the ignimbrite flare-up, the focus of activity is oriented more or less east-west. At about 6.5 million years during the development of the Chuhuilla and Guacha magma systems, activity rotates to a northwestern trend. This trend largely governs the remainder of the flare-up, although activity becomes more centralized around the Guacha caldera. The small, recent eruptions after ~2.5 Ma show more of a northeastern alignment.

5.3 Zircon Crystallization Times

Several different approaches have been used to constrain magma residence times for individual systems. Many studies take the entire spectra of overlapping zircon ages as the residence time (Brown & Fletcher 1999; Brown & Smith 2004; Bachmann et al. 2007b). However, other studies have observed that this approach does not distinguish autocrystic zircons from antecrystic zircon populations that

may represent solidified portions of the magma chamber and opt for constraining residence times to the mean of the youngest distinguishable zircon age peaks (Charlier 2005).

In the APVC, zircon age spectra reveal broadly unimodal peaks with only minor inflections and smaller peaks (Fig. 4). The peak of the PDF curves approximate the time period where zircon ages overlap strongly with no significant age gaps >1σ. This represents a time period over which zircon is continuously crystallizing in the system. The presence of older rim ages (Fig. 6) suggests that solidified magmas may be incorporated at eruption. Additionally, the peaks include "antecrysts" that can be temporally linked to prior APVC eruptions. These antecrysts, however, do not represent residuum from prior eruptions because of the large distances that separate individual eruptive centers. Therefore, APVC antecrysts with ages that overlap strongly with the autocryst population are likely significant to the timescales of magma development prior to eruption, even if older ages may represent solidified portions of the system.

The best estimate for the duration of magma that accumulates in the shallow crust prior to the eruption of each of ignimbrite is the distribution of the pre-eruption peak in the PDF distribution. This timespan is more aptly called the zircon crystallization time than the residence time for several reasons. First of all, it likely includes zircon ages from solidified portions of the magma chamber that are incorporated into subsequent melts, as suggested by rim ages as old or older than

some interior ages. Second of all, zircons record the time at which magma cooled below zircon saturation temperature and began to crystallize and not necessarily the time at which the magma formed. Thus, zircons ages yield a minimum age of a magma.

Zircon crystallization times were determined for each ignimbrite by identifying the oldest zircon in the overlapping zircon age spectra and subtracting the $^{40}Ar/^{39}Ar$ eruption age from the zircon age (Fig. 14). In cases where the biotite age is questionable, the youngest zircon ages were used instead as the eruption age. Ignimbrites with n > 30 likely yield the best estimate of magma accumulation times, although ignimbrites with lower n values provide first order estimates.

Zircon crystallization times are summarized in Table 3. Overall, data yield protracted zircon crystallization times averaging ~630 ka, although they range from ~400 ka to >1000 ka. Even the shortest timescales are longer than most previously reported residence times (see review by: Costa 2008). Weighted mean ages represent the most common crystallization age and likely bear little significance (Bachmann et al. 2007b). Only 6 out of 16 zircon crystallization times yield MSWD values that fall within the 95% confidence interval for the given n value that suggests the mean is consistent with analytical uncertainty. Most indicate excess scatter, although the Artola ignimbrite yields a low MSWD that suggests error is underestimated. High MSWD values are consistent with protracted crystallization governing APVC ignimbrites.

Ignimbrite	Eruption Age (Ma)	Oldest Peak Zircon Age (Ma)	Weighted Mean of Peak (Ma)	MSWD	N	Zircon Residence Times (ka)
Purico	0.98 ± .03	1.44 ± .08	1.27 ± .08	**4.4**	16	460 ± 85
Puripica Chico	1.70 ± .02	2.31 ± .07	2.05 ± .05	**7.4**	40	610 ± 73
Laguna Colorada	1.98 ± .03	2.88 ± .18	2.38 ± .11	**3.1**	18	900 ± 180
Pastos Grandes	2.89 ± .01	3.76 ± .18	3.33 ± .07	**4.2**	51	870 ± 180
Tara	3.49 ± .01	3.92 ± .11	3.65 ± .05	**1.6**	38	430 ± 110
Atana	3.96 ± .02	4.41 ± .26	4.17 ± .03	0.77	49	450 ± 260
Toconao	4.00 ± .12	4.90 ± .25	4.50 ± .08	1.07	22	900 ± 280
Puripicar	4.09 ± .02	4.80 ± .11	4.49 ± .05	**2.2**	45	710 ± 110
Chuhuilla	5.45 ± .02	6.59 ± .30	6.01 ± .11	1.5	34	1140 ± 300
Guacha	5.65 ± .01	6.44 ± .16	5.95 ± .08	**2.1**	46	790 ± 160
Toconce	6.52 ± .19	7.23 ± .25	6.67 ± .15	**2.4**	17	710 ± 310
Panizos	6.79 ± .02	7.43 ± .34	7.15 ± .16	0.47	15	640 ± 340
Sifon	8.33 ± .06	9.07 ± .25	8.67 ± .07	**1.6**	40	740 ± 260
Vilama	8.41 ± .02	9.20 ± .33	8.78 ± .12	0.76	29	790 ± 330
Artola	~9.2	10.2 ± .60	9.59 ± .18	**0.3**	29	1000 ± 880
San Antonio	~9.1	10.1 ± .30	9.53 ± .16	0.83	25	1000 ± 300

Table 3. Summary of calculated zircon residence times. Eruption ages compiled in Salisbury et al. (2011). The oldest peak zircon age represents the oldest zircon comprising the peak of the PDF curve for each ignimbrite. Bolded MSWD values fall outside the accepted 95% confidence interval.

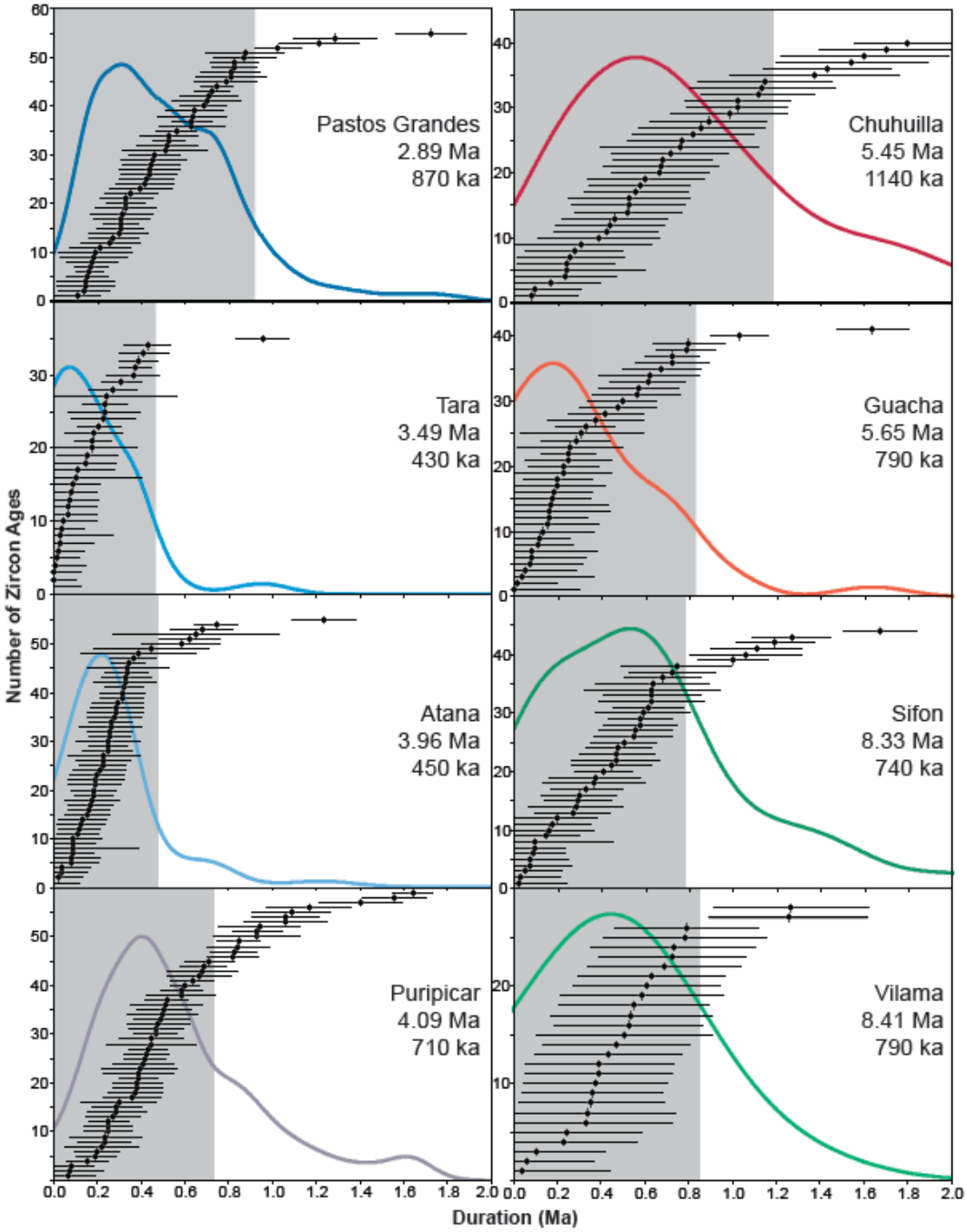
Pastos Grandes
2.89 Ma
870 ka
Chuhuilla
5.45 Ma
1140 ka
Tara
3.49 Ma
430 ka
Guacha
5.65 Ma
790 ka
Atana
3.96 Ma
450 ka
Sifon
8.33 Ma
740 ka
Puripicar
4.09 Ma
710 ka
Vilama
8.41 Ma
790 ka
Number of Zircon Ages
Duration (Ma)

Figure 14. Zircon crystallization times for 8 supereruptions in the APVC. Zircon ages and PDF curves are plotted starting at eruption age (x = 0) for each ignimbrite. Text gives ignimbrite name, eruption age, and approximate zircon crystallization time. Gray shaded region indicates the region of the zircon age spectra representing the zircon crystallization time.

There is no correlation between zircon crystallization time and erupted volume (Fig. 15). Other studies have noted that small volume eruptions frequently exhibit more variation in residence times than voluminous eruptions (Simon et al. 2008). While the small volume ignimbrites do show significant variation in zircon crystallization times (~400 – 900 ka), the large volume (<1000 km^3) also show large variability (~400 – 1100 ka). The largest APVC eruption yields among the shortest zircon crystallization time. This suggests that erupted volume is not a strong control on zircon crystallization time and that other factors are likely in play.

There is slight decreasing in zircon crystallization times over the span of the APVC (Fig. 15), although this may be attributed to better precision and thus lower errors in younger zircon populations. It is notable, though, that some of the oldest eruptions have very long accumulation times. This may be attributed to intrusion into colder, less thermally evolved crust than some of the later eruptions.

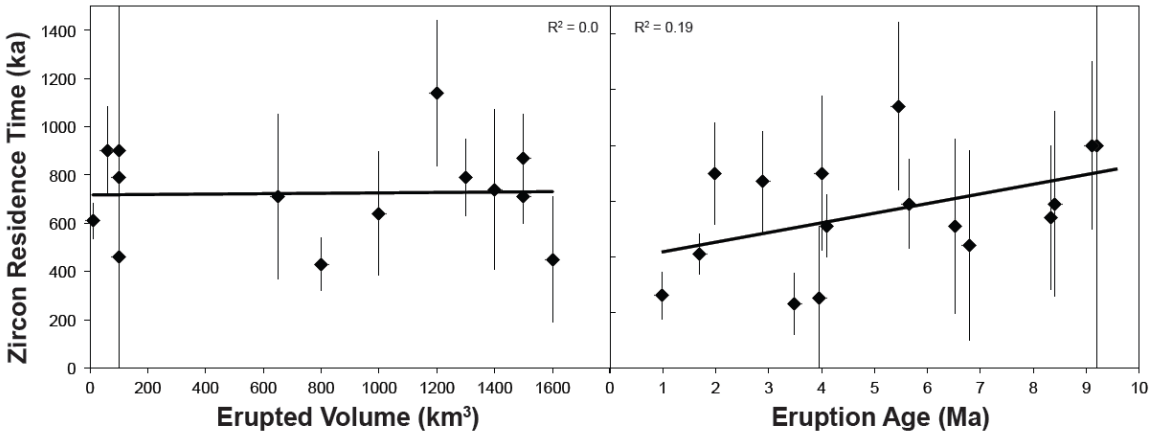

Figure 15. Zircon crystallization times compared to erupted volume and eruption age. Line and reported R^2 value demonstrate virtually nonexistent correlation.

Long zircon crystallization times of ~500 ka to >1 Ma for the APVC are consistent with modeled timescales for the development of large, catastrophic caldera-forming eruptions built by incremental magma supply over time in a thermally primed crust (Jellinek & DePaolo 2003). Previous studies have suggested incremental assembly of large magma chambers in the APVC to explain the volume of material erupted (de Silva & Zandt 2006). Long zircon crystallization times appear to support this model of assembly occurring over long time periods prior to eruption.

While zircon crystallization times provide reasonable estimates for the longevity of a system built by multiple increments of magma intrusion, they do not reflect the residence time of a single magma. In the Tara, Atana, and Guacha age spectra, a statistically significant population subset can be identified within the zircon crystallization time by using probability plots (Fig. 16). Probability plots rank

zircon ages against a normal distribution. Normally distributed ages should define a straight line, while deviations from normality plot off the straight line.

Plotting the zircon age spectra defining the zircon crystallization time for the Guacha, Tara, and Atana ignimbrites on probability plots shows that significant portions of the age spectra for all three ignimbrites are normally distributed (Fig. 16). The Tara ignimbrite contains five older ages identifiable as outliers and 33 that define a straight line. The entire Atana zircon crystallization time spectrum (49 ages) is normally distributed. Guacha contains 13 ages that can be considered outliers and 34 normally distributed ages.

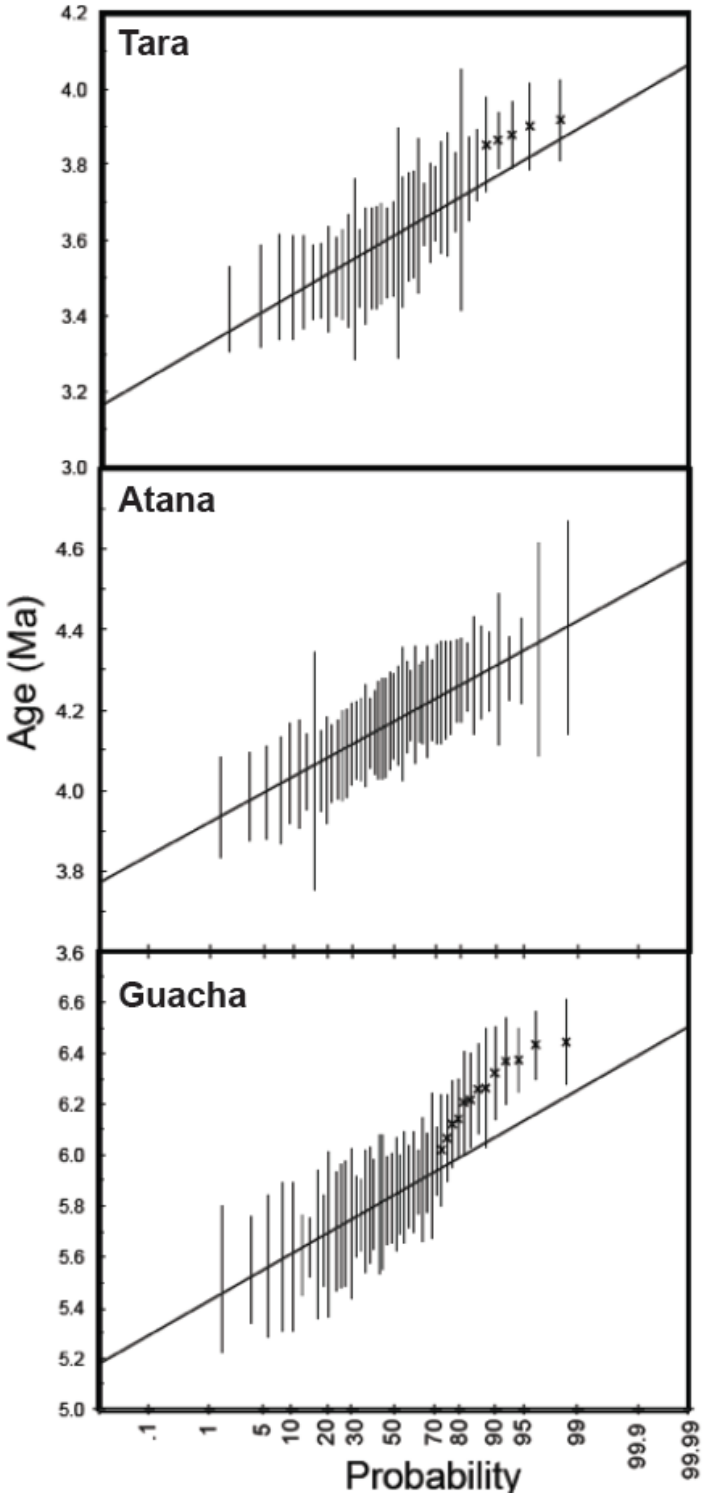
Tara
Atana
Guacha
Age (Ma)
Probability
.1
1
5
10
20
30
50
70
80
90
95
99
99.9
99.99

Figure 16. Probability plots for the Tara, Atana, and Guacha zircon age spectra. Vertical lines represent ranked zircon ages with 1σ errors. Best-fit line plots through normally distributed population, while vertical lines overprinted with "x" are ages that plot outside of the normal population.

Normality can be assessed statistically using a Shapiro-Wilk normality test (Shapiro & Wilk 1965). This test uses the *W* statistic to detect departures from normality for a distribution. A distribution with a high *W* value for a given sample size confirms the null hypothesis that the distribution is normally distributed, while a low value rejects the null hypothesis. Normality is confirmed at the 95% confidence level for the distribution identified from probability plots for all three ignimbrites (Table 4). Additionally, the weighted mean ages of the normal distributions all yield MSWD values approaching unity.

Ignimbrite	**Tara**	**Guacha**	**Atana**
Weighted Population Mean (Ma)	3.59 ± 0.11	5.74 ± 0.14	4.17 ± 0.10
N	33	34	49
W	0.94	0.94	0.97
Hypothesis accepted at 95% confidence level?	Yes	Yes	Yes

Table 4. Population statistics of normally distributed zircon ages for the Tara, Guacha, and Atana ignimbrites. W is the Shapiro-Wilk test statistics

These strongly normal distributions and acceptable MSWD values support interpretation of the distributions as a single population of zircon ages. Normally distributed zircon ages would be expected in a magma cooling through the zircon saturation temperature, with no additional heat input. These values can be considered a better estimate for the true residence time of the magma driving the

eruption of the system as opposed to the longevity of the system. The age spans for the normally distributed populations approach estimates of residence times calculated at other large caldera systems, with residence times of ~310, ~450, and ~280 ka for the Tara, Atana, and Guacha ignimbrite respectively (Fig. 17). If the mean of the distribution is interpreted as the zircon crystallization age of the magma as done in other studies (i.e. Reid et al. 1997), then residence times for Guacha and Tara average ~100 ka while Atana is ~200 ka.

The zircon age distributions of the other supereruptions in this study are not as conducive to determining residence times with this technique. Distributions for the Chuhuilla, Pastos Grandes, Puripicar, and Sifon all exhibit a stepped behavior to the distribution, with no statistically definable, normally distributed sub-population. In some cases (i.e. Chuhuilla, Puripicar), the entire distribution of the zircon crystallization time is normally distributed; however, this is likely more representative of the development of the system as a whole as opposed to a single magma. The Pastos Grandes and Sifon zircon crystallization time spectra are not normally distributed.

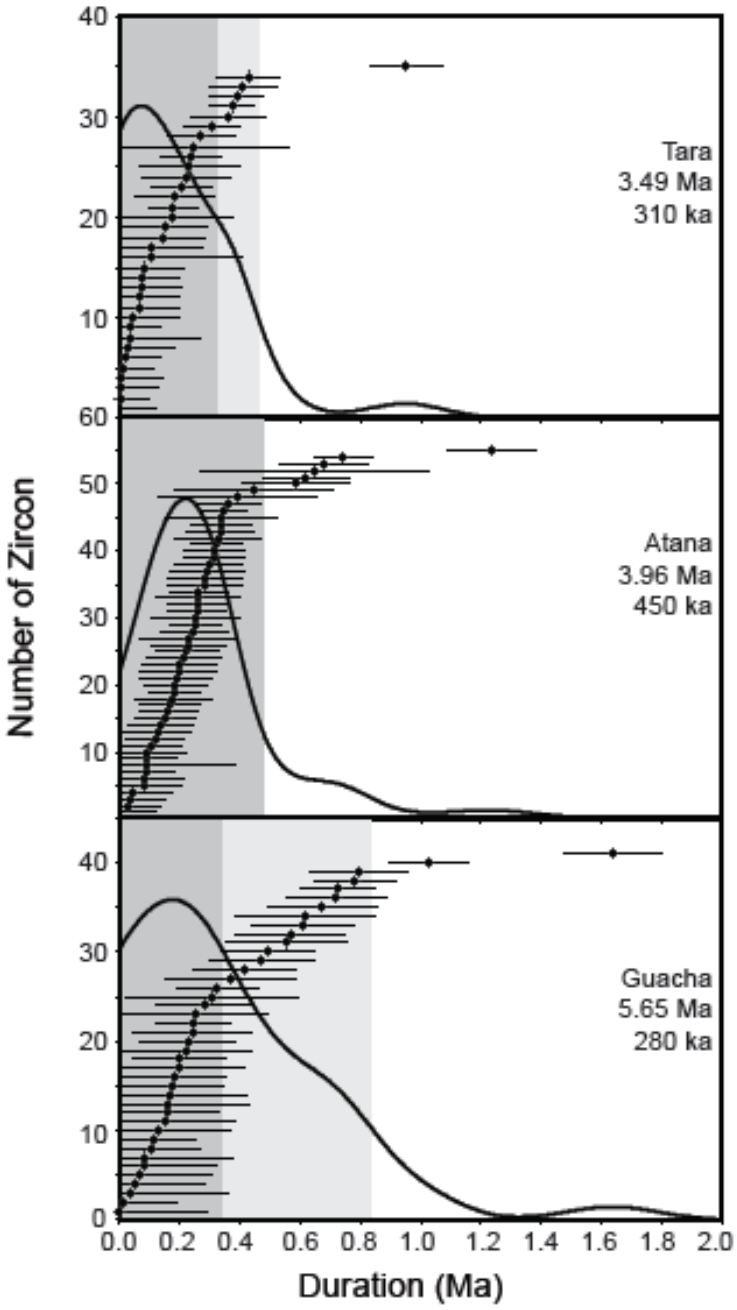

Figure 17. Normally distributed portions of zircon age spectra vs. zircon crystallization time. Dark shaded regions represent portions of age spectra that are normally distributed. Light shaded regions represent zircon crystallization time.

5.4 Contrasting Styles of Magma Development

Considerable variation in the zircon crystallization time among APVC ignimbrites suggests that different processes may govern magma emplacement and crystallization in separate systems. Two end members of zircon crystallization can be identified. The first consists of ignimbrites like Tara and Atana that have relatively homogeneous zircon populations with very clearly defined crystallization peaks, and short zircon crystallization times, and discernable magma residence times. The second includes Pastos Grandes, Chuhuilla, and Sifon type ignimbrites that consist of heterogeneous zircon populations with very broadly distributed peaks yielding long zircon crystallization histories and a characteristic stepped pattern in the zircon populations comprising the peaks (Figs. 8, 9, 10).

Studies have long argued that prolonged zircon crystallization histories in large volcanic systems can best be explained by the presence of large crystal mushes in the shallow crust (Hildreth 1981; Bachmann & Bergantz 2004; Hildreth & Wilson 2007). In this model, zircon crystallization takes place in pods of higher melt fraction material within the crystal mush as the melt cooled through its zircon saturation temperature and eventually solidified. Each melt pod contains its own zircon population that records a unique crystallization history, resulting in protracted zircon crystallization times over the duration of the crystal mush zone (Miller & Wooden 2004; Bachmann et al. 2007c).

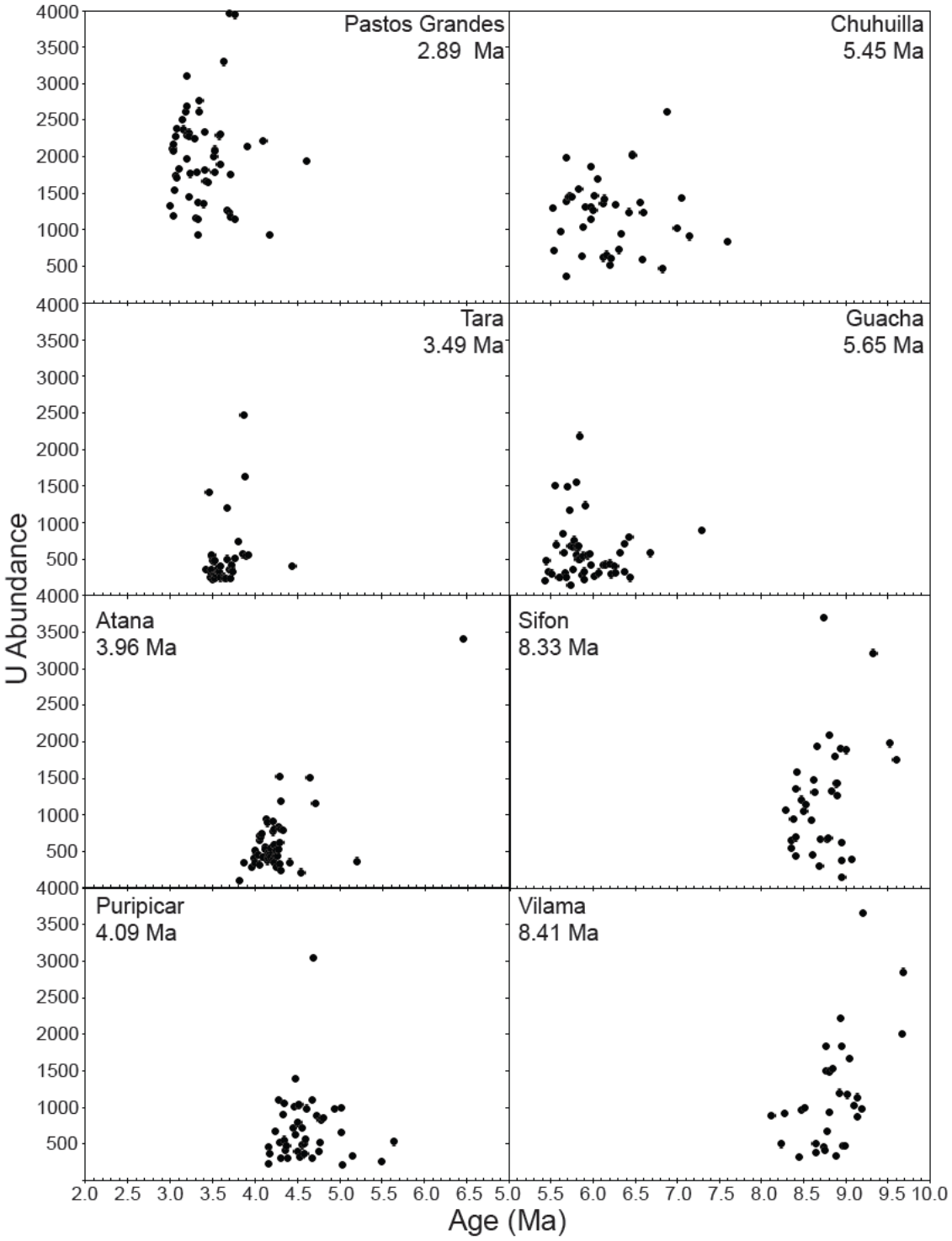
Pastos Grandes
2.89 Ma
Chuhuilla
5.45 Ma
Tara
3.49 Ma
Guacha
5.65 Ma
Atana
3.96 Ma
Sifon
8.33 Ma
Puripicar
4.09 Ma
Vilama
8.41 Ma
U Abundance
Age (Ma)

Figure 18. U abundances in zircon for 8 supereruptions in the APVC. Eruption age as reported in Salisbury et al. (2011) given.

High U and Th concentrations in zircon crystals has been proposed as support for crystal mush models (Miller & Wooden 2004; Storm et al. 2011). U and Th are concentrated in melts with high degrees of fractional crystallization as long as U and Th remain incompatible with the crystalizing phases. The presence of high-U zircons indicate that they formed in very crystalline magma bodies, while low-U zircon crystals likely formed in more melt-rich magmas (Miller & Wooden 2004).

In the APVC, zircon crystals yield a broad range of U abundances, with high variability between ignimbrites (Fig. 18). For example, the Pastos Grandes, Chuhuilla, Sifon, and Vilama ignimbrites all contain highly variable U abundances in zircon ranging from <500 ppm to >3000 ppm. The Tara, Guacha, Atana, and Puripicar ignimbrites have zircon U abundances mostly <1000 ppm.

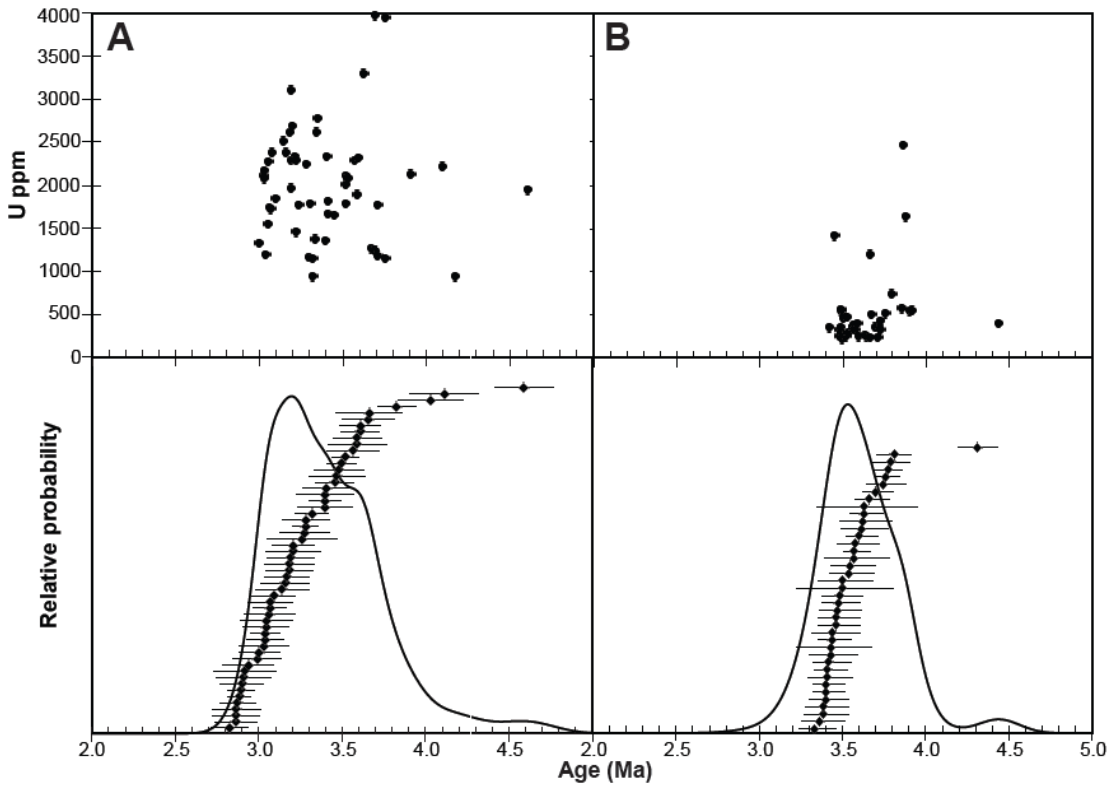

Figure 19. Variations in U abundance compared to the distribution of zircon ages for two ignimbrites. A. The Pastos Grandes ignimbrite shows a stepped zircon age distribution over ~900 ka that correlates with a wide range of U abundance measured in zircon. B. The Tara ignimbrite shows a highly continuous zircon age distribution correlation with a narrow range of U abundance.

The extent of variation in U abundance in zircon correlates well with the pattern of the zircon age populations. Ignimbrites exhibiting heterogeneous zircon populations contain highly variable U concentrations measured in zircon (Fig. 19A). The ignimbrites with homogeneous zircon populations have more concentrated, low U values that likely crystallized in high melt fraction magmas (Fig. 19B).

Zircon saturation temperatures offer further insight into the difference in magma chamber environments. Experimental studies by Watson and Harrison (1983) determined the conditions for zircon saturation in silicic magmas of varying composition determined by the cation ratio [M = (Na + K +2Ca)/(Al*Si)] and zirconium concentration. Applying this thermometer to APVC ignimbrites yields temperatures ranging from ~730 – 815°C (Fig 20). Ignimbrites with very heterogeneous crystal populations (Sifon, Chuhuilla, and Pastos Grandes), yield low saturation temperatures from 750 – 760°C. Ignimbrites with homogeneous zircon populations (Atana, Tara), yield higher zircon saturation temperatures from 785 – 795°C. Higher zircon saturation temperatures promote zircon dissolution and have the potential to obliterate antecrystic zircon crystals while low zircon saturation temperatures are less likely to dissolve incorporated zircons (Watson 1996). This suggests that the ignimbrites with more homogeneous zircon populations may record short zircon residence times because older zircon phenocrysts are dissolved, while heterogeneous zircon populations are the product of low temperature magmas preserving older zircon crystals.

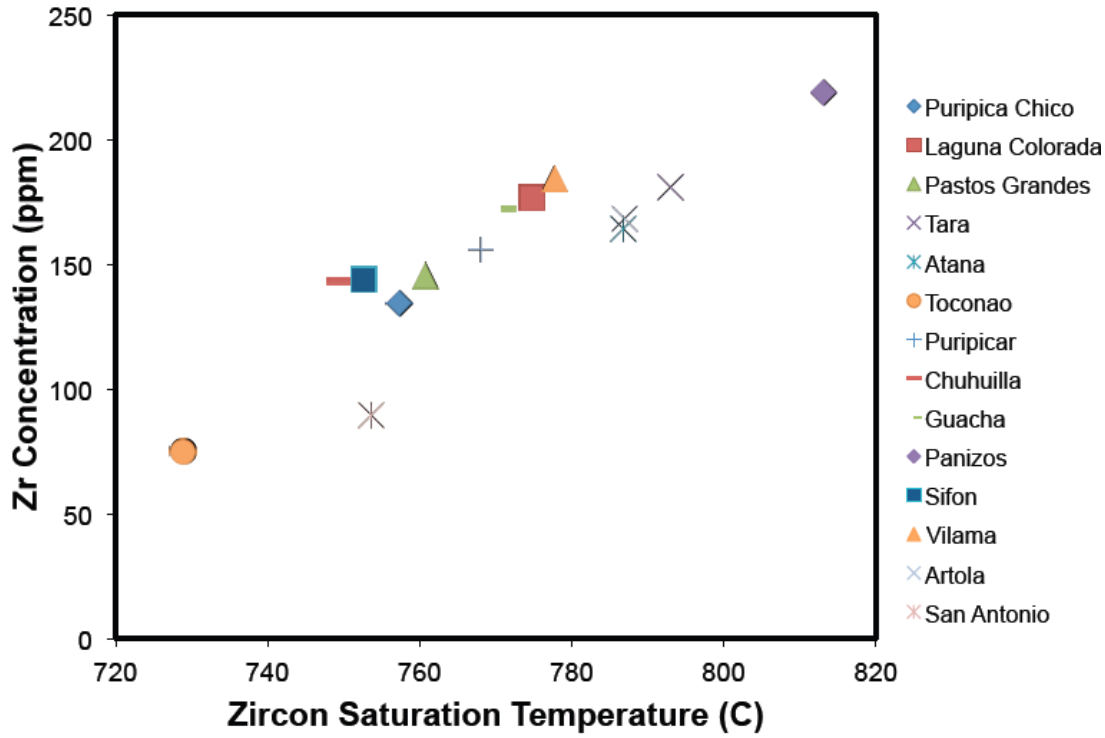

Figure 20. Zircon saturation temperatures for ignimbrites examined in this study calculated based on whole rock pumice samples.

Zircon crystallization times, the pattern of distribution of zircon ages, ranges in U abundances, and zircon saturation temperatures suggest that there are different styles of magma development leading up to ignimbrite eruptions in the APVC. While conditions vary greatly, there appear to be two end members: low melt fraction systems and high melt fraction systems. Low melt fraction systems exhibit strongly heterogeneous zircon populations with highly variable U abundances and low zircon saturation temperatures. Low melt fraction systems are consistent with crystal mush models where melt is segregated from a larger body of crystal mush into

smaller regions or melt pods that record unique crystallization conditions (Fig. 21). Under these conditions, zircon crystallizes in a wide variety of environments within the system, leading to highly variable U abundances in zircon.

High melt fraction systems have short zircon crystallization times, discernable magma residence times, a narrow range of U abundances, and high zircon saturation temperatures. These factors reflect zircon crystallization in a single melt as opposed to multiple melt pockets (Fig 21). The duration of the melt is best estimated based on the magma residence times determined in the previous section. This is further supported by the U abundances. While the normally distributed portion of the Tara zircon spectrum yields very low U-abundances, the slightly older group of 5 zircon ages between 3.85 – 3.92 Ma that are separate from the normally distributed population display slightly more variable U abundances than the bulk population of zircon ages between 3.49 – 3.80 Ma. Three of these ages are interior measurements. This group of zircon ages provides evidence that the hot melt intruded into an older crystal mush and a small portion of the mush was incorporated into the melt.

Finally, the spatial distribution of these two end members of magma chambers suggests a possible mechanism for developing low melt fraction vs. high melt fraction systems. Ignimbrites containing the strongest evidence for low melt fraction systems—Sifon, Chuhuilla, and Pastos Grandes—are found on the periphery of the APVC (Fig. 3). Ignimbrites with high melt fraction behavior—Tara and

Atana—are found near the focus of APVC activity, which is largely centered around 23°S near the Guacha caldera (Salisbury et al. 2011).

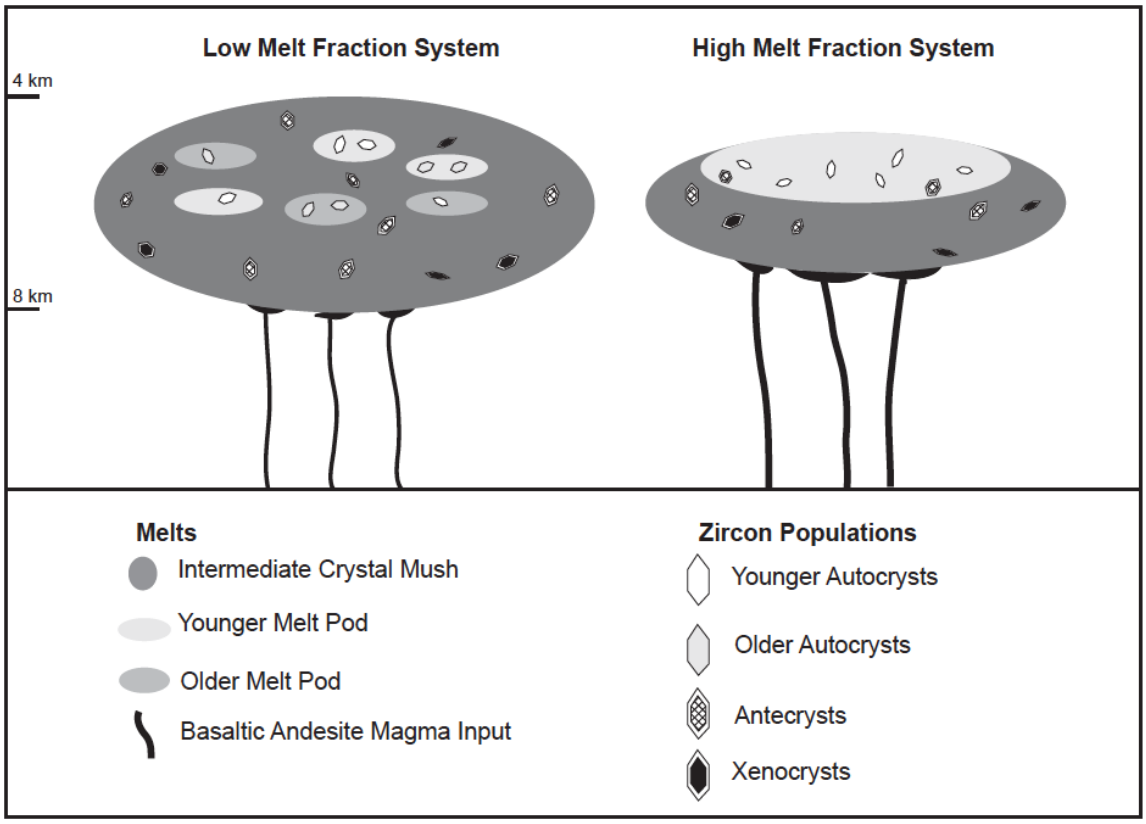

Figure 21. Cartoon representing two different end members of magma "chambers" feeding large ignimbrite eruptions. Low melt fraction systems contain small pockets of melt in which zircons crystallize over long periods of time. The surrounding crystal mush incorporates zircon antecrysts and occasional zircon xenocrysts. High melt fraction systems contain a concentrated region of melt in which zircons crystallize over a relatively short timescale. This melt is contained within a larger crystal mush, which contains zircon antecrysts and xenocrysts that may be incorporated at eruption.

5.5 Integrating Crystallization Histories and Eruptive Histories

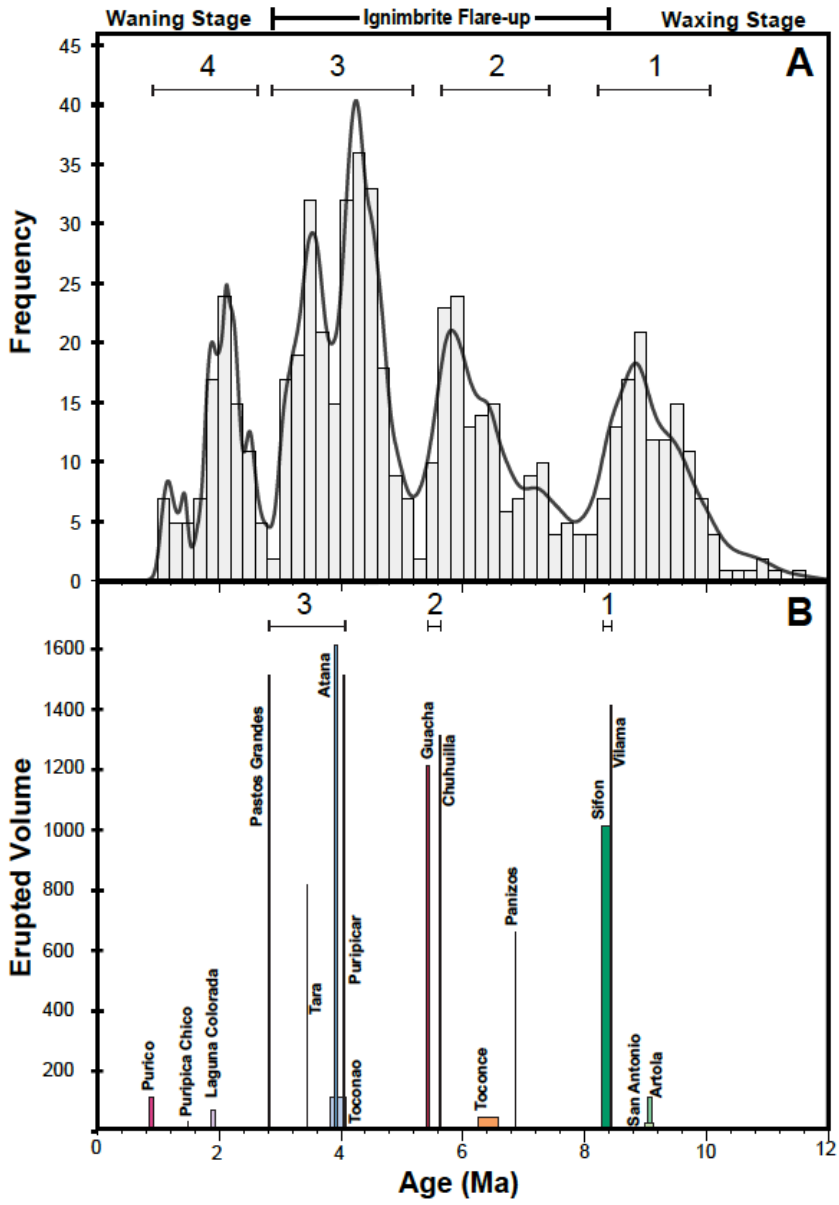

Figure 22. Zircon crystallization periods compared to eruptive pulses over the three stages of APVC development. A. Histogram and accompanying PDF curve for total zircon ages determined for APVC ignimbrites. Numbers and accompanying brackets represent the approximate duration of each period of zircon crystallization. B. Eruption age vs. volume plot adapted from Salisbury et al. (2011). Width of bars approximates eruption ages with error. Numbers and accompanying brackets represent the duration of the major eruptive pulses defining the ignimbrite flare-up.

Overlapping zircon age spectra from ignimbrites erupting on opposite sides of the APVC provide evidence that the APMB experiences periods of increased output into the shallow crust. Four periods of overlapping age spectra have been identified (Fig. 4, Figs. 8 – 11). Combining all zircon ages collected for the APVC reveals pulses in zircon crystallization with distinct breaks between crystallization periods on the regional scale (Fig. 22A). Comparing this to the eruptive record provides insight into the development of each eruptive pulse of the ignimbrite flare-up.

The four periods of zircon crystallization in the APVC correlate well with the eruptive pulses identified in previous studies (de Silva & Gosnold 2007; Salisbury et al. 2011) and provide insight into the timescales of development of the ignimbrite flare-up (Fig. 22). The first crystallization period begins with small volume eruptions from the Artola and San Antonio ignimbrites, which represent the waxing stages of surface volcanism. The Vilama and Sifon ignimbrites comprise the first eruptive pulse of the ignimbrite flare-up between 8.41 – 8.33 Ma. Both of these ignimbrites contain zircon crystallization histories that not only overlap with each other, but also with the peak crystallization of Artola and San Antonio. This

suggests that the first pulse of the ignimbrite flare-up correlates with plutonic development in the APVC extending back as far as ~10 Ma.

The second pulse of the ignimbrite flare-up between 5.60 – 5.45 Ma includes eruptions of the Guacha and Chuhuilla ignimbrites. The zircon record reflects a period of continuous crystallization leading up to second eruptive pulse that includes the development of Panizos and Toconce in addition to Guacha and Chuhuilla as far back as ~7.5 Ma.

The peak of the flare-up occurs between 4.06 and 2.89 Ma with voluminous eruptions of the Puripicar, Atana, Tara, and Pastos Grandes ignimbrites. The zircon record shows nearly continuous crystallization from ~5.2 Ma onward, beginning with the development of the Puripicar magma system.

The last period of zircon crystallization correlates with multiple small ignimbrite eruptions comprising the waning stage of activity. Crystallization is continuous from ~2.8 Ma onward. This data set is missing several younger APVC eruptions, which extend the eruptive record to ~80 ka. Zircon studies of late Pleistocene domes erupted between ~80-90 ka show evidence for continuous crystallization between the eruption of Purico eruptions (Tierney 2011), although further study is needed to investigate this more recent record.

Overall, the three eruptive pulses of the APVC ignimbrite flare-up are preceded by ~1.5 to 2 million years of continuous zircon crystallization that reflect periods of

continuous magma accumulation in the upper crust. The first two periods of zircon crystallization have early, small eruptions prior to the eruptive pulses that comprise the flare-up, while the third period is recorded by large eruptions that define the climax of the ignimbrite flare-up.

The fact that the pulsating nature of eruptions in the APVC is reflected in the plutonic record revealed through U-Pb zircon dating suggests that these pulses are a product of thermal pulsing from the deeper regional source, the APMB. Previous studies have suggested that the eruptive pulses reflect episodicity in the increase in mantle power that drives the ignimbrite flare-up. Each period of crystallization may reflect a transient increase in mantle power, which drives output from the APMB into the shallow crust (de Silva & Gosnold 2007). The eruptive record in conjunction with the plutonic record reveal that these mantle pulses occur on million year timescales over the 10 million history of overall increase in mantle power input that led to the development of the APVC.

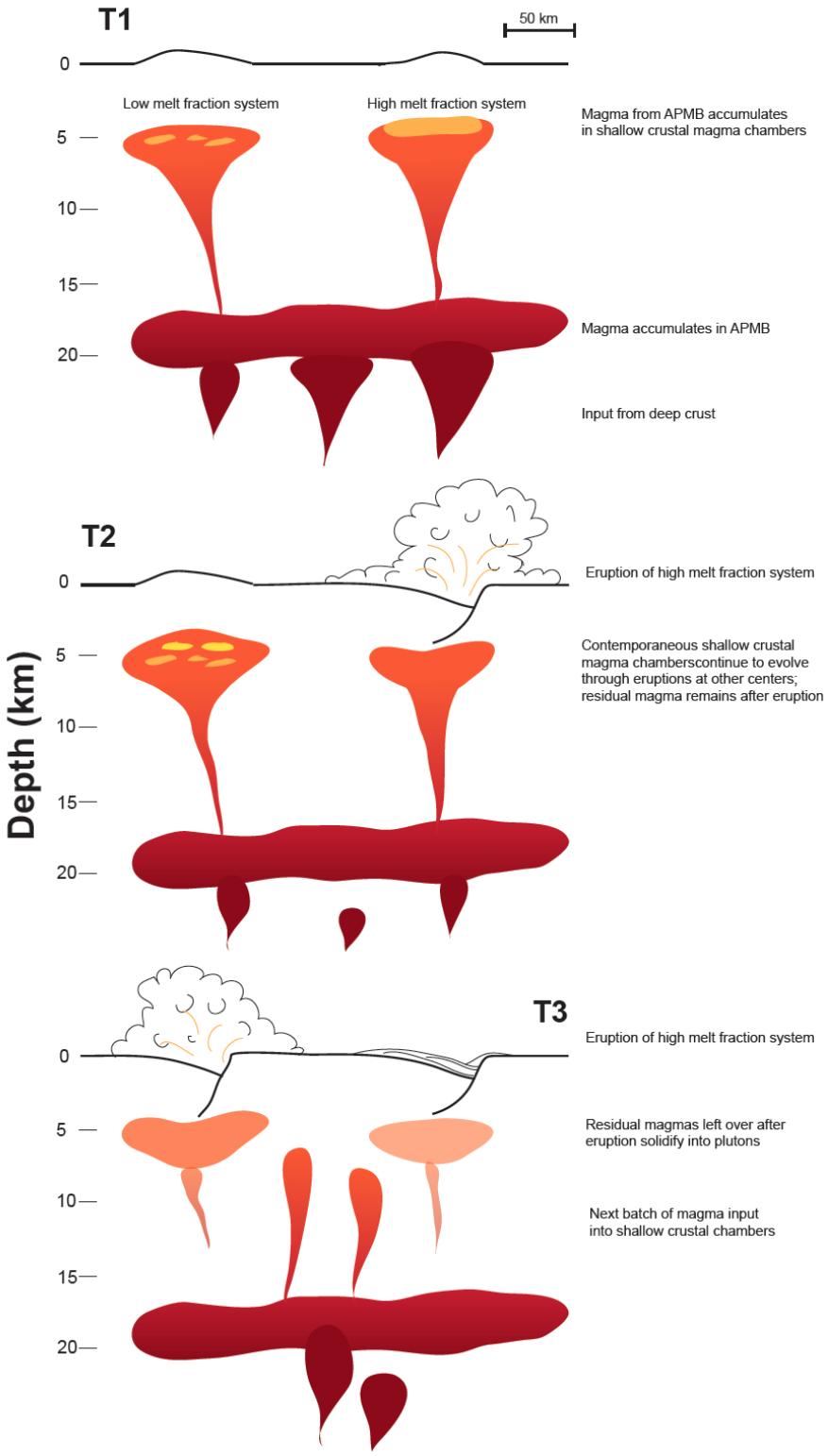
T1
50 km
0
Low melt fraction system
High melt fraction system
Magma from APMB accumulates in shallow crustal magma chambers
5
10
15
20
Magma accumulates in APMB
Input from deep crust
T2
0
Eruption of high melt fraction system
Depth (km)
5
Contemporaneous shallow crustal magma chamberscontinue to evolve through eruptions at other centers; residual magma remains after eruption
10
15
20
T3
0
Eruption of high melt fraction system
5
Residual magmas left over after eruption solidify into plutons
10
Next batch of magma input into shallow crustal chambers
15
20

Figure 23. Integrated model for the regional development of the APVC. T1) Large influx of mantle-derived material into the APMB (~20 km) feeds material into shallow crustal storage zones (8-4 km). The two magmas evolve contemporaneously, despite potential differences in melt fraction between the systems. Melt-rich regions are represented by yellow within orange crystal mushes. T2) Eruption occurs in the high melt fraction center while magma continues to accumulate at the low melt fraction center, resulting in protracted crystallization histories. The intensity of mantle-derived input into the APMB wanes. T3) Eruption occurs at the low melt fraction system. Any residual material left over from previous eruptions begins to solidify into a pluton. Input into the APMB intensifies, sending melt into the shallow crust to begin the next period of crystallization and the continuation of the ignimbrite flare-up.

5.5 Integrated Model for APVC Magmatism

Figure 23 provides an overview of the final model for regional APVC magmatism. The APMB at ~20 km depth provides a regional source for magmas feeding ignimbrite eruptions in the APVC. This is evidenced by the presence of entirely contemporaneous zircon populations in magmas from eruptive centers separated by up to 200 km, or the entire width of APVC volcanism. Combined zircon crystallization histories from all ignimbrites studied record four periods of continuous zircon crystallization lasting 1.5 – 2.0 Ma, which likely reflect pulses of magma input into and out of the APMB from the mantle. The first three of these zircon crystallization periods ends with a pulse of voluminous ignimbrite volcanism, while the fourth covers the waning stages of low-volume APVC eruptions.

Each eruptive center is underlain by a shallow-crustal magma chamber between 4-8 km depth fed by input from the APMB. Zircon ages reveal protracted crystallization times in these chambers ranging from ~400 – 1100 ka. These long timescales are

attributed to continuous influx of magma into the system from the APMB. Additionally, there appear to be two different types of magma chambers—high melt fraction and low melt fraction—as evidenced by variations in zircon populations, measured U abundances, and zircon saturation temperatures. Low melt fraction ignimbrites are found towards the periphery of the APVC while high melt fraction ignimbrites are focused towards the center. This may reflect variations in the intensity of input into different portions, which results in a more elevated geotherm in some areas that supports shorter residence times than less evolved regions that promote longer-lived crystal mushes.

6.0 Conclusions

This study originally set out to address three objectives using zircon crystallization histories of ignimbrites erupted over the spatiotemporal distribution of the APVC. The overall goal was to develop a regional model for how the batholith-scale plutonic system is built.

Objective 1 – Use zircon crystallization histories to determine the timescales of magma development and storage in the APVC

Zircon ages reveal protracted timescales of magma storage prior to eruption in the APVC. The shortest zircon crystallization times are ~400 ka while the longest exceed 1 Ma. The high variability is likely due to varying degrees of crystallinity, melt fraction, and melt composition within individual chambers. These timescales exceed those reported in previous studies, but support modeled timescales of magma accumulation in large ignimbrite eruptions.

Objective 2 – Investigate relationships between zircon crystallization histories over the spatial and temporal span of the APVC

Zircon crystallization histories reveal strong evidence for contemporaneous crystallization between ignimbrites separated by 10s to 100s of km reflecting a shared regional source for these magmas. Because developing a shallow crustal magma system at 4-8 km depth that covers 200 km is highly unlikely, the shared source is attributed to a deeper region. The APMB—a zone of partial melt presently detectable in the APVC at ~20 km depth—is the most probable shared source for magmas feeding the shallow crustal magma storage areas where zircon crystallizes.

While there is abundant evidence for close relationship between ignimbrites on a temporal scale, there is very little evidence for inheritance of zircon crystals left behind from previous eruptions at multicyclic calderas. This suggests that the magmas feeding eruptions at the same caldera separated but >1 Ma apart are not related to one another.

Objective 3 – Understand the relationship between the plutonic record and the eruptive history of the APVC

Zircon crystallization reflects the pulsating nature of the ignimbrite flare-up seen on the surface. There are four identifiable periods of zircon crystallization that correlate well with the eruptive pulses. Zircon crystallizes continuously within the APVC for up to 2 Ma prior to each pulse of the ignimbrite flare-up. This likely reflects pulses of magma input into the APMB from even deeper sources close to the mantle.

References Cited

Allmendinger, R. et al., 1997. The evolution of the Altiplano-Puna plateau of the Central Andes. *Annual Review of Earth and Planetary Sciences*, 25, pp.139–174.

Bachmann, O. & Bergantz, G., 2004. On the Origin of Crystal-poor Rhyolites: Extracted from Batholithic Crystal Mushes. *Journal of Petrology*, 45(8), pp.1565–1582.

Bachmann, O., Oberli, F., Dungan, M., Meier, M., et al., 2007a. 40Ar/39Ar and U–Pb dating of the Fish Canyon magmatic system, San Juan Volcanic field, Colorado: Evidence for an extended crystallization history. *Chemical Geology*, 236(1-2), pp.134–166.

Bachmann, O., Charlier, B.L.A. & Lowenstern, J.B., 2007b. Zircon crystallization and recycling in the magma chamber of the rhyolitic Kos Plateau Tuff (Aegean arc). *Geology*, 35(1), p.73.

Bachmann, O., Miller, C.F. & de Silva, S.L., 2007c. The volcanic–plutonic connection as a stage for understanding crustal magmatism. *Journal of Volcanology and Geothermal Research*, 167(1-4), pp.1–23.

Bacon, C.R. & Lowenstern, J.B., 2005. Late Pleistocene granodiorite source for recycled zircon and phenocrysts in rhyodacite lava at Crater Lake, Oregon. *Earth and Planetary Science Letters*, 233(3-4), pp.277–293.

Best, M. & Christiansen, E., 1991. Limited extension during peak Tertiary volcanism, Great Basin of Nevada and Utah. *Journal of Geophysical Research*.

Brown, S.J.A. & Fletcher, I.R., 1999. SHRIMP U-Pb dating of the preeruption growth history of zircons from the 340 ka Whakamaru Ignimbrite, New Zealand: Evidence for> 250 ky magma residence times. *Geology*, (27), pp.1035–1038.

Brown, S.J.A. & Smith, R.T., 2004. Crystallisation history and crustal inheritance in a large silicic magma system: 206Pb/238U ion probe dating of zircons from the 1.2 Ma Ongatiti ignimbrite, Taupo Volcanic Zone. *Journal of Volcanology and Geothermal Research*, 135(3), pp.247–257.

Charlier, B.L.A., 2005. Magma Generation at a Large, Hyperactive Silicic Volcano (Taupo, New Zealand) Revealed by U-Th and U-Pb Systematics in Zircons. *Journal of Petrology*, 46(1), pp.3–32.

Cherniak, D., Hanchar, J. & Watson, E., 1997. Diffusion of tetravalent cations in zircon. *Contributions to Mineralogy and Petrology*, 127(4), pp.383–390.

Chmielowski, J. & Zandt, G., 1999. The Central Andean Altiplano-Puna magma body. *Geophysical Research Letters*.

Costa, F., 2008. Residence times of silicic magmas associated with calderas. In J. Gottsmann & J. Marti, eds. Developments in Volcanology, pp. 1–55.

de Silva, S.L., 1989. Correlation of large ignimbrites--Two case studies from the Central Andes of northern Chile. *Journal of volcanology and geothermal …*.

de Silva, S.L. & Gosnold, W.D., 2007. Episodic construction of batholiths: Insights from the spatiotemporal development of an ignimbrite flare-up. *Journal of Volcanology and Geothermal Research*, 167(1-4), pp.320–335.

de Silva, S.L. & Zandt, G., 2006. Large scale silicic volcanism: The result of thermal maturation of the crust. *Advances in Geosciences*, 1, pp.215–230.

de Silva, S.L. et al., 2006. Large ignimbrite eruptions and volcano-tectonic depressions in the Central Andes: a thermomechanical perspective. *Geological Society, London, Special Publications*, 269(1), pp.47–63.

Folkes, C.B. et al., 2011. A reconnaissance of U-Pb zircon ages in the Cerro Galán system, NW Argentina: Prolonged magma residence, crystal recycling, and crustal assimilation. *Journal of Volcanology and Geothermal Research*, 206(3-4), pp.136–147.

Harrison, M.T. & Watson, E.B., 1983. Kinetics of zircon dissolution and zirconium diffusion in granitic melts of variable water content. *Contributions to Mineralogy and Petrology*.

Hildreth, W., 1981. Gradients in silicic magma chambers: implications for lithospheric magmatism. *Journal of Geophysical Research*.

Hildreth, W. & Wilson, C.J.N., 2007. Compositional Zoning of the Bishop Tuff. *Journal of Petrology*, 48(5), pp.951–999.

Hora, J.M. et al., 2010. Volcanic biotite-sanidine 40Ar/39Ar age discordances reflect Ar partitioning and pre-eruption closure in biotite. *Geology*, 38(10), pp.923–926.

Iyer, H., Evans, J. & Zandt, G., 1981. A deep low-velocity body under the Yellowstone caldera, Wyoming: Delineation using teleseismic P-wave residuals and tectonic interpretation: Summary. *Geological Society of America Bulletin*, 92(11), pp.792–792798.

Jellinek, A.M. & DePaolo, D.J., 2003. A model for the origin of large silicic magma chambers: precursors of caldera-forming eruptions. *Bulletin of Volcanology*,

65(5), pp.363–381.

Kay, S. & Coira, B.L., 2009. Shallowing and steepening subduction zones, continental lithospheric loss, magmatism, and crustalflow under the Central Andean Altiplano-Puna Plateau. In S. Kay, V. Ramos, & W. Dickinson, eds. *Backbone of the Americas: shallow subduction, plateau uplift, and ridge and terrane collision*. Geological Society of America Memoir 204, pp. 229–259.

Lindsay, J.M., de Silva, S.L. & Trumbull, R., 2001a. La Pacana caldera, N. Chile: a re-evaluation of the stratigraphy and volcanology of one of the world's largest resurgent calderas. *Journal of Volcanology …*.

Lindsay, J.M., Schmitt, A.K. & Trumbull, R., 2001b. Magmatic evolution of the La Pacana caldera system, Central Andes, Chile: Compositional variation of two cogenetic, large-volume felsic ignimbrites. *Journal of …*.

Lipman, P.W., 2007. Incremental assembly and prolonged consolidation of Cordilleran magma chambers: Evidence from the Southern Rocky Mountain volcanic field. *Geosphere*, 3(1), p.42.

Lipman, P.W., 1984. The roots of ash flow calderas in western North America: windows into the tops of granitic batholiths. *Journal of Geophysical Research*.

Miller, J.S. & Wooden, J.L., 2004. Residence, resorption and recycling of zircons in Devils Kitchen rhyolite, Coso volcanic field, California. *Journal of Petrology*, 45(11), pp.2155–2170.

Miller, J.S. et al., 2007. Zircon growth and recycling during the assembly of large, composite arc plutons. *Journal of Volcanology and Geothermal Research*, 167(1-4), pp.282–299.

Ort, M.H., 1993. Eruptive processes and caldera formation in a nested downsagcollapse caldera: Cerro Panizos, central Andes Mountains. *Journal of Volcanology and Geothermal Research*, 56(3), pp.221–252.

Reid, M.R., 2000. In situ U-Pb ages of zircons from the Bishop Tuff: No evidence for long crystal residence times. *Geology*, (28), pp.443–446.

Reid, M.R., Coath, C. & Harrison, M.T., 1997. Prolonged residence times for the youngest rhyolites associated with Long Valley Caldera: 230Th--238U ion microprobe dating of young zircons. *Earth and Planetary Science Letters*, 150, pp.27–39.

Salisbury, M.J. et al., 2011. 40Ar/39Ar chronostratigraphy of Altiplano-Puna volcanic complex ignimbrites reveals the development of a major magmatic province.

Geological Society of America Bulletin, 123(5-6), pp.821–840.

Schmitt, A.K., 2003. The Geysers - Cobb Mountain Magma System, California (Part 1): U-Pb zircon ages of volcanic rocks, conditions of zircon crystallization and magma residence times. *Geochimica et Cosmochimica Acta*, 67(18), pp.3423–3442.

Schmitt, A.K., 2011. Uranium Series Accessory Crystal Dating of Magmatic Processes. *Annual Review of Earth and Planetary Sciences*, 39(1), pp.321–349.

Schmitt, A.K. et al., 2001. Magma evolution in the Purico ignimbrite complex, northern Chile: evidence for zoning of a dacitic magma by injection of rhyolitic melts following mafic recharge. *Contributions to Mineralogy and Petrology*, 140(6), pp.680–700.

Schmitt, A.K. et al., 2003. U–Pb zircon chronostratigraphy of early-Pliocene ignimbrites from La Pacana, north Chile: implications for the formation of stratified magma chambers. *Journal of Volcanology and Geothermal Research*, 120(1-2), pp.43–53.

Shapiro, S.S. & Wilk, M.B., 1965. An analysis of variance test for normality (complete samples). *Biometrika*, 52(3/4), pp.591–611.

Simon, J.I. & Reid, M.R., 2005. The pace of rhyolite differentiation and storage in an "archetypical" silicic magma system, Long Valley, California. *Earth and Planetary Science Letters*, 235(1-2), pp.123–140.

Simon, J.I., Renne, P.R. & Mundil, R., 2008. Implications of pre-eruptive magmatic histories of zircons for U–Pb geochronology of silicic extrusions. *Earth and Planetary Science Letters*, 266(1-2), pp.182–194.

Soler, M.M. et al., 2007. Geology of the Vilama caldera: A new interpretation of a large-scale explosive event in the Central Andean plateau during the Upper Miocene. *Journal of Volcanology and Geothermal Research*, 164(1-2), pp.27–53.

Storm, S. et al., 2011. Decoupled crystallization and eruption histories of the rhyolite magmatic system at Tarawera volcano revealed by zircon ages and growth rates. *Contributions to Mineralogy and Petrology*, 163(3), pp.505–519.

Tappa, M.J. et al., 2011. The plutonic record of a silicic ignimbrite from the Latir volcanic field, New Mexico. *Geochemistry Geophysics Geosystems*, 12(10).

Tierney, C., 2011. *Timescales of Large Silicic Magma Systems: Implications from Accessory Minerals in Pleistocene Lavas of the Altiplano-Puna Volcanic Complex, Central Andes* S. L. de Silva, ed., Oregon State University.

Vazquez, J.A. & Reid, M.R., 2002. Time scales of magma storage and differentiation of voluminous high-silica rhyolites at Yellowstone caldera, Wyoming. *Contributions to Mineralogy and Petrology*, 144(3), pp.274–285.

Walker, B.A., Grunder, A.L. & Wooden, J.L., 2010. Organization and thermal maturation of long-lived arc systems: Evidence from zircons at the Aucanquilcha volcanic cluster, northern Chile. *Geology*, 38(11), pp.1007–1010.

Watson, E., 1996. Dissolution, growth and survival of zircons during crustal fusion: kinetic principles, geological models and implications for isotopic inheritance. *Transactions of the Royal Society of Edinburgh: Earth Sciences*, 87, pp.43–56.

Watson, E.B. & Harrison, M.T., 1983. Zircon saturation revisited: temperature and composition effects in a variety of crustal magma types. *Earth and Planetary Science Letters*, 64, pp.295–304.

White, S.M., Crisp, J.A. & Spera, F.J., 2006. Long-term volumetric eruption rates and magma budgets. *Geochemistry Geophysics Geosystems*, 7(3).

Zandt, G., Leidig, M. & Chmielowski, J., 2003. Seismic detection and characterization of the Altiplano-Puna magma body, central Andes. *Pure and Applied Geophysics*, 160, pp.789–807.

Appendix

Artola

Sample	Grain	Core/Rim	$^{238}U/^{206}Pb$	1σ $^{238}U/^{206}Pb$	207Pb/206Pb	1σ 207Pb/206Pb	% 206Pb*	206Pb/238U age [Ma]	1σ 206Pb/238U age [Ma]	U (ppm)	U/Th
83002	1	R	6.13E+02	3.20E+01	9.52E-02	9.05E-03	93.7	9.93	0.57	269	2.8
83002	2	R	6.70E+02	3.01E+01	6.30E-02	2.27E-03	97.9	9.47	0.43	2045	1.0
83002	3	R	6.46E+02	3.76E+01	8.03E-02	7.27E-03	95.6	9.62	0.59	150	2.8
83002	4	R	6.19E+02	3.33E+01	7.00E-02	4.62E-03	97.0	10.2	0.6	342	3.0
83002	5	R	6.98E+02	3.14E+01	5.92E-02	5.06E-03	98.4	9.17	0.42	426	3.0
83002	6	R	6.69E+02	3.54E+01	7.18E-02	7.99E-03	96.7	9.40	0.52	309	2.6
83002	7	R	6.30E+02	3.43E+01	7.48E-02	6.51E-03	96.4	9.94	0.56	224	1.7
83002	8	R	6.14E+02	3.40E+01	8.22E-02	4.44E-03	95.4	10.1	0.6	315	3.5
83002	9	R	5.13E+02	2.27E+01	2.61E-01	2.22E-02	72.6	9.20	0.69	329	3.2
83002	10	R	6.76E+02	2.96E+01	7.39E-02	7.48E-03	96.5	9.29	0.43	214	2.6
83002	11	R	5.65E+02	2.57E+01	1.81E-01	7.44E-03	82.8	9.53	0.54	343	2.1
83002	12	R	5.91E+02	3.47E+01	1.27E-01	7.24E-03	89.7	9.84	0.65	216	1.5
83002	13	R	5.93E+02	2.95E+01	1.55E-01	1.67E-02	86.1	9.45	0.59	124	3.6
83002	14	R	6.56E+02	3.26E+01	8.02E-02	5.50E-03	95.7	9.49	0.49	505	3.3
83002	15	R	2.25E+02	1.14E+01	5.76E-01	9.84E-03	32.3	9.33	1.75	244	3.2
83002	16	R	3.73E+01	2.11E+00	7.92E-01	7.00E-03	4.7	8.21	13.31	199	2.6
83002	17	R	6.72E+02	3.69E+01	7.29E-02	8.69E-03	96.6	9.36	0.54	248	2.7
83002	18	R	6.14E+02	3.32E+01	9.37E-02	7.18E-03	93.9	9.94	0.58	166	1.7
83002	19	R	6.84E+02	3.24E+01	5.80E-02	3.91E-03	98.5	9.36	0.45	488	2.3
83002	20	R	6.65E+02	2.86E+01	5.01E-02	1.82E-03	99.5	9.69	0.42	1812	0.9
83002	21	R	1.24E+02	8.43E+00	6.49E-01	1.05E-02	22.9	11.9	4.7	489	2.3

83002	22	R	6.74E+02	3.16E+01	7.55E-02	4.58E-03	96.3	9.28	0.45	353	2.2
83002	23	R	5.15E+02	2.50E+01	2.36E-01	1.52E-02	75.7	9.55	0.69	253	2.0
83002	24	R	4.86E+02	2.74E+01	2.44E-01	6.85E-03	74.7	9.98	0.78	304	1.9
83002	25	R	6.80E+02	2.96E+01	6.38E-02	5.12E-03	97.8	9.32	0.42	260	1.0
83002	26	R	4.02E+02	1.66E+01	3.33E-01	9.34E-03	63.3	10.2	0.7	241	3.1
83002	27	R	6.47E+02	2.83E+01	9.31E-02	8.56E-03	94.0	9.44	0.45	173	1.9
83002	28	R	6.56E+02	2.54E+01	6.39E-02	6.61E-03	97.7	9.68	0.39	384	1.6
83002	29	R	6.58E+02	2.67E+01	6.81E-02	4.91E-03	97.2	9.61	0.40	414	2.9
83002	30	R	6.52E+02	2.70E+01	6.87E-02	6.31E-03	97.1	9.66	0.42	276	1.2
83002	31	R	5.82E+02	2.31E+01	1.35E-01	1.01E-02	88.7	9.88	0.47	246	1.4
83002	32	R	5.71E+02	2.34E+01	1.56E-01	6.17E-03	86.0	9.79	0.48	373	2.8

Atana

Sample	Grain	Core/Rim	$^{238}U/^{206}Pb$	1σ $^{238}U/^{206}Pb$	207Pb/206Pb	1σ 207Pb/206Pb	% 206Pb*	206Pb/238U age [Ma]	1σ 206Pb/238U age [Ma]	U (ppm)	U/Th
88055	1	R	1.52E+03	3.71E+01	9.07E-02	7.61E-03	94.3	4.09	0.11	419	1.9
88055	2	R	1.20E+03	3.11E+01	8.74E-02	6.54E-03	94.7	5.20	0.15	364	4.6
88055	3	R	1.37E+03	2.87E+01	5.86E-02	3.91E-03	98.4	4.70	0.10	1155	2.7
88055	4	R	1.00E+03	1.52E+01	5.29E-02	1.45E-03	99.1	6.45	0.10	3412	4.0
88055	5	R	1.45E+03	3.60E+01	9.34E-02	7.46E-03	94.0	4.26	0.12	429	1.9
88055	6	C	1.51E+03	4.22E+01	1.04E-01	1.10E-02	92.6	4.04	0.14	455	2.8
88055	7	C	1.52E+03	3.45E+01	8.84E-02	5.19E-03	94.6	4.12	0.10	551	3.1
88055	8	R	1.43E+03	3.66E+01	1.10E-01	7.87E-03	91.8	4.24	0.12	477	2.7
88055	9	R	1.32E+03	3.26E+01	9.17E-02	1.22E-02	94.2	4.64	0.14	1506	1.0

88055	12	R	1.46E+03	3.18E+01	8.46E-02	6.47E-03	95.1	4.28	0.10	520	1.6
88055	13	R	1.47E+03	3.21E+01	7.94E-02	5.51E-03	95.7	4.27	0.10	829	2.1
88055	14	C	1.61E+03	5.26E+01	1.64E-01	2.85E-02	84.9	3.49	0.18	154	2.7
88055	15	R	1.45E+03	3.93E+01	9.77E-02	6.44E-03	93.4	4.24	0.13	505	2.7
88055	16	R	1.55E+03	3.37E+01	8.31E-02	5.67E-03	95.3	4.05	0.09	649	3.1
88055	17	R	1.53E+03	3.73E+01	8.29E-02	6.97E-03	95.3	4.09	0.11	415	1.4
88055	18	R	1.51E+03	3.28E+01	6.84E-02	4.72E-03	97.2	4.22	0.09	799	1.8
88055	19	R	1.54E+03	3.48E+01	7.22E-02	4.68E-03	96.7	4.08	0.10	745	0.8
88055	20	R	1.47E+03	3.92E+01	1.01E-01	8.50E-03	93.0	4.15	0.13	484	1.7
88055	21	R	1.53E+03	3.65E+01	7.60E-02	4.81E-03	96.2	4.14	0.10	887	3.0
88055	22	C	1.48E+03	3.44E+01	6.82E-02	5.47E-03	97.2	4.32	0.11	788	2.8
88055	23	C	1.49E+03	2.89E+01	6.98E-02	3.31E-03	97.0	4.28	0.09	1520	2.5
88055	24	R	1.50E+03	3.82E+01	1.24E-01	1.18E-02	90.0	3.96	0.13	283	2.3
88055	25	R	1.55E+03	4.05E+01	9.52E-02	8.65E-03	93.7	4.00	0.12	345	3.4
88055	26	R	1.51E+03	3.44E+01	7.05E-02	5.50E-03	96.9	4.22	0.10	582	3.2
88055	27	C	1.56E+03	4.87E+01	8.64E-02	6.06E-03	94.9	4.00	0.13	505	3.1
88055	28	R	1.96E+02	3.90E+00	8.21E-02	2.20E-03	95.5	31.5	0.7	502	3.1
88055	29	R	1.44E+03	4.33E+01	1.03E-01	7.99E-03	92.7	4.22	0.14	343	1.8
88055	30	R	1.55E+03	3.69E+01	7.05E-02	5.85E-03	96.9	4.13	0.10	938	3.6
88055	32	C	1.40E+03	4.84E+01	1.12E-01	1.69E-02	91.6	4.30	0.19	239	2.6
88055	34	R	1.50E+03	3.87E+01	8.36E-02	9.80E-03	95.2	4.17	0.12	447	3.2
88055	35	R	1.46E+03	4.58E+01	8.42E-02	7.60E-03	95.1	4.29	0.14	323	1.6
88055	36	C	1.27E+03	5.09E+01	1.64E-01	2.27E-02	84.9	4.41	0.26	350	2.4
88055	37	R	1.49E+03	3.33E+01	6.62E-02	4.05E-03	97.4	4.30	0.10	799	3.2
88055	38	R	1.49E+03	3.79E+01	6.83E-02	5.08E-03	97.2	4.29	0.11	614	2.6
88055	39	R	1.57E+03	3.64E+01	7.49E-02	5.51E-03	96.3	4.05	0.10	704	2.9
88055	40	R	1.49E+03	3.46E+01	8.64E-02	6.49E-03	94.8	4.19	0.11	537	2.0
88055	43	R	1.50E+03	2.62E+01	6.29E-02	3.24E-03	97.9	4.30	0.08	1182	2.1

88055	44	C	1.55E+03	3.37E+01	7.96E-02	5.65E-03	95.7	4.07	0.09	689	3.0
88055	45	C	1.51E+03	3.20E+01	8.73E-02	5.67E-03	94.7	4.12	0.10	531	2.2
88055	46	C	1.51E+03	4.07E+01	1.01E-01	1.31E-02	93.0	4.05	0.13	318	1.8
88055	48	C	1.47E+03	3.89E+01	1.02E-01	8.45E-03	92.9	4.14	0.13	366	1.2
88055	49	C	1.41E+03	6.23E+01	1.91E-01	2.36E-02	81.5	3.81	0.23	98	1.7
88055	50	R	1.50E+03	4.89E+01	7.87E-02	7.73E-03	95.8	4.21	0.15	380	2.6
88055	51	R	1.53E+03	3.00E+01	6.49E-02	4.20E-03	97.6	4.21	0.09	912	2.5
88055	52	C	1.51E+03	3.99E+01	8.33E-02	8.99E-03	95.2	4.16	0.12	410	1.9
88055	53	C	1.63E+03	4.47E+01	8.08E-02	1.38E-02	95.6	3.86	0.13	340	2.3
88055	54	R	1.50E+03	2.77E+01	8.78E-02	7.26E-03	94.7	4.14	0.09	450	1.8
88055	55	C	1.57E+03	4.04E+01	8.36E-02	6.69E-03	95.2	3.99	0.11	411	1.6
88055	56	R	1.45E+03	3.70E+01	9.89E-02	8.22E-03	93.3	4.25	0.12	282	3.1
88055	57	R	1.34E+03	4.46E+01	1.04E-01	1.15E-02	92.6	4.54	0.18	210	1.9
88055	58	C	1.52E+03	3.91E+01	6.63E-02	4.30E-03	97.4	4.21	0.11	766	1.3
88055	59	C	5.83E+02	1.55E+01	5.19E-01	1.15E-02	39.6	4.44	0.42	923	1.2
88055	60	R	1.52E+03	4.11E+01	7.66E-02	8.97E-03	96.1	4.19	0.12	425	4.7
88055	61	R	1.51E+03	3.22E+01	7.07E-02	7.83E-03	96.9	4.22	0.10	592	3.1
Lari-96h-6	2	C	8.46E-04	5.10E-05	2.85E-02	5.16E-03	41.7	2.27	0.75		
Lari-96h-6	2	R	8.93E-04	7.50E-05	2.92E-02	8.33E-03	81.4	4.61	0.76		
Lari-96h-6	3	C	6.81E-04	3.50E-05	1.63E-02	2.48E-03	91.9	4.04	0.25		
Lari-96h-6	3	R	6.26E-04	3.20E-05	1.31E-02	2.06E-03	88.8	3.58	0.22		
Lari-96h-6	3	R	6.90E-04	3.90E-05	9.83E-03	1.39E-03	90.5	3.83	0.39		
Lari-96h-6	5	C	1.25E-03	6.20E-05	7.13E-02	5.38E-03	50.2	4.05	0.59		
Lari-96h-6	5	R	8.03E-04	4.80E-05	1.38E-02	2.77E-03	74.9	3.9	0.61		
Lari-96h-6	6	R	7.12E-04	3.20E-05	1.38E-02	1.70E-03	90.4	4.15	0.24		
Lari-96h-6	6	C	7.42E-04	4.60E-05	1.27E-02	2.34E-03	76.5	3.59	0.51		
Lari-96h-6	8	C	1.01E-03	1.23E-04	5.37E-02	1.16E-02	54.4	3.53	1.02		
Lari-96h-6	8	R	7.32E-04	3.30E-05	8.42E-03	1.44E-03	100	4.58	0.28		

Lari-96h-6	13	C	2.94E-03	1.18E-04	2.58E-01	1.39E-02	31.5	3.88	1.39
Lari-96h-6	18	C	7.10E-04	3.80E-05	1.57E-02	2.35E-03	86.5	3.91	0.26
Lari-96h-6	19	C	9.95E-04	5.00E-05	4.02E-02	4.88E-03	67.9	4.35	0.53
Lari-96h-6	25	C	6.85E-04	3.40E-05	5.48E-03	1.20E-03	100	4.19	0.33
Lari-96h-6	26	C	6.64E-04	5.70E-05	9.81E-03	1.93E-03	84.5	3.45	0.74
Lari-96h-6	30	C	6.41E-04	4.30E-05	4.82E-03	9.80E-04	91.8	3.58	0.46

*Lari-96h-6 ages previously reported in Schmitt et al. 2003

Chuhuilla

Sample	Grain	Core/Rim	$^{238}U/^{206}Pb$	1σ $^{238}U/^{206}Pb$	207Pb/206Pb	1σ 207Pb/206Pb	% 206Pb*	206Pb/238U age [Ma]	1σ 206Pb/238U age [Ma]	U (ppm)	U/Th
6050	1	C	1.00E+03	3.60E+01	5.23E-02	2.14E-03	99.2	6.47	0.23	2029	1.5
6050	1	R	9.96E+02	3.68E+01	5.48E-02	2.59E-03	98.9	6.47	0.24	2014	1.5
6050	2	C	8.45E+02	3.68E+01	5.64E-02	2.60E-03	98.7	7.59	0.33	833	1.1
6050	2	R	1.04E+03	4.43E+01	6.15E-02	3.81E-03	98.0	6.16	0.26	660	6.1
6050	3	C	8.96E+02	3.78E+01	5.96E-02	2.96E-03	98.3	7.15	0.31	906	1.9
6050	3	R	1.01E+03	4.20E+01	6.41E-02	3.49E-03	97.7	6.34	0.27	943	4.7
6050	4	C	1.05E+03	3.87E+01	7.17E-02	4.28E-03	96.7	6.02	0.23	1461	2.1
6050	4	R	1.07E+03	4.24E+01	5.91E-02	2.73E-03	98.4	6.01	0.24	1266	4.6
6050	5	C	1.06E+03	3.90E+01	5.26E-02	2.49E-03	99.2	6.11	0.22	1357	3.8
6050	5	R	1.13E+03	4.43E+01	6.09E-02	2.41E-03	98.1	5.69	0.22	1397	4.3
6050	6	C	1.06E+03	3.89E+01	5.34E-02	3.72E-03	99.1	6.13	0.23	1427	2.0
6050	6	R	1.13E+03	4.43E+01	5.42E-02	2.69E-03	99.0	5.72	0.22	1458	3.5
6050	7	C	8.95E+02	2.97E+01	5.13E-02	1.10E-03	99.4	7.24	0.24	4923	3.4
6050	7	R	1.00E+03	4.10E+01	5.81E-02	2.27E-03	98.5	6.43	0.26	1243	3.6
6050	8	C	1.04E+03	4.39E+01	6.53E-02	5.10E-03	97.5	6.12	0.26	616	6.2

6050	8	R	1.10E+03	4.44E+01	5.83E-02	3.55E-03	98.5	5.87	0.24	633	5.4
6050	9	C	1.01E+03	4.22E+01	1.24E-01	5.77E-03	90.0	5.83	0.27	1561	3.7
6050	9	R	8.42E+02	3.34E+01	2.51E-01	6.97E-03	73.9	5.75	0.32	1451	4.8
SDS5	1	R	3.32E+02	1.60E+01	5.42E-01	8.09E-03	36.6	7.21	1.13	907	
SDS5	2	R	9.34E+02	5.06E+01	6.61E-02	1.20E-02	97.5	6.82	0.39	462	
SDS5	3	R	8.72E+02	4.46E+01	9.22E-02	4.45E-03	94.1	7.05	0.38	1439	
SDS5	4	R	1.09E+03	5.07E+01	5.34E-02	3.90E-03	99.1	5.97	0.28	1150	
SDS5	5	R	1.10E+03	4.52E+01	4.84E-02	3.36E-03	99.7	5.91	0.24	1312	
SDS5	6	R	1.14E+03	4.68E+01	5.71E-02	3.00E-03	98.6	5.68	0.23	1991	
SDS5	7	R	1.17E+03	4.31E+01	5.84E-02	7.93E-03	98.4	5.54	0.21	713	
SDS5	8	R	1.08E+03	4.46E+01	5.64E-02	3.39E-03	98.7	5.97	0.25	1318	
SDS5	9	R	1.03E+03	4.13E+01	5.91E-02	5.57E-03	98.4	6.22	0.25	610	
SDS5	10	R	1.32E+03	5.04E+01	5.88E-02	6.42E-03	98.4	4.89	0.19	780	
SDS5	11	R	1.10E+03	4.64E+01	5.85E-02	3.86E-03	98.4	5.89	0.25	1040	
SDS5	12	R	8.91E+02	4.14E+01	1.67E-01	1.36E-02	84.6	6.20	0.36	523	
SDS5	13	R	4.44E+02	4.04E+01	4.43E-01	3.11E-02	49.3	7.24	1.77	1219	
SDS5	14	C	9.29E+02	4.63E+01	4.75E-02	3.65E-03	99.8	6.99	0.35	1020	
SDS5	15	R	9.78E+02	4.49E+01	5.53E-02	3.50E-03	98.8	6.59	0.30	1231	
SDS5	16	R	1.10E+03	6.56E+01	7.73E-02	1.07E-02	96.0	5.69	0.36	361	
SDS5	17	R	1.09E+03	4.70E+01	5.19E-02	3.00E-03	99.3	5.97	0.26	1870	
SDS5	18	R	9.84E+02	3.88E+01	5.66E-02	3.76E-03	98.7	6.56	0.26	1377	
SDS5	19	R	1.14E+03	4.88E+01	5.16E-02	3.58E-03	99.3	5.71	0.24	1447	
SDS5	20	R	9.43E+02	4.03E+01	5.13E-02	2.20E-03	99.3	6.88	0.29	2617	
SDS5	21	R	9.70E+02	4.80E+01	6.32E-02	7.82E-03	97.8	6.58	0.33	589	
SDS5	22	R	1.16E+03	4.63E+01	5.26E-02	3.66E-03	99.2	5.62	0.22	980	
SDS5	23	R	1.04E+03	4.62E+01	4.76E-02	3.25E-03	99.8	6.27	0.28	1340	
SDS5	24	R	1.03E+03	4.73E+01	5.05E-02	4.17E-03	99.4	6.30	0.29	723	
SDS5	25	R	1.05E+03	4.53E+01	6.76E-02	3.10E-03	97.3	6.05	0.27	1693	

SDS5	26	R	1.18E+03	4.57E+01	5.36E-02	4.45E-03	99.0	5.53	0.22	1295
SDS5	27	R	1.23E+03	5.10E+01	5.54E-02	4.43E-03	98.8	5.24	0.22	1122

Guacha

Sample	Grain	Core/Rim	$^{238}U/^{206}Pb$	1σ $^{238}U/^{206}Pb$	207Pb/206Pb	1σ 207Pb/206Pb	% 206Pb*	206Pb/238U age [Ma]	1σ 206Pb/238U age [Ma]	U (ppm)	U/Th
ARIBOL 10007	1	R	1.12E+03	2.94E+01	7.83E-02	6.83E-03	95.9	5.61	0.16	252	1.8
ARIBOL 10007	2	C	1.08E+03	2.11E+01	7.03E-02	5.39E-03	96.9	5.90	0.12	333	3.0
ARIBOL 10007	2	R	1.04E+03	3.15E+01	9.32E-02	8.66E-03	94.0	5.89	0.20	222	3.2
ARIBOL 10007	3	C	1.04E+03	2.81E+01	7.02E-02	5.65E-03	96.9	6.07	0.17	318	2.1
ARIBOL 10007	4	R	1.09E+03	2.03E+01	9.24E-02	3.59E-03	94.1	5.64	0.11	844	2.0
ARIBOL 10007	6	C	9.57E+02	2.17E+01	8.93E-02	7.56E-03	94.5	6.44	0.16	243	1.9
ARIBOL 10007	7	R	1.15E+03	2.76E+01	7.46E-02	6.54E-03	96.4	5.47	0.14	331	2.2
ARIBOL 10007	8	C	1.09E+03	2.89E+01	6.15E-02	4.71E-03	98.0	5.88	0.16	548	2.3
ARIBOL 10007	9	R	1.07E+03	2.68E+01	7.17E-02	5.53E-03	96.7	5.93	0.16	549	2.1
ARIBOL 10007	10	R	1.10E+03	2.70E+01	7.10E-02	9.48E-03	96.8	5.76	0.16	355	2.2
ARIBOL 10007	11	R	1.11E+03	3.29E+01	5.66E-02	4.13E-03	98.7	5.83	0.18	684	1.8
ARIBOL 10007	12	R	1.01E+03	2.60E+01	7.47E-02	6.13E-03	96.4	6.26	0.17	408	3.0
ARIBOL 10007	13	R	1.12E+03	3.91E+01	1.03E-01	1.75E-02	92.8	5.43	0.23	201	2.2
ARIBOL 10007	14	C	1.05E+03	3.55E+01	7.40E-02	8.11E-03	96.4	6.02	0.22	265	3.0
ARIBOL 10007	15	R	1.10E+03	3.11E+01	8.14E-02	8.76E-03	95.5	5.66	0.18	315	3.0
ARIBOL 10007	16	R	1.07E+03	2.20E+01	6.53E-02	7.06E-03	97.6	5.97	0.13	414	3.3
ARIBOL 10007	17	R	1.01E+03	2.06E+01	5.42E-02	3.70E-03	99.0	6.43	0.13	797	2.6
ARIBOL 10007	18	R	1.04E+03	3.34E+01	5.42E-02	5.76E-03	99.0	6.21	0.20	440	2.9
ARIBOL 10007	19	R	1.03E+03	2.49E+01	7.07E-02	5.84E-03	96.9	6.14	0.16	426	2.6
ARIBOL 10007	20	C	1.01E+03	2.76E+01	8.05E-02	7.38E-03	95.6	6.22	0.18	289	2.3

ARIBOL 10007	21	R	1.29E+03	6.78E+01	8.26E-02	8.44E-03	95.3	4.85	0.27	228	2.4
ARIBOL 10007	22	C	1.26E+03	1.85E+02	6.06E-02	4.94E-03	98.2	5.12	0.76	589	2.8
ARIBOL 10007	23	R	1.22E+03	3.23E+01	9.20E-02	1.02E-02	94.1	5.04	0.15	192	2.2
ARIBOL 10007	24	C	1.04E+03	4.07E+01	1.18E-01	2.15E-02	90.9	5.73	0.29	145	2.7
ARIBOL 10007	25	C	8.87E+02	1.94E+01	5.48E-02	3.54E-03	98.9	7.29	0.16	891	11.0
ARIBOL 10007	26	R	1.12E+03	2.50E+01	5.61E-02	8.18E-03	98.7	5.77	0.14	666	2.3
ARIBOL 10007	27	C	1.05E+03	3.38E+01	9.05E-02	1.12E-02	94.3	5.87	0.22	275	3.1
ARIBOL 10007	27	R	1.09E+03	3.18E+01	7.19E-02	5.03E-03	96.7	5.81	0.18	564	3.7
ARIBOL 10007	28	R	9.97E+02	2.51E+01	6.80E-02	6.34E-03	97.2	6.37	0.17	323	2.5
ARIBOL 10007	29	C	1.01E+03	1.86E+01	6.04E-02	5.05E-03	98.2	6.37	0.13	715	1.8
ARIBOL 10007	30	C	1.06E+03	2.54E+01	8.81E-02	7.46E-03	94.6	5.85	0.16	502	1.9
ARIBOL 10007	31	C	9.62E+02	1.81E+01	5.98E-02	4.85E-03	98.3	6.68	0.13	580	4.5
ARIBOL 10007	32	C	1.01E+03	2.81E+01	6.48E-02	5.53E-03	97.6	6.32	0.18	587	2.9
ARIBOL 10007	32	R	1.08E+03	3.02E+01	7.34E-02	7.01E-03	96.5	5.82	0.17	495	2.7
ARIBOL 10007	33	R	1.04E+03	2.67E+01	6.43E-02	1.04E-02	97.7	6.12	0.17	415	2.7
ARIBOL 10007	34	C	9.95E+02	3.40E+01	8.24E-02	7.56E-03	95.4	6.26	0.23	318	2.6
ARIBOL 10007	35	C	1.20E+01	3.07E-01	6.19E-02	1.78E-03	99.4	513	13	301	2.1
SDS10	1	R	1.09E+03	4.47E+01	5.55E-02	3.62E-03	98.8	5.90	0.24	1237	
SDS10	2	R	1.10E+03	4.76E+01	6.46E-02	8.67E-03	97.6	5.81	0.26	673	
SDS10	3	R	1.05E+03	4.65E+01	8.24E-02	1.10E-02	95.4	5.96	0.28	575	
SDS10	4	R	1.14E+03	4.80E+01	5.10E-02	3.53E-03	99.4	5.72	0.24	1166	
SDS10	5	R	1.12E+03	5.62E+01	7.30E-02	6.71E-03	96.6	5.65	0.29	587	
SDS10	6	R	1.17E+03	5.83E+01	9.03E-02	9.39E-03	94.4	5.30	0.28	404	
SDS10	7	R	1.17E+03	5.06E+01	6.47E-02	1.00E-02	97.6	5.45	0.25	472	
SDS10	8	R	1.12E+03	4.37E+01	5.35E-02	4.00E-03	99.1	5.80	0.23	1549	
SDS10	9	R	1.12E+03	5.51E+01	7.61E-02	1.04E-02	96.2	5.60	0.29	247	
SDS10	10	R	1.21E+03	5.33E+01	7.44E-02	1.36E-02	96.4	5.23	0.25	296	
SDS10	11	R	1.17E+03	4.42E+01	5.26E-02	3.36E-03	99.2	5.55	0.21	1503	

SDS10	12	R	1.15E+03	5.79E+01	6.98E-02	9.35E-03	97.0	5.51	0.29	303
SDS10	13	R	1.11E+03	4.43E+01	6.09E-02	7.65E-03	98.1	5.78	0.24	763
SDS10	14	R	1.12E+03	4.23E+01	4.85E-02	3.12E-03	99.7	5.85	0.22	2186
SDS10	15	R	1.12E+03	6.21E+01	7.00E-02	8.85E-03	97.0	5.69	0.33	253
SDS10	16	R	1.14E+03	5.51E+01	7.25E-02	6.12E-03	96.6	5.56	0.28	702
SDS10	17	R	1.11E+03	4.37E+01	7.20E-02	5.93E-03	96.7	5.70	0.23	1488
SDS10	18	R	1.12E+03	4.69E+01	6.40E-02	4.94E-03	97.7	5.73	0.25	677
SDS10	19	R	1.08E+03	4.90E+01	1.08E-01	1.44E-02	92.1	5.60	0.29	249
SDS10	20	R	1.02E+03	4.03E+01	1.23E-01	1.28E-02	90.2	5.81	0.27	655

Laguna Colorada

Sample	Grain	Core/Rim	$^{238}U/^{206}Pb$	1σ $^{238}U/^{206}Pb$	207Pb/206Pb	1σ 207Pb/206Pb	% 206Pb*	206Pb/238U age [Ma]	1σ 206Pb/238U age [Ma]	U (ppm)	U/Th
BOL07024LC	1	R	2.79E+03	1.31E+02	1.40E-01	1.92E-02	88.0	2.12	0.12	194	2.7
BOL07024LC	6	R	2.48E+03	1.17E+02	8.24E-02	1.22E-02	95.4	2.57	0.13	567	3.3
BOL07024LC	7	R	2.22E+03	1.13E+02	1.25E-01	1.39E-02	89.9	2.70	0.16	202	3.3
BOL07024LC	8	R	2.47E+03	1.06E+02	1.01E-01	8.68E-03	93.0	2.52	0.12	375	3.5
BOL07024LC	12	R	3.12E+03	1.23E+02	7.85E-02	1.06E-02	95.9	2.08	0.09	563	4.2
BOL07024LC	12	C	2.09E+03	1.14E+02	1.20E-01	1.60E-02	90.6	2.88	0.18	168	2.7
BOL07024LC	15	R	2.09E+03	9.41E+01	2.84E-01	1.28E-02	69.6	2.24	0.15	434	3.7
BOL07024LC	16	R	2.61E+03	1.04E+02	1.10E-01	1.56E-02	91.9	2.37	0.11	549	3.7
BOL07024LC	19	C	2.84E+03	1.49E+02	1.27E-01	1.52E-02	89.7	2.13	0.13	363	2.9
BOL07024LC	21	C	2.70E+03	1.41E+02	1.54E-01	1.80E-02	86.2	2.15	0.14	327	2.6
BOL07024LC	26	C	2.63E+03	1.16E+02	1.04E-01	1.25E-02	92.6	2.35	0.11	370	1.8
BOL07024LC	26	R	2.21E+03	1.29E+03	1.22E-01	1.98E-02	90.3	2.73	1.72	364	3.6
BOL07024LC	28	R	2.53E+03	1.20E+02	1.14E-01	1.93E-02	91.4	2.42	0.13	301	3.2

BOL07024LC	30	R	2.44E+03	1.19E+02	1.09E-01	1.20E-02	92.0	2.52	0.13	410	3.1
BOL07024LC	32	C	2.38E+03	1.08E+02	9.13E-02	8.16E-03	94.2	2.64	0.13	537	2.7
BOL07024LC	33	R	2.57E+03	1.22E+02	9.83E-02	9.09E-03	93.3	2.44	0.12	447	3.6
BOL07024LC	38	R	1.30E+03	4.89E+01	6.91E-02	7.91E-03	97.1	4.92	0.19	418	3.5
BOL07024LC	42	C	2.60E+03	1.23E+02	1.11E-01	1.59E-02	91.7	2.37	0.13	256	4.0
BOL07024LC	43	C	2.57E+03	1.06E+02	1.26E-01	1.65E-02	89.8	2.34	0.12	478	2.4
BOL07024LC	44	R	2.30E+03	9.83E+01	1.03E-01	1.05E-02	92.7	2.68	0.12	331	2.4

Panizos

Sample	Grain	Core/Rim	$^{238}U/^{206}Pb$	1σ $^{238}U/^{206}Pb$	207Pb/206Pb	1σ 207Pb/206Pb	% 206Pb*	206Pb/238U age [Ma]	1σ 206Pb/238U age [Ma]	U (ppm)	U/Th
07BOL05	1		1.20E+01	4.13E-01	5.87E-02	4.36E-04	99.9	517	17	522	2.3
07BOL06	2		2.19E+01	8.26E-01	5.94E-02	8.57E-04	99.0	285	11	565	7.2
07BOL07	3		6.27E+02	1.39E+02	2.15E-01	9.36E-02	78.5	8.16	2.85	343	9.0
07BOL08	4		2.78E+02	1.05E+01	5.71E-01	8.39E-03	32.9	7.70	1.12	414	1.9
07BOL09	5		8.31E+02	3.37E+01	5.95E-02	3.05E-03	98.3	7.70	0.32	903	1.9
07BOL10	6		8.97E+02	3.25E+01	5.84E-02	3.38E-03	98.4	7.18	0.26	734	14.2
07BOL11	7		7.99E+02	3.18E+01	6.32E-02	3.69E-03	97.8	7.99	0.32	729	4.5
07BOL12	8		8.54E+02	3.62E+01	7.72E-02	5.69E-03	96.0	7.31	0.33	630	1.1
07BOL13	9		9.03E+02	3.83E+01	6.85E-02	5.24E-03	97.1	7.01	0.31	335	1.8
07BOL14	10		8.92E+02	3.18E+01	5.62E-02	3.95E-03	98.7	7.23	0.26	699	4.3
07BOL15	11		5.82E+02	2.66E+01	2.86E-01	4.92E-03	69.4	7.78	0.54	951	2.7
07BOL16	12		1.19E+01	4.50E-01	5.66E-02	2.58E-04	100.1	519	19	1431	1.5
07BOL17	13		1.31E+01	4.96E-01	5.69E-02	5.94E-04	100.0	474	17	328	3.0
07BOL18	14		7.82E+00	2.87E-01	6.49E-02	2.90E-04	100.0	775	27	441	2.4
07BOL19	15		8.87E+02	3.26E+01	6.26E-02	3.56E-03	97.9	7.22	0.27	647	20.8

07BOL20	16	8.00E+02	4.06E+01	1.41E-01	2.26E-02	87.9	7.17	0.47	109	3.2
07BOL21	17	9.52E+02	3.56E+01	6.84E-02	1.13E-02	97.2	6.67	0.27	286	5.6
07BOL22	18	1.40E+01	5.14E-01	5.70E-02	3.33E-04	99.8	443	16	2676	1.3
07BOL23	19	8.72E+02	3.99E+01	5.22E-02	2.64E-03	99.2	7.43	0.34	719	5.4
07BOL24	20	8.61E+02	3.95E+01	7.13E-02	8.39E-03	96.8	7.33	0.36	282	2.5
07BOL25	21	8.19E+02	3.78E+01	1.35E-01	1.09E-02	88.6	7.06	0.38	144	2.9
07BOL26	22	5.97E+00	2.20E-01	2.11E-01	1.21E-03	81.1	820	36	356	3.6
07BOL27	23	8.61E+02	3.98E+01	9.44E-02	7.92E-03	93.8	7.11	0.35	195	3.8
07BOL28	24	3.33E+00	1.18E-01	1.06E-01	2.75E-04	99.7	1688	53	603	2.5
07BOL29	25	8.36E+02	3.41E+01	5.26E-02	3.83E-03	99.2	7.74	0.32	763	5.6
07BOL30	26	1.10E+01	4.30E-01	6.40E-02	5.66E-04	99.3	559	21	261	2.6
07BOL31	27	1.15E+01	4.30E-01	5.85E-02	7.27E-04	100.0	537	19	233	3.6
07BOL32	28	8.73E+02	3.63E+01	6.62E-02	6.63E-03	97.4	7.28	0.31	440	2.6
07BOL33	29	8.75E+02	3.10E+01	5.74E-02	2.55E-03	98.6	7.36	0.26	1239	15.8
07BOL34	30	1.38E+01	4.65E-01	5.67E-02	2.86E-04	99.9	452	15	1002	1.9
07BOL35	31	2.14E+01	7.26E-01	7.27E-02	1.64E-03	97.3	286	10	235	5.0
07BOL36	32	7.77E+02	2.99E+01	1.89E-01	1.26E-02	81.8	6.87	0.34	162	3.1
07BOL37	33	9.03E+02	3.66E+01	7.20E-02	7.59E-03	96.7	6.99	0.30	365	4.3
07BOL38	34	1.66E+01	4.74E-01	5.64E-02	4.53E-04	99.7	376	11	1022	2.0

Pastos Grandes

Sample	Grain	Core/Rim	$^{238}U/^{206}Pb$	1σ $^{238}U/^{206}Pb$	207Pb/206Pb	1σ 207Pb/206Pb	% 206Pb*	206Pb/238U age [Ma]	1σ 206Pb/238U age [Ma]	U (ppm)	U/Th
BOL07027	1	C	6.46E+02	2.42E+01	4.90E-02	1.66E-03	99.6	10.04	0.38	1840	4.5
BOL07027	1	R	1.34E+03	5.03E+01	1.68E-01	7.01E-03	84.5	4.17	0.19	934	5.4
BOL07027	2	C	2.00E+03	7.39E+01	6.51E-02	4.10E-03	97.6	3.22	0.12	1451	1.9

BOL07027	3	C	1.67E+03	6.03E+01	8.26E-02	4.06E-03	95.3	3.76	0.14	3942	1.5
BOL07027	3	R	1.18E+03	5.16E+01	3.21E-01	7.44E-03	64.8	3.63	0.26	1086	7.3
BOL07027	4	C	9.83E+02	4.20E+01	1.58E-01	7.33E-03	85.8	5.72	0.29	706	5.5
BOL07027	5	R	2.00E+03	7.24E+01	6.56E-02	5.98E-03	97.5	3.24	0.12	1765	4.8
BOL07027	6	R	1.97E+03	7.35E+01	6.16E-02	4.42E-03	98.0	3.31	0.12	1783	5.1
BOL07027	7	R	1.94E+03	7.96E+01	7.02E-02	4.58E-03	96.9	3.32	0.14	1142	6.1
BOL07027	7	C	1.96E+03	7.73E+01	6.60E-02	4.34E-03	97.5	3.30	0.13	1159	5.4
BOL07027	8	R	1.57E+03	6.75E+01	2.00E-01	1.18E-02	80.4	3.40	0.19	1352	6.3
BOL07027	9	R	7.99E+02	3.71E+01	5.42E-01	1.01E-02	36.7	3.06	0.46	1418	5.0
BOL07027	10	R	2.05E+03	8.27E+01	5.58E-02	3.99E-03	98.8	3.20	0.13	2288	4.6
BOL07027	11	R	1.96E+03	6.97E+01	5.58E-02	2.35E-03	98.8	3.35	0.12	2771	8.2
BOL07027	12	R	1.89E+03	7.21E+01	6.67E-02	3.01E-03	97.4	3.41	0.13	1665	6.1
BOL07027	13	R	1.69E+03	6.16E+01	9.22E-02	5.86E-03	94.1	3.67	0.14	1262	2.0
BOL07027	14	R	2.02E+03	5.62E+01	5.77E-02	3.86E-03	98.5	3.22	0.09	2280	2.0
BOL07027	15	C	2.11E+03	4.17E+01	7.21E-02	5.32E-03	96.7	3.05	0.06	1545	3.3
BOL07027	15	R	1.81E+03	5.23E+01	6.35E-02	4.29E-03	97.8	3.57	0.10	2286	5.7
BOL07027	16	R	1.73E+03	5.05E+01	6.81E-02	7.13E-03	97.2	3.71	0.11	1182	6.0
BOL07027	17	R	1.41E+03	4.98E+01	5.38E-02	3.67E-03	99.0	4.61	0.16	1937	2.9
BOL07027	18	R	1.67E+03	4.36E+01	5.63E-02	4.26E-03	98.7	3.91	0.10	2135	4.5
BOL07027	19	R	2.14E+03	7.07E+01	7.70E-02	8.12E-03	96.0	3.00	0.10	1326	4.7
BOL07027	20	R	1.80E+03	4.01E+01	5.81E-02	2.88E-03	98.5	3.61	0.08	4420	1.7
BOL07027	21	C	3.72E+02	8.53E+00	5.73E-02	2.03E-03	98.6	17.16	0.40	1822	4.8
BOL07027	21	R	1.79E+03	3.60E+01	6.15E-02	2.98E-03	98.0	3.63	0.07	3298	3.3
BOL07027	22	R	2.03E+03	4.96E+01	6.78E-02	4.79E-03	97.2	3.19	0.08	1968	4.9
BOL07027	23	R	2.13E+03	5.24E+01	6.05E-02	3.29E-03	98.2	3.06	0.08	2277	3.9
BOL07027	24	R	1.89E+03	5.09E+01	5.73E-02	3.85E-03	98.6	3.45	0.09	1650	3.3
BOL07027	25	R	2.09E+03	5.88E+01	8.03E-02	1.17E-02	95.6	3.04	0.10	1188	5.2
BOL07027	26	C	1.91E+03	3.94E+01	5.98E-02	4.81E-03	98.3	3.41	0.07	1817	5.0

BOL07027	26	R	1.87E+03	4.71E+01	5.26E-02	4.26E-03	99.2	3.52	0.09	1788	5.2
BOL07027	27	C	1.75E+03	4.79E+01	6.24E-02	5.40E-03	97.9	3.71	0.10	1762	5.1
BOL07027	27	R	7.03E+02	1.83E+01	5.84E-01	9.24E-03	31.2	2.95	0.28	1269	2.5
BOL07027	28	R	2.04E+03	6.67E+01	6.21E-02	2.26E-03	98.0	3.19	0.10	3110	5.6
BOL07027	29	C	1.76E+03	6.41E+01	5.22E-02	1.81E-03	99.2	3.70	0.13	3967	1.4
BOL07027	29	R	1.82E+03	6.81E+01	5.52E-02	3.62E-03	98.8	3.60	0.13	2309	6.9
BOL07027	30	C	1.95E+03	7.49E+01	6.55E-02	4.12E-03	97.5	3.32	0.13	934	6.4
BOL07027	30	R	2.16E+03	8.37E+01	5.20E-02	3.04E-03	99.2	3.06	0.12	1742	4.7
BOL07027	31	C	1.75E+03	7.47E+01	6.62E-02	4.98E-03	97.4	3.70	0.16	1237	6.1
BOL07027	31	R	1.97E+03	7.80E+01	5.54E-02	5.80E-03	98.8	3.33	0.13	1369	5.7
SDS5	1	R	2.02E+03	9.03E+01	4.69E-02	3.34E-03	99.9	3.29	0.14	2244	
SDS5	2	C	1.73E+03	8.19E+01	5.97E-02	6.05E-03	98.3	3.76	0.18	1145	
SDS5	3	R	2.16E+03	8.28E+01	5.62E-02	3.88E-03	98.7	3.03	0.12	2102	
SDS5	4	R	1.87E+03	7.07E+01	1.33E-01	6.51E-03	88.9	3.15	0.13	2511	
SDS5	5	R	2.06E+03	7.37E+01	6.16E-02	3.77E-03	98.0	3.16	0.11	2377	
SDS5	6	R	1.59E+03	7.06E+01	5.39E-02	3.12E-03	99.0	4.10	0.18	2213	
SDS5	7	R	2.09E+03	9.00E+01	6.83E-02	7.88E-03	97.2	3.10	0.14	1839	
SDS5	8	R	2.16E+03	9.31E+01	5.74E-02	5.52E-03	98.6	3.03	0.13	2165	
SDS5	9	R	8.55E+02	3.65E+01	5.38E-02	3.26E-03	99.0	7.55	0.32	2422	
SDS5	10	R	2.06E+03	8.92E+01	5.48E-02	5.28E-03	98.9	3.19	0.14	2614	
SDS5	11	R	1.19E+03	4.97E+01	3.86E-01	1.01E-02	56.6	3.16	0.26	1505	
SDS5	12	R	2.01E+03	8.12E+01	1.09E-01	5.15E-03	91.9	3.03	0.13	2075	
SDS5	13	R	1.78E+03	8.14E+01	1.83E-01	6.40E-03	82.5	3.08	0.17	2385	
SDS5	14	R	1.95E+03	8.08E+01	4.51E-02	4.25E-03	100.1	3.41	0.14	2335	
SDS5	15	C	1.82E+03	7.88E+01	5.95E-02	3.70E-03	98.3	3.59	0.16	1893	
SDS5	16	R	1.95E+03	8.65E+01	5.89E-02	3.23E-03	98.4	3.35	0.15	2622	
SDS5	17	R	4.44E+02	1.77E+01	6.68E-01	1.08E-02	20.5	3.07	0.75	1063	
SDS5	18	R	1.87E+03	7.02E+01	4.70E-02	3.54E-03	99.9	3.53	0.13	2078	

SDS5	19	R	2.04E+03	8.93E+01	5.62E-02	3.56E-03	98.7	3.22	0.14	2330
SDS5	20	R	1.84E+03	7.92E+01	6.17E-02	3.62E-03	98.0	3.52	0.15	2009
SDS5	21	R	2.04E+03	9.02E+01	5.76E-02	3.57E-03	98.5	3.20	0.14	2689
SDS5	22	R	1.86E+03	8.33E+01	5.54E-02	3.17E-03	98.8	3.52	0.16	2101
SDS5	23	R	2.03E+03	9.65E+01	9.35E-02	5.17E-03	93.9	3.07	0.15	1716

Puripica Chico

Sample	Grain	Core/Rim	$^{238}U/^{206}Pb$	1σ $^{238}U/^{206}Pb$	207Pb/206Pb	1σ 207Pb/206Pb	% 206Pb*	206Pb/238U age [Ma]	1σ 206Pb/238U age [Ma]	U (ppm)	U/Th
07BOI-023-PD	1	R	2.76E+03	7.33E+01	1.74E-01	1.03E-02	83.6	2.04	0.07	1538	2.6
07BOI-023-PD	2	R	1.39E+03	8.91E+01	5.11E-01	1.50E-02	40.6	1.96	0.35	1401	1.7
07BOI-023-PD	3	R	3.25E+03	8.78E+01	7.45E-02	5.74E-03	96.4	2.00	0.06	1300	2.7
07BOI-023-PD	4	R	3.06E+03	6.67E+01	7.69E-02	7.64E-03	96.1	2.12	0.05	1177	3.2
07BOI-023-PD	5	R	2.96E+03	7.73E+01	7.88E-02	6.83E-03	95.8	2.18	0.06	1055	2.9
07BOI-023-PD	6	R	3.56E+03	9.58E+01	8.48E-02	8.17E-03	95.0	1.81	0.05	1101	3.2
07BOI-023-PD	7	R	3.51E+03	9.51E+01	9.15E-02	9.63E-03	94.2	1.83	0.06	768	3.7
07BOI-023-PD	8	C	3.41E+03	7.73E+01	8.70E-02	5.84E-03	94.8	1.89	0.04	1199	3.1
07BOI-023-PD	9	R	2.31E+03	6.09E+01	1.25E-01	1.50E-02	89.9	2.60	0.09	1147	4.0
07BOI-023-PD	10	R	3.25E+03	8.65E+01	1.01E-01	6.20E-03	92.9	1.94	0.06	1167	3.1
07BOI-023-PD	11	R	3.11E+03	8.05E+01	9.45E-02	9.61E-03	93.8	2.04	0.06	662	4.4
07BOI-023-PD	12	R	2.99E+03	7.69E+01	6.71E-02	5.01E-03	97.3	2.19	0.06	1286	3.2
07BOI-023-PD	13	R	3.57E+03	9.01E+01	7.08E-02	5.55E-03	96.8	1.84	0.05	1440	3.5
07BOI-023-PD	14	R	2.83E+03	7.91E+01	7.89E-02	4.52E-03	95.8	2.28	0.06	1645	4.6
07BOI-023-PD	15	C	2.54E+03	5.90E+01	7.85E-02	7.53E-03	95.9	2.53	0.06	956	3.3
07BOI-023-PD	16	R	5.72E+02	1.40E+01	7.30E-01	1.65E-02	12.6	1.52	0.41	405	4.5
07BOI-023-PD	17	R	2.57E+03	7.68E+01	2.65E-01	1.28E-02	72.0	1.90	0.09	911	3.1

07BOI-023-PD	18	R	3.16E+03	8.91E+01	8.43E-02	8.57E-03	95.1	2.03	0.06	737	3.1
07BOI-023-PD	19	R	2.93E+03	6.38E+01	6.81E-02	4.71E-03	97.2	2.23	0.05	1804	3.3
07BOI-023-PD	20	R	5.07E+01	3.85E+00	8.13E-01	4.85E-03	1.9	2.57	13.65	1266	3.2
07BOI-023-PD	21	R	2.87E+03	6.18E+01	6.03E-02	3.98E-03	98.2	2.29	0.05	1948	1.9
07BOI-023-PD	23	R	3.45E+03	9.95E+01	7.97E-02	8.71E-03	95.7	1.87	0.06	978	2.4
07BOI-023-PD	24	R	3.16E+03	8.47E+01	7.08E-02	6.72E-03	96.8	2.07	0.06	1332	3.8
07BOI-023-PD	25	R	2.58E+03	5.78E+01	7.84E-02	5.84E-03	95.9	2.49	0.06	1057	3.3
07BOI-023-PD	26	R	2.96E+03	7.80E+01	7.53E-02	5.19E-03	96.3	2.19	0.06	1212	3.4
07BOI-023-PD	27	C	1.42E+03	3.15E+01	6.33E-02	5.07E-03	97.8	4.55	0.11	880	4.3
07BOI-023-PD	28	R	3.37E+03	7.80E+01	8.29E-02	5.87E-03	95.3	1.91	0.05	1198	2.3
07BOI-023-PD	29	R	3.07E+03	7.24E+01	6.90E-02	4.57E-03	97.1	2.13	0.05	1432	3.3
07BOI-023-PD	30	R	3.13E+03	7.44E+01	7.80E-02	8.11E-03	95.9	2.07	0.05	1123	3.5
07BOI-023-PD	31	R	3.07E+03	7.21E+01	7.63E-02	6.37E-03	96.1	2.11	0.05	948	3.4
07BOI-023-PD	31	C	2.64E+03	6.30E+01	5.57E-02	4.03E-03	98.8	2.50	0.06	2514	2.6
07BOI-023-PD	32	R	2.81E+03	7.77E+01	8.87E-02	7.94E-03	94.6	2.27	0.07	862	4.2
07BOI-023-PD	33	R	2.29E+03	7.04E+01	3.21E-01	2.61E-02	64.8	1.92	0.13	532	4.1
07BOI-023-PD	33	C	2.85E+03	8.10E+01	1.66E-01	8.99E-03	84.7	2.00	0.07	1234	2.2
07BOI-023-PD	34	R	2.86E+03	6.67E+01	7.38E-02	7.13E-03	96.5	2.26	0.06	1114	3.0
07BOI-023-PD	35	R	3.01E+03	1.28E+02	1.87E-01	1.85E-02	82.0	1.85	0.11	791	3.0
07BOI-023-PD	36	R	2.80E+03	6.18E+01	1.82E-01	1.05E-02	82.6	2.00	0.06	1169	3.3
07BOI-023-PD	37	R	2.96E+03	7.02E+01	7.16E-02	4.49E-03	96.7	2.20	0.05	1535	2.7
07BOI-023-PD	38	R	3.24E+03	7.35E+01	8.56E-02	8.86E-03	95.0	1.98	0.05	1051	3.4
07BOI-023-PD	39	R	2.97E+03	8.66E+01	1.83E-01	1.28E-02	82.5	1.89	0.07	1065	3.4
07BOI-023-PD	39	C	2.98E+03	7.58E+01	8.80E-02	6.24E-03	94.6	2.14	0.06	846	3.7
07BOI-023-PD	40	R	3.46E+03	1.01E+02	1.11E-01	9.99E-03	91.8	1.80	0.06	894	2.5
07BOI-023-PD	41	R	2.44E+03	6.32E+01	1.70E-01	5.60E-03	84.2	2.31	0.07	1482	2.9
07BOI-023-PD	42	C	2.32E+03	1.06E+02	2.13E-01	2.44E-02	78.6	2.29	0.16	435	5.3
07BOI-023-PD	43	R	3.10E+03	5.04E+01	6.06E-02	2.89E-03	98.1	2.12	0.03	2881	1.6

07BOI-023-PD	44	R	3.54E+03	8.73E+01	1.02E-01	6.72E-03	92.9	1.78	0.05	988	3.1
07BOI-023-PD	45	R	5.00E+02	1.89E+01	6.85E-01	1.75E-02	18.4	2.47	0.80	661	4.9
07BOI-023-PD	46	R	2.77E+03	6.91E+01	1.22E-01	9.85E-03	90.3	2.19	0.07	1005	4.0
07BOI-023-PD	47	R	1.42E+03	1.01E+02	5.33E-01	2.96E-02	37.7	1.81	0.47	948	3.6
07BOI-023-PD	48	R	2.33E+03	5.83E+01	6.46E-02	3.98E-03	97.6	2.79	0.07	1027	3.9
07BOI-023-PD	49	R	3.13E+03	9.81E+01	9.37E-02	1.07E-02	93.9	2.03	0.07	867	4.2

Puripicar

Sample	Grain	Core/Rim	$^{238}U/^{206}Pb$	1σ $^{238}U/^{206}Pb$	207Pb/206Pb	1σ 207Pb/206Pb	% 206Pb*	206Pb/238U age [Ma]	1σ 206Pb/238U age [Ma]	U (ppm)	U/Th
83015	1	R	1.20E+03	4.85E+01	1.36E-01	1.18E-02	88.5	4.83	0.23	192	2.6
83015	2	R	1.38E+03	2.77E+01	7.07E-02	6.08E-03	96.9	4.61	0.10	985	3.4
83015	3	R	1.50E+03	3.09E+01	7.54E-02	6.07E-03	96.3	4.24	0.10	669	4.7
83015	4	R	8.42E+02	1.69E+01	5.75E-02	2.49E-03	98.6	7.64	0.16	1163	8.0
83015	5	C	1.43E+03	2.74E+01	6.71E-02	3.16E-03	97.3	4.48	0.09	1388	3.8
83015	6	R	1.63E+02	5.94E+00	7.49E-01	7.63E-03	10.1	4.09	2.05	572	2.0
83015	7	R	1.50E+03	3.11E+01	6.67E-02	4.03E-03	97.4	4.28	0.09	1104	6.3
83015	8	R	1.35E+03	2.71E+01	6.75E-02	3.99E-03	97.3	4.72	0.10	890	3.2
83015	9	C	1.09E+03	3.29E+01	1.10E-01	1.03E-02	91.8	5.49	0.19	260	2.6
83015	10	R	1.47E+03	3.09E+01	9.94E-02	7.44E-03	93.2	4.17	0.10	372	2.4
83015	11	R	1.27E+03	2.73E+01	6.77E-02	4.37E-03	97.2	5.02	0.11	653	2.6
83015	13	C	1.40E+03	2.72E+01	7.42E-02	4.25E-03	96.4	4.51	0.09	786	1.9
83015	14	R	1.19E+03	3.02E+01	9.40E-02	1.01E-02	93.9	5.15	0.15	335	2.4
83015	16	R	1.13E+03	2.28E+01	2.28E-01	6.74E-03	76.8	4.46	0.13	1008	1.7
83015	17	R	1.14E+03	1.81E+01	5.07E-02	2.08E-03	99.4	5.73	0.09	6350	6.2
83015	19	C	1.31E+03	2.52E+01	5.87E-02	3.07E-03	98.4	4.94	0.10	982	2.8

83015	20	C	1.44E+03	3.24E+01	8.41E-02	6.25E-03	95.1	4.34	0.11	556	2.3
83015	21	R	1.39E+03	4.13E+01	1.40E-01	1.41E-02	88.0	4.16	0.16	228	1.8
83015	22	R	1.10E+03	4.44E+01	2.07E-01	2.18E-02	79.4	4.76	0.30	391	2.6
83015	23	R	1.42E+03	4.02E+01	9.05E-02	7.42E-03	94.3	4.38	0.14	470	2.9
83015	24	R	1.42E+03	4.93E+01	9.80E-02	1.15E-02	93.4	4.31	0.17	309	2.1
83015	25	R	1.45E+03	5.22E+01	8.22E-02	3.89E-03	95.4	4.33	0.16	905	2.1
83015	26	R	1.50E+03	3.00E+01	5.76E-02	5.18E-03	98.5	4.34	0.09	1054	5.6
83015	27	R	1.38E+03	3.91E+01	8.81E-02	6.05E-03	94.6	4.50	0.14	391	3.1
83015	28	R	1.34E+03	3.10E+01	6.20E-02	3.98E-03	98.0	4.80	0.11	853	3.8
83015	29	R	1.21E+03	4.01E+01	1.06E-01	9.28E-03	92.4	5.03	0.19	217	3.2
83015	30	C	1.33E+03	2.63E+01	1.14E-01	5.46E-03	91.3	4.51	0.10	1022	5.9
83015	31	R	1.43E+03	3.84E+01	7.22E-02	8.15E-03	96.7	4.45	0.13	712	1.7
83015	32	R	1.26E+03	3.64E+01	1.25E-01	9.17E-03	89.9	4.68	0.16	310	3.3
83015	33	C	2.12E+01	7.25E-01	6.29E-02	2.05E-03	98.6	294	10	115	1.1
83015	34	R	1.38E+03	4.88E+01	1.08E-01	8.78E-03	92.1	4.39	0.17	298	6.0
83015	35	C	1.42E+03	3.29E+01	9.10E-02	1.06E-02	94.3	4.36	0.12	411	2.1
83015	36	C	1.34E+03	4.36E+01	9.83E-02	7.00E-03	93.3	4.59	0.16	361	2.6
83015	37	R	1.39E+03	2.83E+01	5.60E-02	3.23E-03	98.7	4.68	0.10	1104	3.1
83015	38	C	1.39E+03	3.29E+01	1.42E-01	1.02E-02	87.7	4.16	0.12	460	3.4
83015	39	C	1.11E+03	2.74E+01	7.65E-02	4.73E-03	96.1	5.64	0.15	528	2.2
83015	40	C	1.35E+03	3.30E+01	9.03E-02	9.72E-03	94.4	4.58	0.13	497	3.2
83015	41	C	1.43E+03	3.42E+01	6.95E-02	5.44E-03	97.0	4.47	0.11	620	3.2
83015	42	C	1.39E+03	2.82E+01	7.47E-02	5.01E-03	96.3	4.56	0.10	712	2.2
83015	43	R	1.38E+03	3.53E+01	8.10E-02	6.19E-03	95.5	4.56	0.13	481	2.5
83015	44	R	1.39E+03	3.42E+01	6.96E-02	8.19E-03	97.0	4.59	0.12	558	3.2
83015	45	R	1.39E+03	1.89E+01	5.23E-02	2.18E-03	99.2	4.69	0.06	3042	11.4
83015	46	R	1.42E+03	2.71E+01	6.27E-02	4.33E-03	97.9	4.52	0.09	1034	2.8
83015	47	R	1.48E+03	3.31E+01	7.52E-02	5.50E-03	96.3	4.29	0.10	514	5.4

83015	48	R	1.21E+03	3.79E+01	1.03E-01	1.44E-02	92.7	5.02	0.20	993	3.9
83015	49	R	1.32E+03	3.78E+01	8.36E-02	8.18E-03	95.2	4.76	0.15	396	3.5
83015	50	C	1.33E+03	4.30E+01	7.52E-02	5.59E-03	96.3	4.77	0.16	522	4.0
83015	51	R	1.34E+03	2.68E+01	6.65E-02	7.20E-03	97.4	4.77	0.11	821	1.9
83015	52	R	1.37E+03	4.06E+01	8.98E-02	7.76E-03	94.4	4.54	0.15	324	4.5
83015	53	R	1.57E+03	3.48E+01	8.28E-02	1.13E-02	95.3	4.02	0.11	549	3.5
83015	1	R						4.38	0.11		
83015	1	C						4.47	0.11		
83015	2	C						4.48	0.16		
83015	2	R						4.32	0.12		
83015	3	C						4.91	0.12		
83015	3	R						4.57	0.14		
83015	5	C						5.18	0.18		
83015	5	R						4.93	0.14		
83015	6	C						4.53	0.20		
83015	7	C						4.48	0.17		
83015	8	C						4.61	0.16		
83015	9	C						4.34	0.11		
83015	18	C						5.15	0.19		
83015	18	R						4.92	0.11		
83015	20	C						5.26	0.20		
83015	20	R						3.73	1.74		

Sifon

Sample	Grain	Core/Rim	$^{238}U/^{206}Pb$	1σ $^{238}U/^{206}Pb$	207Pb/206Pb	1σ 207Pb/206Pb	% 206Pb*	206Pb/238U age [Ma]	1σ 206Pb/238U age [Ma]	U (ppm)	U/Th

83001	1	R	3.15E+02	1.13E+01	5.06E-01	1.33E-02	41.1	8.50	0.94	343	2.0
83001	2	R	7.48E+02	1.56E+01	7.85E-02	4.92E-03	95.9	8.35	0.19	553	3.8
83001	3	C	6.80E+02	1.75E+01	8.82E-02	5.55E-03	94.6	9.07	0.25	393	8.6
83001	4	C	1.51E+01	7.56E-01	8.04E-01	8.88E-03	3.1	13.2	30.7	987	1.8
83001	5	R	4.69E+02	1.02E+01	3.52E-01	1.14E-02	60.8	8.45	0.36	507	5.0
83001	6	R	6.43E+02	1.14E+01	2.22E-01	9.81E-03	77.6	7.87	0.22	566	4.5
83001	7	R	7.54E+02	1.50E+01	6.77E-02	3.45E-03	97.2	8.40	0.17	693	4.1
83001	8	C	6.98E+02	1.40E+01	1.05E-01	9.99E-03	92.5	8.61	0.22	454	1.3
83001	9	C	7.23E+02	1.18E+01	5.61E-02	2.34E-03	98.7	8.90	0.15	1435	15.5
83001	10	C	7.58E+02	1.30E+01	5.85E-02	3.14E-03	98.4	8.47	0.15	1211	9.3
83001	11	R	7.49E+02	1.57E+01	7.21E-02	4.70E-03	96.7	8.40	0.19	438	2.3
83001	12	R	7.67E+02	1.26E+01	5.35E-02	2.41E-03	99.1	8.42	0.14	1583	9.3
83001	13	R	7.63E+02	1.49E+01	6.16E-02	3.64E-03	98.0	8.37	0.17	939	7.8
83001	14	R	7.08E+02	1.32E+01	7.32E-02	4.48E-03	96.6	8.87	0.18	1800	2.6
83001	15	R	6.20E+02	3.00E+01	2.42E-01	2.83E-02	75.0	7.87	0.70	732	1.7
83001	16	R	7.55E+02	1.48E+01	5.60E-02	2.88E-03	98.7	8.51	0.17	1051	2.0
83001	17	R	7.43E+02	1.44E+01	6.17E-02	3.07E-03	98.0	8.60	0.17	925	8.9
83001	18	R	7.05E+02	1.68E+01	7.07E-02	4.42E-03	96.9	8.96	0.22	620	6.1
83001	19	R	7.94E+02	1.58E+01	6.97E-02	5.44E-03	97.0	7.95	0.17	520	2.1
83001	21	R	8.08E+02	1.65E+01	5.28E-02	2.97E-03	99.2	8.00	0.17	1013	3.4
83001	22	R	7.42E+02	1.10E+01	5.01E-02	1.45E-03	99.5	8.74	0.13	3697	4.4
83001	23	R	7.47E+02	1.32E+01	5.48E-02	2.81E-03	98.9	8.62	0.16	1484	3.9
83001	24	C	5.39E+02	2.52E+01	2.94E-01	2.10E-02	68.3	8.26	0.73	473	4.5
83001	26	C	7.25E+02	1.34E+01	5.57E-02	3.08E-03	98.8	8.88	0.17	1427	12.3
83001	27	R	6.79E+02	1.25E+01	5.19E-02	1.89E-03	99.3	9.52	0.18	1979	5.8
83001	28	C	6.73E+02	2.09E+01	1.02E-01	7.14E-03	92.8	8.96	0.31	149	1.7
83001	29	C	7.23E+02	1.32E+01	7.57E-02	2.01E-03	96.2	8.66	0.16	1942	2.0
83001	30	C	5.75E+02	2.26E+01	1.91E-01	7.64E-03	81.5	9.20	0.48	217	1.5

83001	31	C	7.02E+02	1.78E+01	7.24E-02	6.27E-03	96.7	8.96	0.24	381	2.5
83001	32	C	6.73E+02	1.25E+01	5.20E-02	1.66E-03	99.3	9.60	0.18	1757	7.0
83001	33	R	7.65E+02	1.46E+01	7.05E-02	4.95E-03	96.9	8.25	0.17	309	3.6
83001	34	R	7.12E+02	1.75E+01	8.46E-02	6.03E-03	95.1	8.69	0.23	303	2.2
83001	35	R	7.46E+02	1.47E+01	5.69E-02	1.97E-03	98.6	8.63	0.17	1313	13.6
83001	36	R	7.33E+02	1.24E+01	5.09E-02	1.99E-03	99.4	8.80	0.15	2096	1.1
83001	37	C	7.23E+02	1.29E+01	5.26E-02	2.39E-03	99.2	8.94	0.16	1912	7.6
83001	38	C	7.28E+02	1.48E+01	6.15E-02	3.52E-03	98.0	8.77	0.18	671	3.5
83001	39	R	6.63E+02	1.14E+01	1.51E-01	6.17E-03	86.6	8.52	0.19	1147	6.7
83001	40	C	7.69E+02	1.33E+01	5.05E-02	2.00E-03	99.4	8.41	0.15	1358	2.0
83001	41	R	7.23E+02	1.59E+01	7.29E-02	5.34E-03	96.6	8.70	0.21	663	3.1
83001	42	C	7.23E+02	1.33E+01	5.63E-02	3.06E-03	98.7	8.90	0.17	1262	6.6
83001	44	R	5.49E+02	1.45E+01	2.80E-01	7.58E-03	70.1	8.32	0.35	391	3.4
83001	46	R	7.29E+02	1.22E+01	5.62E-02	2.71E-03	98.7	8.83	0.15	1322	8.2
83001	49	R	5.81E+02	4.28E+01	1.87E-01	3.68E-02	82.0	9.16	1.05	1086	1.2
83001	50	C	6.48E+02	1.09E+01	5.02E-02	1.16E-03	99.5	10.0	0.2	2875	12.9
83001	51	R	7.36E+02	1.54E+01	9.10E-02	9.97E-03	94.3	8.35	0.22	652	4.2
83001	52	R	6.80E+02	1.25E+01	1.51E-01	4.77E-03	86.6	8.29	0.18	1061	2.3
83001	53	R	6.94E+02	1.20E+01	5.05E-02	1.31E-03	99.5	9.33	0.16	3218	8.3
83001	54	C	7.30E+02	1.37E+01	5.70E-02	3.62E-03	98.6	8.80	0.17	681	6.0
83001	55	C	6.13E+02	1.57E+01	2.32E-01	7.99E-03	76.2	8.10	0.30	376	2.9
83001	56	R	7.17E+02	1.38E+01	5.40E-02	2.67E-03	99.0	9.00	0.18	1887	17.3
84048	1	C						8.49	0.21		
84048	3	C						9.38	0.25		
84048	4	C						9.44	0.21		
84048	5	C						8.92	0.22		
84048	6	C						8.17	0.20		
84048	6	R						9.05	0.20		

84048	7	C	9.02	0.43
84048	8	C	8.42	0.36
84048	9	C	7.96	0.38
84048	19	C	373.15	6.84
84048	22	C	8.79	0.20
84048	23	C	8.96	0.26

Tara

Sample	Grain	Core/Rim	$^{238}U/^{206}Pb$	1σ $^{238}U/^{206}Pb$	207Pb/206Pb	1σ 207Pb/206Pb	% 206Pb*	206Pb/238U age [Ma]	1σ 206Pb/238U age [Ma]	U (ppm)	U/Th
BOL-06-013	1	C	1.77E+03	6.52E+01	1.34E-01	1.58E-02	88.8	3.32	0.15	261	3.2
BOL-06-013	2	C	1.65E+03	6.90E+01	1.27E-01	9.85E-03	89.7	3.60	0.17	243	2.7
BOL-06-013	3	C	1.72E+03	6.47E+01	1.44E-01	9.98E-03	87.5	3.36	0.15	331	1.8
BOL-06-013	4	R	1.69E+03	4.11E+01	1.30E-01	8.24E-03	89.2	3.49	0.10	539	2.3
BOL-06-013	5	C	1.55E+03	3.85E+01	1.11E-01	9.38E-03	91.7	3.90	0.11	542	1.8
BOL-06-013	6	C	1.57E+03	7.44E+01	1.46E-01	1.03E-02	87.2	3.66	0.21	237	1.7
BOL-06-013	7	C	1.72E+03	3.69E+01	8.35E-02	4.33E-03	95.2	3.67	0.08	1204	4.7
BOL-06-013	7	R	1.61E+03	4.74E+01	9.43E-02	5.62E-03	93.8	3.85	0.12	565	3.9
BOL-06-013	8	C	1.67E+03	4.72E+01	1.25E-01	1.68E-02	89.9	3.55	0.13	348	2.1
BOL-06-013	9	R	1.54E+03	4.81E+01	1.47E-01	1.40E-02	87.1	3.71	0.15	236	1.7
BOL-06-013	10	R	1.73E+03	4.32E+01	1.06E-01	8.68E-03	92.4	3.53	0.10	473	2.6
BOL-06-013	11	R	6.47E+02	1.45E+01	5.53E-01	1.22E-02	35.2	3.59	0.30	398	2.4
BOL-06-013	12	R	1.73E+03	4.63E+01	1.26E-01	1.27E-02	89.8	3.42	0.11	352	1.9
BOL-06-013	13	C	1.69E+03	5.50E+01	1.16E-01	1.02E-02	91.1	3.55	0.14	351	2.2
BOL-06-013	14	R	1.63E+03	8.14E+01	1.52E-01	2.38E-02	86.5	3.52	0.24	243	3.5
BOL-06-013	15	C	1.69E+03	4.93E+01	1.14E-01	8.90E-03	91.4	3.57	0.12	374	2.7

BOL-06-013	16	R	1.55E+03	4.53E+01	1.52E-01	9.46E-03	86.5	3.67	0.13	503	1.4
BOL-06-013	17	R	7.30E+01	2.26E+00	8.09E-01	7.19E-03	2.4	2.19	3.96	246	1.5
BOL-06-013	18	R	1.50E+03	3.89E+01	1.98E-01	1.18E-02	80.5	3.56	0.13	354	3.4
BOL-06-013	19	C	1.65E+03	4.23E+01	9.30E-02	8.96E-03	94.0	3.76	0.11	507	3.5
BOL-06-013	20	R	1.69E+03	4.36E+01	8.39E-02	5.56E-03	95.2	3.73	0.10	423	2.9
BOL-06-013	21	R	1.71E+03	6.39E+01	1.15E-01	1.11E-02	91.1	3.52	0.15	261	2.0
BOL-06-013	22	C	1.77E+03	4.88E+01	8.99E-02	7.18E-03	94.4	3.50	0.10	476	1.4
BOL-06-013	23	R	1.73E+03	5.84E+01	1.18E-01	1.25E-02	90.8	3.48	0.14	256	2.3
BOL-06-013	24	C	1.71E+03	4.13E+01	8.29E-02	7.88E-03	95.3	3.70	0.10	357	3.6
BOL-06-013	25	R	1.73E+03	5.58E+01	9.55E-02	9.70E-03	93.7	3.57	0.13	320	2.5
BOL-06-013	26	R	1.61E+03	4.16E+01	8.28E-02	5.72E-03	95.3	3.92	0.11	552	4.4
BOL-06-013	27	C	9.12E+02	7.38E+01	4.32E-01	2.90E-02	50.7	3.67	0.75	280	4.3
BOL-06-013	28	R	1.67E+03	5.76E+01	1.11E-01	1.12E-02	91.7	3.63	0.14	257	3.2
BOL-06-013	29	R	1.58E+03	4.16E+01	1.99E-01	1.31E-02	80.5	3.36	0.12	380	1.9
BOL-06-013	30	R	1.42E+03	3.69E+01	7.74E-02	5.60E-03	96.0	4.44	0.12	399	2.5
BOL-06-013	30	C	1.01E+03	2.43E+01	6.82E-02	5.16E-03	97.2	6.27	0.16	444	2.8
BOL-06-013	31	R	1.35E+03	5.19E+01	3.13E-01	2.41E-02	65.9	3.22	0.24	325	2.1
BOL-06-013	32	R	1.89E+03	7.45E+01	5.85E-02	3.13E-03	98.4	3.45	0.14	1413	4.0
BOL-06-013	33	R	1.25E+03	1.09E+02	2.82E-01	2.54E-02	69.9	3.71	0.54	413	3.4
BOL-06-013	34	C	1.61E+03	3.42E+01	8.68E-02	4.75E-03	94.8	3.88	0.09	1630	3.6
BOL-06-013	35	R	1.75E+03	7.03E+01	9.56E-02	8.65E-03	93.7	3.53	0.15	291	2.5
BOL-06-013	36	R	1.75E+03	5.24E+01	1.00E-01	1.06E-02	93.1	3.51	0.12	460	2.0
BOL-06-013	37	R	1.90E+03	7.98E+01	8.39E-02	9.47E-03	95.2	3.32	0.15	401	2.3
BOL-06-013	38	R	1.60E+03	5.12E+01	1.38E-01	1.16E-02	88.3	3.64	0.14	239	2.0
BOL-06-013	39	R	1.77E+03	6.46E+01	9.94E-02	8.82E-03	93.2	3.48	0.14	331	2.2
BOL-06-013	40	R	9.12E+02	4.34E+01	4.47E-01	3.17E-02	48.7	3.54	0.54	313	3.3
BOL-06-013	41	R	1.82E+03	4.93E+01	7.56E-02	5.97E-03	96.2	3.49	0.10	555	2.0
BOL-06-013	42	R	1.86E+03	7.81E+01	9.54E-02	1.12E-02	93.7	3.34	0.15	376	2.2

BOL-06-013	43	R	1.68E+03	3.16E+01	6.01E-02	2.31E-03	98.2	3.86	0.07	2468	3.5
BOL-06-013	44	C	1.72E+03	5.95E+01	1.15E-01	1.25E-02	91.2	3.50	0.14	216	2.0
BOL-06-013	45	R	1.69E+03	3.98E+01	6.98E-02	5.16E-03	97.0	3.80	0.09	739	3.1
BOL-06-013	45	C	1.63E+03	6.52E+01	1.09E-01	1.07E-02	92.0	3.72	0.16	370	2.2
BOL-06-013	46	R	1.59E+03	4.20E+01	1.72E-01	1.16E-02	83.9	3.49	0.12	352	1.6
BOL-06-013	47	C	6.43E+02	1.54E+01	5.44E-01	1.15E-02	36.4	3.73	0.32	333	2.3

Toconao

Sample	Grain	Core/Rim	$^{238}U/^{206}Pb$	1σ $^{238}U/^{206}Pb$	207Pb/206Pb	1σ 207Pb/206Pb	% 206Pb*	206Pb/238U age [Ma]	1σ 206Pb/238U age [Ma]	U (ppm)	U/Th
88052B	2	R	6.87E+02	2.29E+01	6.38E-02	7.02E-03	97.8	9.26	0.32	352	3.3
88052B	4	R	1.05E+03	4.20E+01	7.64E-02	5.05E-03	96.1	5.99	0.25	436	2.6
88052B	5	R	1.40E+03	5.09E+01	6.23E-02	5.17E-03	97.9	4.61	0.17	1942	4.9
88052B	8	R	1.38E+03	5.19E+01	6.16E-02	3.34E-03	98.0	4.68	0.18	1218	5.5
88052B	11	C	2.68E+02	1.97E+01	6.75E-01	8.68E-03	19.6	4.81	2.39	653	4.1
88052B	14	R	1.40E+03	4.77E+01	7.83E-02	4.37E-03	95.9	4.49	0.16	918	3.3
88052B	19	C	1.48E+03	5.26E+01	9.15E-02	6.77E-03	94.2	4.19	0.16	379	2.7
88052B	19	R	1.14E+03	4.74E+01	1.65E-01	9.41E-03	84.8	4.90	0.25	1116	4.4
88052B	22	R	1.45E+03	7.71E+01	2.00E-01	2.73E-02	80.4	3.67	0.31	383	2.3
88052B	26	R	1.36E+03	6.18E+01	7.61E-02	5.29E-03	96.2	4.65	0.22	436	2.5
88052B	30	M	1.06E+03	4.33E+01	6.52E-02	7.23E-03	97.6	6.02	0.25	342	4.8
88052B	30	R	9.71E+02	3.59E+01	5.02E-02	1.82E-03	99.5	6.70	0.25	2209	4.8
88052B	30	C	1.05E+01	4.46E-01	6.10E-02	5.15E-04	99.8	583	24	478	1.3
88052B	32	R	1.34E+03	5.28E+01	7.53E-02	7.09E-03	96.3	4.73	0.19	407	2.3
88052B	33	R	1.30E+03	5.46E+01	6.92E-02	4.83E-03	97.1	4.89	0.21	811	4.5
88052B	34	R	1.42E+03	6.40E+01	7.47E-02	7.04E-03	96.3	4.48	0.21	450	3.8

88052B	36	R	9.71E+02	5.43E+01	3.53E-01	1.95E-02	60.7	4.11	0.43	119	1.8
88052B	36	C	1.38E+03	6.46E+01	1.37E-01	1.12E-02	88.4	4.19	0.23	177	1.4
88052B	38	R	1.46E+03	5.66E+01	6.43E-02	3.75E-03	97.7	4.40	0.17	807	1.7
88052B	38	C	1.46E+03	5.43E+01	5.51E-02	5.06E-03	98.9	4.45	0.17	669	1.7
88052B	39	C	1.19E+03	3.70E+01	6.03E-02	6.63E-03	98.2	5.38	0.17	532	1.7
88052B	43	R	1.41E+03	5.08E+01	6.62E-02	5.62E-03	97.4	4.53	0.17	642	2.9
88052B	44	R	6.83E+02	2.62E+01	5.70E-02	5.54E-03	98.6	9.39	0.37	436	2.4
88052B	46	C	1.47E+03	5.70E+01	8.82E-02	7.25E-03	94.6	4.24	0.18	326	3.0
88052B	48	C	1.33E+03	5.14E+01	1.04E-01	5.90E-03	92.6	4.58	0.19	420	2.4
TOC-97h-2	2	R	7.30E-04	3.90E-05	5.30E-03	1.04E-03	80.9	3.54	0.59		
TOC-97h-2	2	C	7.36E-04	2.70E-05	9.62E-03	1.16E-03	94.3	4.68	0.31		
TOC-97h-2	3	C	7.56E-04	3.00E-05	6.02E-03	6.60E-04	100	4.15	0.36		
TOC-97h-2	4	C	6.87E-04	3.70E-05	5.93E-03	9.00E-04	100	4.43	0.24		
TOC-97h-2	4	R	7.52E-04	2.00E-05	6.28E-03	6.80E-04	91.7	4.44	0.16		
TOC-97h-2	7	R	9.53E-03	2.41E-03	9.43E-01	2.43E-01	11.7	9.32	10.19		
TOC-97h-2	7	R	3.18E-03	3.68E-04	2.61E-01	4.61E-02	14.2	3.4	4.13		
TOC-97h-2	7	R	1.96E-03	3.72E-04	1.16E-01	2.50E-02	46.5	7.3	4.28		
TOC-97h-2	7	R	1.18E-03	1.02E-04	5.58E-02	5.95E-03	72.6	6.17	1.55		
TOC-97h-2	7	C	7.21E-04	4.90E-05	8.47E-03	1.41E-03	94.9	4.21	0.48		
TOC-97h-2	8	C	6.83E-04	4.30E-05	4.95E-03	1.05E-03	89.4	3.66	0.48		
TOC-97h-2	8	R	7.20E-04	1.80E-05	6.29E-03	5.40E-04	95.5	4.43	0.14		
TOC-97h-2	9	C	7.77E-04	2.40E-05	6.07E-03	7.00E-04	97.4	4.87	0.24		

*TOC-97h-2 ages previously reported in Schmitt et al. 2003

Toconce

Sample	Grain	Core/Rim	$^{238}U/^{206}Pb$	1σ $^{238}U/^{206}Pb$	207Pb/206Pb	1σ 207Pb/206Pb	% 206Pb*	206Pb/238U age [Ma]	1σ 206Pb/238U age [Ma]	U (ppm)	U/Th
09033GG_z_r	2		9.00E+02	2.50E+01	8.54E-02	1.24E-02		6.90	0.22	600	8.2
09033GG_z_r	3		9.36E+02	3.16E+01	9.93E-02	1.08E-02		6.51	0.25	452	8.3
09033GG_z_r	4		8.53E+02	2.47E+01	8.96E-02	7.70E-03		7.22	0.23	400	8.4
09033GG_z_r	5		9.59E+02	2.93E+01	1.35E-01	1.42E-02		6.05	0.24	471	8.4
09033GG_z_r	6		9.44E+02	2.24E+01	8.98E-02	5.45E-03		6.54	0.17	1069	8.5
09033GG_z_r	7		9.93E+02	2.33E+01	5.65E-02	4.91E-03		6.50	0.16	2031	8.4
09033GG_z_r	8		8.83E+02	2.70E+01	7.44E-02	7.86E-03		7.13	0.24	593	8.3
09033GG_z_r	9		9.82E+02	2.22E+01	4.95E-02	4.09E-03		6.63	0.15	2561	8.4
09033GG_z_r	9		5.24E+02	1.09E+01	4.09E-01	1.44E-02		6.69	0.36	538	8.4
09033GG_z_r	9		8.40E+02	1.84E+01	7.50E-02	6.08E-03		7.47	0.18	1155	8.3
09033GG_z_r	9		9.45E+02	2.30E+01	8.84E-02	8.90E-03		6.54	0.18	605	8.4
09033GG_z_r	9		8.49E+02	1.61E+01	5.36E-02	1.71E-03		7.62	0.15	5248	8.4
09033GG_z_r	9		8.56E+02	2.54E+01	8.61E-02	1.21E-02		7.23	0.25	308	8.2
09033GG_z_r	9		8.44E+02	1.67E+01	1.44E-01	4.52E-03		6.76	0.16	2332	8.3
09033GG_z_r	9		9.50E+02	1.98E+01	5.96E-02	4.21E-03		6.76	0.15	1135	8.3
09033GG_z_r	12		8.98E+02	2.21E+01	9.31E-02	6.94E-03		6.83	0.19	672	8.3
09033GG_z_r	13		9.35E+02	2.49E+01	9.31E-02	1.03E-02		6.57	0.20	580	8.4
09033GG_z_r	14		8.87E+02	2.31E+01	7.76E-02	1.01E-02		7.06	0.21	514	8.3
09033GG_z_r	15		9.96E+02	2.73E+01	8.37E-02	8.50E-03		6.25	0.19	565	8.3
09033GG_z_r	16		8.44E+02	1.65E+01	1.78E-01	4.84E-03		6.42	0.16	2569	8.4

Vilama

Sample	Grain	Core/Rim	$^{238}U/^{206}Pb$	1σ $^{238}U/^{206}Pb$	207Pb/206Pb	1σ 207Pb/206Pb	% 206Pb*	206Pb/238U age [Ma]	1σ 206Pb/238U age [Ma]	U (ppm)	U/Th
BOL06042	1	R	7.15E+02	2.53E+01	6.51E-02	9.11E-03	97.6	8.88	0.34	338	3.4
BOL06042	2	R	5.76E+02	2.54E+01	1.79E-01	8.41E-03	83.0	9.39	0.53	1124	8.5
BOL06042	3	R	7.26E+02	3.26E+01	6.50E-02	4.19E-03	97.6	8.75	0.40	407	2.4
BOL06042	4	R	6.98E+02	2.79E+01	5.67E-02	3.98E-03	98.7	9.19	0.37	976	3.0
BOL06042	5	R	7.39E+02	2.78E+01	5.10E-02	3.01E-03	99.4	8.77	0.33	1498	4.5
BOL06042	6	R	7.63E+02	2.49E+01	7.49E-02	4.75E-03	96.3	8.23	0.28	496	4.0
BOL06042	7	R	7.97E+02	3.14E+01	5.17E-02	2.89E-03	99.3	8.12	0.32	888	3.4
BOL06042	8	R	7.76E+02	3.10E+01	5.61E-02	2.76E-03	98.7	8.27	0.33	915	1.8
BOL06042	9	R	7.04E+02	2.87E+01	5.62E-02	3.80E-03	98.7	9.14	0.38	876	7.6
BOL06042	10	R	7.61E+02	2.72E+01	5.54E-02	2.84E-03	98.8	8.47	0.30	959	12.0
BOL06042	11	R	7.11E+02	2.89E+01	6.06E-02	3.33E-03	98.2	8.99	0.37	473	4.5
BOL06042	12	R	7.23E+02	2.73E+01	5.26E-02	1.75E-03	99.2	8.94	0.34	2223	5.0
BOL06042	13	R	7.14E+02	2.70E+01	5.91E-02	3.63E-03	98.4	8.96	0.34	471	2.6
BOL06042	14	R	7.05E+02	2.98E+01	8.81E-02	5.19E-03	94.6	8.74	0.39	456	4.2
BOL06042	15	R	7.07E+02	2.57E+01	4.73E-02	1.38E-03	99.9	9.20	0.33	3658	13.9
BOL06042	16	R	7.25E+02	2.67E+01	6.22E-02	4.03E-03	98.0	8.78	0.33	669	1.9
BOL06042	17	R	7.34E+02	2.81E+01	5.27E-02	2.10E-03	99.2	8.80	0.34	1491	8.2
BOL06042	18	R	7.07E+02	2.58E+01	5.25E-02	2.22E-03	99.2	9.14	0.33	1137	6.4
BOL06042	19	R	7.36E+02	2.86E+01	6.42E-02	5.64E-03	97.7	8.65	0.35	382	5.8
BOL06042	20	R	6.70E+02	2.46E+01	4.97E-02	2.27E-03	99.6	9.68	0.35	2853	32.0
BOL06042	21	R	7.43E+02	2.84E+01	5.75E-02	3.72E-03	98.6	8.64	0.33	501	3.9
BOL06042	22	R	7.11E+02	2.74E+01	5.22E-02	2.54E-03	99.2	9.10	0.35	1018	8.0
BOL06042	23	R	7.16E+02	2.65E+01	5.33E-02	2.51E-03	99.1	9.02	0.33	1171	8.4
BOL06042	24	R	7.39E+02	2.72E+01	5.12E-02	1.81E-03	99.4	8.77	0.32	1841	9.1
BOL06042	25	R	7.14E+02	2.63E+01	5.31E-02	1.92E-03	99.1	9.04	0.33	1667	6.2

BOL06042	26	R	7.22E+02	2.99E+01	5.26E-02	1.71E-03	99.2	8.95	0.37	1837	5.2
BOL06042	27	R	7.31E+02	2.78E+01	5.62E-02	2.37E-03	98.7	8.80	0.34	935	5.9
BOL06042	28	R	6.68E+02	2.51E+01	5.22E-02	1.29E-03	99.2	9.67	0.36	1999	9.6
BOL06042	29	R	7.36E+02	2.82E+01	4.72E-02	1.98E-03	99.9	8.85	0.34	1527	7.1
BOL06042	30	R	7.58E+02	2.79E+01	5.49E-02	2.57E-03	98.9	8.51	0.32	990	9.6
BOL06042	31	R	7.43E+02	3.39E+01	7.45E-02	6.77E-03	96.4	8.45	0.40	314	4.0
BOL06042	32	R	6.99E+02	2.91E+01	7.93E-02	9.41E-03	95.8	8.92	0.40	1200	2.7

1 s.e. = 1σ standard error
n.d. = not detected
All ages relative to standard zircon AS3 (1099.1 Ma) and corrected for ^{230}Th disequilibrium using D230 = 0.2
UO+/U+ calibration: range = 7.17-8.73; AS3 age reproducibility = 2.1% (1 standard deviation; n = 142)
Common Pb correction using Southern California anthropogenic ^{207}Pb/^{206}Pb = 0.8283
U concentrations estimated from standard zircon 91500 (U = 81 ppm); uncertainty approx. 13% (rel.)
U/Th mass ratio from ^{208}Pb/^{206}Pb vs. Th/U for AS3 standard zircon